Understanding the Performance of Highway Embankments on Degraded Permafrost

by

Hamid Batenipour

A Thesis submitted to the Faculty of Graduate Studies of

The University of Manitoba

in partial fulfilment of the requirements of the degree of

DOCTOR OF PHILOSOPHY

Department of Civil Engineering

University of Manitoba

Winnipeg

Abstract

Roads and highways in cold regions are negatively affected by settlement of embankments in areas of degraded or degrading permafrost, particularly in areas with mean annual temperatures close to 0°C where permafrost is locally discontinuous. Climate warming and human activities can lead to increases in the temperature of permafrost and to thawing. In regions of discontinuous permafrost, thawing may produce thickening of the active layer, large settlements and non-recoverable shear deformations. These can cause potentially dangerous trafficability issues.

The research program involved a test site on Provincial Road PR391, about 18 km northwest of Thompson, Manitoba. The foundation material of PR391 is currently classified as "degraded (thawed) permafrost". The purpose of this research was to investigate and understand the performance of highway embankments on thawed permafrost. The research involved field instrumentation and data collection, laboratory testing, thermal modelling and frost heave predictions.

The results of the field instrumentation and data collection show net heat flow into the ground, as well as development of cyclic seasonal gradients of total head. This is believed to be a significant original contribution to understanding the effects of climate change on highway infrastructure. The results also show that displacements

observed at the PR391 embankment are a combination of consolidation and shearing strain of the foundation material. Most studies of embankments concentrate on vertical settlements. This research shows that horizontal movements are also present, a contribution that helps explain the mechanism of lateral spreading. The results of the laboratory testing show that the mechanical and shearing properties of the soil collected from the PR391 embankment are not significantly affected by differences in temperature once water in the soil has actually thawed. The results of the thermal modelling show reasonable trends in simulated ground temperatures compared with the data obtained from the thermistors underneath the embankment. The frost heave prediction of PR391 shows that in situ frost heave characteristics can be estimated by applying the Segregation Potential (SP) frost heave method in field conditions. This provides a valuable field study to the limited number of such studies of Segregation Potential, which are normally done under laboratory conditions.

Acknowledgements

I would like to express my gratitude to my co-advisors Dr. Marolo Alfaro and Dr. Jim Graham for their unending patience, encouragement, and mentoring during this research. Dr. Marolo Alfaro and Dr. Jim Graham made time for all my questions and provided support to me both personally and professionally.

Thank you to the engineering professors including Dr. Scott Ormiston and Dr. Jitendra Sharma for their advice and encouragement.

Thanks to Ken Kalynuk and Kerry Lynch for their help in the field and laboratory as well as guidance and support. Thanks to geotechnical graduate students and civil undergraduate students for their friendship, discussions and assistance during this research. I would like to specifically acknowledge my colleague and fellow PhD student Mr. David Kurz for his collaboration during this research. Our respective programs were parallel but separate.

Financial support is acknowledged from Manitoba Infrastructure and Transportation, the University of Manitoba, and the National Science and Engineering Research Council of Canada.

A big thanks to my family: Mansoureh Pourghadiri, Amir and Soheila Batenipour for their love and support during my studies.

Table of Contents

List of Tables

List of Figures

ix

List of Copyrighted Material for which Permission was Obtained

CHAPTER 1:   Introduction

1.1 General Overview

Changes in meteorological conditions, precipitation, solar radiation, wind speed, and other factors induce temperature changes not only at ground level, but also at greater depths. The changes in temperature affect civil engineering infrastructure, particularly in areas with mean annual temperatures close to 0°C where discontinuous permafrost may be locally present. Permafrost is defined as ground, whether soil or rock, that remains at or below a temperature of 0°C for a minimum period of two years (Williams 1986). The characteristics of permafrost vary with climatic, topographic, geographic, hydrologic and geological factors.

Climate warming and human activities can lead to increases in ground temperature and thickening of the active layer - the top layer of soil that freezes during winter months and thaws during summer. Seasonal cycles of freezing and thawing can cause large settlements and non-recoverable shear deformations in fine-grained soils (Brown 1967).

As the literature review in Chapter 2 will show, the mean annual air temperatures in Canada are increasing more rapidly close to the 0°C isotherm than further north or further south (CCCSN 2009) (IPCC 2007). These temperature changes will degrade

existing permafrost and affect many forms of civil engineering infrastructure, unless mitigated by engineering interventions.

Frozen soil is stronger and less compressible than unfrozen soil. Frozen silty sands, silts, and silty clays frequently contain layers of ice, often in distinct lenses that form as a result of migration of water to negative potentials at the freezing front (Konrad 2008). Heaving is produced in seasonally frozen soils as a result of increasing the volume of water in the void spaces as it freezes, and more importantly as a result of ice segregation during freezing, which produces alternating bands of frozen soil and ice.

When thawing occurs, whether as a result of seasonal warming, climate warming over a longer period, or changes in heat transfer due to human or engineering activities, water from the melting ice moves towards the ground surface or moves laterally to be absorbed by surrounding soils. Resulting decrease in effective stresses produces deformations and weakening of foundations for highway sub-bases, cuts and fills, buildings and pipelines, airport runways and rail beds. Because the ice lenses are typically irregular in thickness and extent, out-migration of water often produces differential settlements, lateral spreading, and reduced stability that lead to serviceability issues (Hinkel et al. 2003).

Although the permafrost regions in northern Canada are not heavily populated, their economic importance has increased substantially in recent decades owing to the presence of mineral, petrocarbon and hydroelectric resources. Additional shipping into northern Canada can also be expected due to the thawing of summer ice in the Arctic Ocean. New roads and railways will have to be constructed in northern Canada over soils with engineering properties that may degrade with climate warming and land use. Design, construction, and maintenance of this new infrastructure will have to take account of future warming (Hinkel et al. 2003).

Highway construction in northern Canada follows generally similar practices to those in warmer regions. Embankment fills usually have high thermal conductivity, leading to heat transfer into underlying layers and thawing of previously frozen foundation soil (Batenipour et al. 2009b). Alteration of existing ground cover can change the energy regime (Nelson & Outcalt 1982). Asphalt surfacing also absorbs heat from the sun and transfers it to the embankment. This often leads to thawing of underlying ice-rich permafrost and subsidence of the road bed. In general, degradation of permafrost begins at the toe of embankments and extends later beneath its centre (Andersland & Ladanyi 2004). Melting of permafrost also reduces strength and increases pore water pressures when the hydraulic conductivity of the foundation soil is low. This leads to differential settlements, lateral spreading, and instability which can be sufficiently large to make the road inoperable. Several methods are currently used to prevent or reduce thawing of permafrost and

development of deformations. These include above-ground construction, use of thermosyphons, and buildings on piles or gravel pads above original ground level (Hinkel et al. 2003) and (Holubec 2008).

1.2 Background

Construction in permafrost regions requires special practices where soil profiles contain ice lenses. In order to improve local design and maintenance procedures, Manitoba Infrastructure and Transportation (MIT) and the University of Manitoba (UM) are collaborating on several projects that involve field instrumentation, laboratory testing and numerical modelling. To properly understand the context of this Ph.D. research program, this section provides an introductory summary.

The research program is a project on Provincial Road PR391, about 18 km northwest of Thompson, Manitoba (the research site will be described in more detail in Chapter 3). The most recent geotechnical site investigation on PR391 has shown no presence of permafrost in the foundation of the embankment (Previous investigations confirmed the presence of ice in the foundation). Therefore, the foundation material of PR391 is currently classified as "degraded (thawed) permafrost". The purpose of this research is to investigate and understand the performance of highway embankments on thawed permafrost. The research on PR391 consists of (1) a detailed geotechnical site investigation, (2) field

instrumentation, (3) data collection, (4) laboratory testing, (5) constitutive analysis and (6) numerical simulations. This provides new insight into the nature and cause of the embankment deformations and the mechanism producing functional failure (serviceability limit state). It also provides an improved ability to identify sections 'at risk' that require immediate remedial attention and evaluates suitable remedial measures for constructing of highways and road embankments, and the treatment of existing highways on thawed permafrost.

A comprehensive laboratory testing program has been completed, focusing on the effects of low temperatures (about 0°C) on the consolidation and shearing properties of the soil at the PR391 test site. The one-dimensional consolidation (oedometer) tests and consolidated undrained triaxial tests with pore pressure measurement (CIŪ tests) were completed at temperatures of 3°C and 21°C. Soil characterization tests (such as Atterberg limits and grain size distribution) have been undertaken to understand thoroughly the properties of the foundation material underneath the PR391 embankment and the effect of temperature change on the mechanical properties of soil. All tests were done in general accordance with the appropriate ASTM standards. Testing was done in the University of Manitoba's Geotechnical Laboratories. Testing and analysis have been done by the author with the help of the author's colleague Mr. David Kurz, the laboratory technicians, and undergraduate summer students.

Instrument clusters were installed at the PR391 site embankment, including thermistor strings at 1m intervals, vibrating wire piezometers and standpipes, surface settlement plates, slope inclinometers, and lateral displacement extensometers. The temperature, pore water pressure, and vertical and horizontal deformations of embankment have been monitored. Data have been collected from the instruments and analyzed during the first two years of operation, that is, over two freeze-thaw cycles. Results provide a better understanding of the deformation of embankment, changes of temperature, changes of pore water pressure and flow in the ground.

The numerical modelling of the PR391 embankment has been developed to simulate the thermal changes and frost heave characteristics of highway embankments. Thermal conductivity values of the soil from the PR391 test site embankment have been measured in the laboratory and used as an input in the thermal modelling. The modelling permits simulation of temperature changes under the embankment. These temperature changes affect the behaviour of the foundation soils and allow simulation of frost heave characteristics of foundations on degraded permafrost. The focus of this modelling is primarily to study the application of the frost heave approach known as the Segregation Potential (SP) method (Konrad & Morgenstern 1982) to field conditions. The goal is to back-calculate the segregation potentials from the site observations and collected frost heave data by using the SP method, and to compare the results with other published results.

1.3 Hypotheses and Objectives

The purpose of this research program is to investigate and understand the performance of highway embankments on degraded permafrost. This program includes three major areas of work: laboratory testing, field instrumentation, and numerical modelling. As a result, three hypotheses are presented that are closely inter-related.

Hypothesis #1

Soil properties measured at room temperatures may give faulty estimates of deformations at the lower temperatures in thawed permafrost.

Hypothesis #2

Deformations of highways and road embankments on thawed permafrost are associated with compression and shear strains, including creep strains in the foundation soils.

Hypothesis #3

Frost heave prediction using segregation potential can be used in the field to examine the frost susceptibility of the soil

To examine the three hypotheses, the objectives of the research program are to identify:

1. Mechanisms producing (functional) failure in road embankments on thawed permafrost

2. Improved ability to identify sections 'at risk' in highways and road embankments on thawed permafrost

3. Suitable remedial measures in the highways and road embankments on thawed permafrost

1.4 Organization of Thesis

The thesis is organized as follows: Chapter 2 provides a literature review required in order to understand the work and concepts presented in this thesis. It also provides justification for the research program that has been undertaken. The research site description, geotechnical site investigation and field instrumentation are presented in Chapter 3. Chapter 4 describes the laboratory testing used in the research program and the analysis of the test results. Data collected and analyzed from the site are presented in Chapter 5. Chapter 6 provides the development of the frost heave prediction and thermal modelling used in this research and presents the model results. The results of laboratory testing, field instrumentation and numerical modelling are discussed in Chapter 7 to bring together the results of the preceding chapters, and to compare them to the original hypotheses and objectives. Chapter 8 discusses processes, strategies and remedial measures to improve road

embankment stability. Finally Chapter 9 summarizes the conclusions and recommendations of this research program.

CHAPTER 2:   Literature Review

2.1 Introduction

The focus of this research is to understand the performance of highway embankments on degraded permafrost. An important goal is to understand and describe the mechanisms producing functional failure in roads and other structures placed on thawed permafrost. This chapter provides a review and background information on warming of foundations in cold regions, climate warming, thawed permafrost and the implications of these processes on the design and performance of engineering projects. The review examines the effect of temperature on the behaviour of clay, as well as the frost heave process in soils and related factors.

2.2 Natural and Engineered Warming of Foundations in Cold Regions

Permafrost, or perennially frozen ground, is a critical component of cold regions in the Arctic. Permafrost regions occupy approximately one-fifth of the land area of the earth and half of the surface of Canada (Brown 1967). The effects of climate warming on permafrost can severely disrupt ecosystems and human infrastructure such as roads, buildings, bridges, utilities, pipelines, and airstrips. The susceptibility of engineering works to thaw-induced damage is particularly relevant to First Nations communities in northern Canada. The territories occupied by these communities are

rich in mineral, petrocarbon and hydroelectric resources that will require future infrastructure projects if they are to be developed successfully. Climate warming and human activities can lead to increases in the temperature of permafrost and thickening of the active layer (the top layer of soil that thaws during summer months and freezes again during winter) (Brown 1967). Such changes can lead to extensive settlements of the ground surface, with severe damage to infrastructure.

2.2.1 Permafrost in Canada

Permafrost is defined as a ground condition, whether soil or rock, that remains at or below a temperature of 0°C for a minimum period of two years (Williams 1986). Permafrost includes ground that freezes in one winter and remains frozen through the following summer and into the next winter. The permafrost regions in Canada currently occupy more than 50% of the ground surface, primarily in northern regions and at higher elevations in the western mountains (Brown 1967). Figure 2.1 shows the distribution of permafrost in Canada. Different zones of permafrost have been identified in Canada on the basis of the distribution and frequency of perennially frozen ground. In the continuous zone, permafrost is everywhere present beneath the ground surface except beneath large bodies of water that do not freeze to the bottom. In the discontinuous zone, there are discontinuities in the permafrost both in its horizontal and vertical extents and the permafrost is interspersed with areas of unfrozen ground. Some researchers subdivide discontinuous permafrost into

regions which are predominantly unfrozen but contain some permafrost; and other regions which are predominantly permafrost but contain some unfrozen soils (Brown 1967) and (Heginbottom 2000). The mean annual temperature at the ground surface, the thermal properties of the substrate, the amount of heat flowing from the earth's interior, the insulating cover of vegetation and snow, and drainage are all factors that determine the thickness of permafrost (Hinkel et al. 2003) and (Osterkamp & Lachenbruch 1990). Changes in meteorological conditions, precipitation, solar radiation, wind speed, and other factors induce temperature changes, not only at ground level but also at greater depths. Permafrost in the continuous zone is several hundreds to more than 305m thick and the active layer is generally 0.3m to 1m thick (Brown 1967). In the northern part of the discontinuous zone, the thickness of permafrost varies from about 15m to 60m. In the southern part of the zone, permafrost occurs in scattered islands ranging in area from a few square metres to several hectares, and varying in thickness from a few metres to a maximum of about 15m (Brown 1960).

Although the presence of ice is not by itself a requirement in the definition of permafrost, ground ice is nevertheless related to many of the distinctive features and problems in permafrost areas. Ice can occur within permafrost as small individual crystals within soil pores, as lenses of nearly pure ice parallel to the ground surface, and as variously shaped intrusive masses formed when water is attracted to a freezing front in soil or rock and subsequently frozen (Hinkel et al. 2003).

2.2.2 Climate Warming

Net heat flow is the main control on the occurrence of permafrost. Permafrost can exist only in areas where the average temperature produced by the amount of heat lost from the ground in winter and gained from the atmosphere in summer, plus geothermal heat, remains continuously below 0°C. Fluctuations in air temperature during the year produce corresponding temperature fluctuations about the mean annual ground temperature to depths of about 6m to 15m (Brown 1967).

Without considering its origin, the Intergovernmental Panel on Climate Change (IPCC) showed that the global climate warming in Canada over the past thirty to forty years is clearly producing significant effects on permafrost (Figure 2.2, (IPCC 2007)). Temperature increases lead to thawing of ground ice and an overall reduction in the extent of permafrost, with a significant effect on the distribution of permafrost (Smith et al. 2005). In general, as the ground warms, the thickness of the active layer increases and the icy permafrost below the active layer thaws. Climate warming also leads to changes in vegetation. In the long term, these changes will affect permafrost conditions in areas where vegetation changes lead to further changes in the relationship between air climate and soil temperature (Heginbottom 2000).

Data from the IPCC showed that the global average of surface temperatures has increased by about 0.74°C over the past hundred years. Warming in the last century

has occurred in two phases, from the 1910s to the 1940s (0.35°C), followed by a slight cooling (0.1°C) and then a rapid warming from the 1970s to the end of 2006 (0.55°C). The warmest years of the series are 1998 and 2005, and 11 of the 12 warmest years since 1850 have occurred in the last 12 years (1995 to 2006). The largest temperature increases in recent decades have occurred over land areas in the Northern Hemisphere from about 40°-70°N. Seasonally, warming has been slightly greater in winter months. Warming of the oceans, rising sea levels, glaciers melting, sea ice retreating in the Arctic and diminished snow cover in the Northern Hemisphere also confirms the presence of global climate warming (IPCC 2007).

Figure 2.2 shows the mean annual air temperature and 5-year running means for Environment Canada stations in five northern regions. The figure shows the increases of temperature, particularly in the western Arctic. Figure 2.3 depicts variations of annual air temperature in the Arctic (north of 60° N) from 1900 to 2003. In general, temperature increased from 1900 to the mid-1940s, then decreased until about the mid-1960s, and increased more quickly thereafter. The general trends of the arctic temperature changes are similar to those of global temperature changes (McBean et al. 2005).

Environment Canada has produced a report that predicts climate changes on a regional basis (CCCSN 2009). Twenty-four international modelling centres from IPCC for 9 arctic Canada zones (shown in Figure 2.4) contributed to the international

modelling dataset. The baseline period for the modelling is 1971-2000. Four models with best results were selected for each of the 9 zones. They were run as an ensemble to capture the range of future temperatures by season for moderate (A1B) and high (A2) greenhouse gas emission scenarios. Results were produced that compare the baseline with the periods 2011-2040, 2041-2070, and 2071- 2100 for each of the four seasons within the 9 regions. Ensemble projections using the selected models were used to produce the final results for both the A1B, and A2 emission cases. The projected temperature changes are all in relation to the 1971-2000 baseline period. Table 2.1 shows the results for changes in mean annual temperature from the 'best four models' for each sector for each of the standard projection periods. The results show increases in mean annual temperature for all sectors. In general, increases of 5°C to 6°C over 100 years can be seen across the arctic. The site of the author's research program is located in the C1 Region in Figure 2.4, where the projected increase from the current 1971-2000 baseline to the 2040-2070 period is 2.7°C to 2.9°C for the moderate and high emission scenarios respectively (CCCSN 2009).

Climate warming also affects permafrost temperatures and consequently will result in disappearance of some current areas of permafrost. Permafrost in northern Canada has typically warmed in recent decades. Data from the northern Mackenzie Valley in the continuous permafrost zone (Smith et al. 2005) show that permafrost temperature between depths of 20m to 30m has increased in the 1990s (Figure 2.5).

15

Data from southern Mackenzie Valley, where permafrost is close to 0°C and thin (less than 10m to 15m thick) show smaller changes in temperature of permafrost (Figure 2.6), likely due to the absorption of latent heat required to thaw the ice-rich permafrost (Smith et al. 2005). Similar results are reported for the eastern and high Canadian Arctic regions mainly in the late 1990s (Smith et al. 2005). Warming of 0.15°C per year at a depth of 15m occurred between 1995 and 2001 and warming of about 0.06°C per year has occurred since 1996 at a depth of about 30m. In contrast, cooling of permafrost was observed from the late 1980s to the early 1990s at a depth of 5m at Iqaluit in the eastern Canadian Arctic. This cooling, however, was followed by warming of 0.4°C per year between 1993 and 2000 (Smith et al. 2005). Similar trends in temperature change were observed in Northern Quebec along the southern shore of Hudson Strait, where permafrost cooling was observed between the mid-1980s and mid-1990s at a depth of 10m (Allard, Wang & Pilon 1995). The cooling was followed by warming that began in 1996 (Brown, Hinkel & Nelson 2000).

2.2.3 Warming Caused by Engineering Infrastructure

Other controls on the distribution, nature and extent of permafrost include variations in geology, vegetation and topographic features such as slope aspect and slope angle. These changes affect insulation, depth of thaw, runoff, and moisture content.

Disturbances in permafrost terrain caused by human activities can result in disruption of the thermal equilibrium which enhances thawing of permafrost (Péwé 1954) (Brown 1997). The disturbance can occur due to human-induced (anthropogenic) construction, removal or change of the vegetation cover for agricultural purposes, off-road activities, contaminant input, or natural causes such as fire or heavy summer rains.

Construction activities such as the clearing of rights-of-way and the grading and the traversing of drainage courses have a potential for disturbing permafrost. In permafrost terrain, construction-related disturbance can lead to permafrost degradation accompanied by thaw settlement and slope instability, which may cause dangerous trafficability issues as well as having adverse effects on the landscape (Claridge & Mirza 1981). Use of off-road winter vehicles such as snowmobiles in rural landscapes can accelerate the change of vegetation and lead to thaw of permafrost (Slaughter et al. 1990). The settlement of thawed permafrost due to the removal of vegetation can also be very severe (Linell 1973). A controlled experiment study from the Permafrost National Test Site near Fairbanks, Alaska, showed that the removal of insulating layers of vegetation caused the permafrost table to move downward as much as 6.7m over a 26 year period.

(Brown 1997) provided a comprehensive review of a wide range of anthropogenic disturbances affecting permafrost terrain and the active layer. Figure 2.7 shows the

complex interactions of the active layer and permafrost with atmosphere, vegetation and biological, hydrological and geomorphological processes. The figure illustrates that the active layer thickens and degradation of ice-rich permafrost occurs when vegetation and organic layers decrease or are removed. Changes in snow cover and soil moisture further modify the response of the active layer to thermal changes at the ground surface and in thawing of the frozen soil layer (Brown 1997).

2.2.4 Thawing of Permafrost

As mentioned earlier, fluctuations in air temperature during the year produce corresponding temperature fluctuations about the mean annual ground temperature to depths that depend on latitude, altitude, aspect etc. The amplitude of these fluctuations decreases with depth. The depth at which fluctuations became imperceptible is called the *level of negligible annual amplitude* or *depth of mean zero annual amplitude, DMZAA* (Brown 1969). Below this level, the ground temperature in the permafrost and below increases steadily under the influence of the heat from the Earth's interior. Below the DMZAA, ground temperatures change only in response to long-term climate changes extending over centuries or to longer term changes in upwards heat from deeper in the earth's mantle. Figure 2.8 shows a typical ground temperature profile through permafrost. The figure shows that climate warming shifts the temperature profile to the right, as shown by the gray curves. The surface temperatures are higher in summer and winter, the active layer is

thicker, and the mean annual temperature at the DMZAA is higher (Hinkel et al. 2003).

Thawing of permafrost refers to natural or artificial decreases in the thickness and extent of permafrost due to the changes of temperature. Permafrost degradation changes the boundaries of areas of permafrost. Monitoring in Canada over the last three decades (Halsey, Vitt & Zoltai 1995) indicates a general warming of shallow permafrost across the Canadian permafrost zones and changes in the southern boundary of the discontinuous permafrost zone. In North America, the southern boundary of the discontinuous zone has migrated northward in response to warming.

Thawing of permafrost and changes in the thickness and geographical extent of permafrost can have two effects. The first effect is the *carbon cycle* when greenhouse gases (carbon dioxide and methane) are released from thawing permafrost, which is often organic, and enter the atmosphere. This process facilitates further climate warming due to the ability of carbon dioxide and methane to absorb solar heat rather than reflect it (Hinkel et al. 2003).

The second effect is when the ice in the permafrost thaws and converts to water. Frozen soil is stronger and less compressible than unfrozen soil. Frozen silty sands, silts, and silty clays frequently contain layers of ice, often in distinct lenses that form as a result of water migration to negative water potentials at the freezing front

(Konrad 2008). When thawing occurs, either as a result of warming climate or changes in heat transfer due to human/engineering activities, these ice lenses melt and water moves towards the ground surface. The resulting decrease in effective stresses in the soil causes weakening and subsequent deformation of foundations for buildings and pipelines, airport runways, rail beds, and highway sub-bases, cuts and fills. Because ice lenses are typically irregular in thickness and extent, out-migration of water often produces differential settlements, lateral spreading, and instability that lead to serviceability issues. This irregular settlement of the ground surface is termed *thaw settlement*. Typically, thaw settlement does not occur uniformly, yielding a chaotic surface with small hills and wet depressions known as *thermokarst terrain* (Hinkel et al. 2003).

2.2.5 Engineering Implications

Thermokarst affects civil engineering infrastructure, and in many cases renders it unstable. As mentioned before, thawing of ice-rich permafrost causes large settlements and non-recoverable shear deformations because of its potential for settlement. Although the permafrost regions in northern Canada are not heavily populated, their economic importance has increased substantially in recent decades owing to the presence of mineral, petrocarbon and hydroelectric resources. Improved methods of extraction and transportation to population centres are essential.

Construction in permafrost regions requires special techniques at locations where the terrain contains ice lenses within the soil profile (Hinkel et al. 2003). Construction of highway fills in northern Canada follows broadly the same practices as those in warmer regions. The fills generally have high thermal conductivity, leading to heat transfer into underlying layers and thawing of previously frozen foundation soil (Batenipour et al. 2009b). Asphalt surfacing also absorbs heat from the sun and transfers it to the embankment. Generally, degradation of permafrost begins at the toe of the embankment. Melting reduces strength and increases pore water pressures when the hydraulic conductivity of the foundation soil is low. This leads to differential settlements, lateral spreading, and instability. The resulting disturbance can change the energy regime at the ground surface (Nelson & Outcalt 1982). In turn, this leads to thawing of the underlying ice-rich permafrost and subsidence of the road, which can become unusable several years after construction. Several methods are currently being used to prevent or minimize the thawing of permafrost and development of thermokarst. Three of these methods will be described in the following section.

The first method includes preserving the frozen soil in permafrost by passive cooling (no power required to operate) through pressurized heat exchange pipes termed as thermosyphons (Figure 2.9). This method is being widely applied in Alaska, northern Canada and Russia to protect and cool permafrost. A thermosyphon is a closed two-phase convection device that extracts heat from the ground and

discharges it into the atmosphere. The gas/fluid medium is carbon dioxide or nitrogen that functions in a closed-pipe pressure vessel, under a pressure varying from about 2100kPa to 4800kPa. The thermosyphon draws out the heat from below the buildings or road embankments by a heat exchange mechanism. The outside colder air in winter causes the gas in the pipe above the ground to condense and flow back to the base of the pipe as a liquid. The cold air drops the pressure in the gas and by this means causes the fluid at the bottom of the pipe to evaporate. Exchange of heat operates throughout the winter as long as the air temperature is colder than the ground temperature at the bottom of the thermosyphon. In summer, the accumulated cold in the ground is preserved by a zone of insulation located above the evaporator pipes. Studies in northern Canada show that thermosyphons have operated for about 40 years without any major problems. Some failures of thermosyphons have been reported. These failures were generally the result of a combination of manufacturing problems, poor foundation design, or poor construction procedures (Holubec 2008).

The second method is being used in the construction of pipelines. In order to prevent the thawing of permafrost and severe damage to the oil pipes, the pipelines have been elevated where surveys indicated the presence of excess ice under the Trans-Alaska Pipeline (Figure 2.10, (Hinkel et al. 2003)). To offset the conduction of heat into the ground, many of the pipeline's vertical supports are equipped with heat pipes (thermosyphons) that cool the permafrost in winter, lowering the mean annual

ground temperature and preventing thawing of permafrost during summer. In cases where burial of the line is required, the pipes are enclosed in thick insulation and refrigerated.

The third engineering technique developed for protecting ice-rich permafrost includes constructing heated buildings above original ground level on piles (Figure 2.11) or on gravel pads which sometimes contain large-diameter pipes. Both forms of construction allow air to circulate beneath the structures and prevent transmission of heat to the subsurface ((Hinkel et al. 2003) and (Holubec 2008)).

2.3 Effect of Temperature on Soil Behaviour

The engineering properties of soil can be influenced significantly by temperature variations. Heating or cooling can affect the physical, chemical and mechanical properties of soils in different ways that may include changing the properties of the pore water, and altering the soil particles (Ghahremannejad 2003). These changes in turn produce apparent differences in compressibility and strength of soil. Studies examining the effect of temperature on the mechanical behaviour of clay soils date back to the 1960s (Perkins & Sjursen 2009). Studies from the 1990s were interested in the influence of elevated temperatures from various industrial applications, such as radioactive waste disposal (Houston, Houston & Williams 1985) (Eriksson 1989) (Lingnau et al. 1996). While the majority of these studies

focused on applications involving elevated temperatures, testing programs also often involved testing at temperatures approaching freezing, and this, of course, is the interest of the author's research program.

Temperature has two major effects on soil, thermal expansion-contraction of soil particles (solid and water) and mechanical weakening of the contacts between soil aggregates (Perkins & Sjursen 2009). In general, as temperature increases, water is expelled under drained conditions and particle contacts become weaker (Mitchell & Soga 2005). This rather unexpected result shows that the measured effects of temperature on observed mechanical properties are often contradictory (Tang, Cui & Barnel 2008). They may be due to the influence of temperature on dielectric constant. This section provides a review and background information on the effects of temperature on mechanical properties of clay, including consolidation and shear strength properties.

2.3.1 Thermal Effects on Consolidation

As temperature increases in a saturated clay soil, consolidation may be induced (Perkins & Sjursen 2009). Changes in the volume of soil due to temperature variations have been the subject of many investigations since 1960 (Ghahremannejad 2003).

Change of temperature under constant load can cause contraction or expansion, which can lead to pore water pressure changes. A study by (Houston, Houston & Williams 1985) illustrates the effect of temperature on pore water pressure. This effect is shown in Figure 2.12 for two undisturbed clays (undisturbed Pacific illite and undisturbed Pacific smectite-rich samples) where the pore water pressure increase (Δu) is normalized by the initial consolidation pressure (σ'_{3c}) and plotted versus temperature. As the figure shows, a temperature increase in clay samples prevented from draining in isotropic compression resulted in an increase in pore water pressure. Pore water pressure increased at a faster rate with an increase in temperature when the initial temperature is higher.

Several studies have investigated the effect of temperature on preconsolidation pressure measured in one-dimensional oedometer tests. (Eriksson 1989) performed incremental loading oedometer tests on a silty clay from northern Sweden. The results showed that preconsolidation pressure decreased with increasing temperature (Figure 2.13). The rate of decrease appeared to be greater for temperatures less than 20°C and was approximately 1kPa per 1°C of temperature change (Figure 2.14). Similar results are reported by (Leroueil & Marques 1996). They summarized several studies by plotting preconsolidation pressure (σ_p as used in Figure 2.15) normalized by the preconsolidation pressure measured at 20°C against test temperature. The results in Figure 2.15 show appreciable scatter but

indicate that the preconsolidation pressure measured near 0°C is approximately 20% higher, on average, than that measured at 20°C.

(Tidfors & Sällfors 1989) performed conventional incremental oedometer and constant rate of strain (CRS) tests on five clays from Sweden, three of which were marine clays. Temperature was varied between 7°C and 50°C. Figure 2.16 summarizes the results where the change in preconsolidation pressure per 10°C ($\Delta\sigma'_c$/10°C) normalized by the preconsolidation pressure of the soil (σ'_c) expressed as a percentage is plotted against the soil's liquid limit. The change in preconsolidation pressure is seen to increase as the liquid limit of the clay increased. Provided full drainage is permitted and effective stresses are held constant, the increase of temperature can decrease the volume of saturated, normally consolidated clay specimens (Graham et al. 2001). Figure 2.17 shows results obtained by (Graham et al. 2001) from drained isotropic compression tests on reconstituted illite at three different temperatures. As Figure 2.17 illustrates, increase in temperature causes expansion of the minerals and the water. This can be explained by the *diffuse double layer* theory (Mitchell & Soga 2005). The diffuse double layer occupies the space between the clay surface and the 'free' (hydrostatic) water, and has a thickness less than 10^{-5}mm. The thickness of the diffuse double layers increases with an increase in temperature, with an increase in dielectric constant, with a decrease in the electrolyte concentration and with a decrease in cation valency of the solution (Equation 2.1).

26

Equation 2.1
$$\frac{1}{K} = \left(\frac{\varepsilon_0 DkT}{2n_0 e^2 u^2} \right)^{\frac{1}{2}}$$

where $1/K$ is thickness of the diffuse double layer, n_0 is electrolyte concentration, u is cation valence, D is dielectric constant of the medium, T is temperature, k is the Boltzmann constant (the gas constant per molecule, $1.38*10^{-23}$ J/K), e is the electronic charge ($1.602*10^{-19}$ C) and ε_0 is a constant representing the permittivity of vacuum ($8.8542*10^{-12}$ C^2 J^{-1} m^{-1}).

Change of temperature affects the way in which the minerals support the applied stresses through net repulsive forces in diffuse double layers. The changes are not only through the direct effects of temperature T, but also through reductions in the dielectric constant which also varies with temperature. Figure 2.18 shows that the compressions caused by increases of temperature are not fully reversible when the temperature returns to its original value. (Campanella & Mitchell 1968) also reported similar results (Figure 2.19). Relationships between reversible and nonreversible volume changes appear to differ significantly from soil to soil. (Graham et al. 2001) suggest that an approach based on elastoplasticity will be useful.

When a soil is loaded one-dimensionally under a constant normal stress, its compression has two components (Batenipour et al. 2009a).   One, primary

consolidation, is associated with the hydrodynamic expulsion of water, increasing effective stress, and consequent reorganization of the soil structure. Two, the clay continues to settle even after excess pore water pressures have dissipated and effective stresses are constant. Secondary compression (creep) is the change in volume of soil caused by adjustment of the soil fabric. It is present even during primary consolidation. Volumetric creep strains are typically linear when plotted against with the logarithm of elapsed time. Secondary compression is usually characterized by the index $C_{\alpha e}$, defined as the slope of the curve obtained by plotting void ratio (e) versus log (time) in the normally consolidated range of loading (Yin, Zhu & Graham 2002) (Budhu 2007) (Kelln et al. 2008):

Equation 2.2 $\qquad C_{\alpha e} = \dfrac{e_1 - e_2}{\log(t_2/t_1)} = \dfrac{|\Delta e|}{\log(t_2/t_1)} \; ; t_2 > t_1$

There are different opinions on the effect of temperature on creep or secondary compression. (Habibagahi 1977) and (Mesri 1973) showed that $C_{\alpha e}$ for both normally and overconsolidated samples of inorganic Plaudings clay and for normally consolidated organic Plauding clay was not affected by change of temperature, whereas for organic overconsolidated samples it increased with an increase in temperature (Figure 2.20 and Figure 2.21). (Plum & Esrig 1969) also reported that the secondary compression rates were only slightly affected by increase in temperature. On the other hand, (Campanella & Mitchell 1968), (Houston, Houston

28

& Williams 1985), (Tidfors & Sällfors 1989), (Burghignoli, Desideri & Miliziano 1992), and (Towhata, Kuntiwattanaku & Seko 1993) reported that increasing temperatures produce increases in the rate of creep. An increase in creep rate was explained by the increase in the energy level (Tidfors & Sällfors 1989), or by bond breaking and structural rearrangement (Houston, Houston & Williams 1985) (Burghignoli, Desideri & Miliziano 1992). (Houston, Houston & Williams 1985) examined the effect of temperature on secondary compression for undisturbed Pacific illite. In Figure 2.22, the slope of the linear portion of the thermal consolidation curve is defined as the thermal coefficient of secondary compression, $\Gamma_{\varepsilon\alpha}$, given in percent strain per log cycle. Figure 2.23 illustrates that $\Gamma_{\varepsilon\alpha}$ increases with increasing temperature. The value ranges from about 0.4% /log cycle at 40°C to about 2.1% /log cycle at 200°C. The increase in the rate of secondary compression at the elevated temperatures was quite significant, typically causing secondary compression to dominate the thermal consolidation process.

2.3.2 Thermal Effects on Shear Strength

Several studies have been conducted to examine the influence of temperature on shear strength of clay. The effects of changes in temperature on shear strength and stress-strain behaviour have always been a subject of controversy (Kuntiwattanakul et al. 1995). Conflicting experimental results have been reported in this study area. Many experimental studies strongly asserted that an increase in temperature causes

weakening in clay. On the other hand, there were also many test results indicating that an increase in temperature strengthened the clay. (Ghahremannejad 2003) summarized (Table 2.2) the results of many of the shear experiments that have been carried out on clay at different temperatures. Some of these studies will be reviewed in this section.

Several researchers have found that an increase in temperature causes weakening of clay. (Mitchell 1964) performed consolidated undrained triaxial tests after drained heating on remolded San Francisco Bay mud with temperatures ranging from 4.7°C to 31.4°C and observed a decrease in undrained shear strength as temperature increased. The decrease in undrained shear strength from tests corresponding to an increase in temperature from 4.7°C to 20°C was approximately 10%. (Sherif & Burrous 1969) reported results of unconfined compression tests on normally consolidated kaolinite that experienced a temperature increase after consolidation and observed that unconfined compressive strength decreased with an increase in temperature. These tests were performed at warm temperatures ranging from 24°C to 65°C. (Hueckel & Baldi 1990) performed drained triaxial tests at a given confining stress of 0.5MPa under drained heating at temperatures ranging from 18°C to 115°C and observed a decrease in shearing strength with an increase in temperature (Figure 2.24). Similar observations have been made by (Boudali 1995), (Moritz 1995), and (Marques, Leroueil & Almeida 2004).

On the other hand, some studies have shown that an increase of temperature strengthens clay (Houston, Houston & Williams 1985). (Houston, Houston & Williams 1985) studied the effect of temperatures on peak shear strength of soils. Figure 2.25 shows the stress-strain behaviour of undisturbed illite at various temperatures and effective stress levels. The peak shear strength and stiffness increase with increasing temperature at a given effective confining stress. Their study was carried out using drained heating during consolidation and undrained triaxial shearing. It is important to note that the focus of their work was on elevated temperatures up to 200°C. The behaviour of the high-temperature specimens is significantly different than that of low temperature specimens tested by (Kuntiwattanakul et al. 1995). They also reported similar results from undrained triaxial tests on samples of kaolin clay at various temperatures ranging from 20°C to 90°C. Their study is based on isotropically consolidated undrained triaxial tests carried out using several paths of drained heating and consolidation. (For 90°C tests, specimens were heated under drained conditions). Their test results indicated that the undrained peak shear strength and stiffness of samples increased with increase in temperature.

Thermal expansion of the soil components explains the phenomenon of macroscopic thermal expansion under low stresses. Thermal contraction explains the mechanical weakening of contacts (Tang, Cui & Barnel 2008). This thermal volume change phenomenon has a significant effect on the soil shear strength. The

31

expansion of aggregates induces a decrease of soil strength. Conversely, thermal contraction hardens the soil and increases the shear strength. These two opposing phenomena explain the conflicting results in the research literature in terms of the effect of temperature on shear strength.

Several researchers have investigated the effect of temperature on friction angle. Studies by (Mitchell 1964), (Houston, Houston & Williams 1985), (Hueckel & Pellegrini 1989), (Hueckel & Baldi 1990), (Lingnau et al. 1996), and (Marques, Leroueil & Almeida 2004) showed only small effects of temperature on the friction angle of normally consolidated clays.

2.4 Frost Heave in Soils

Frost heave occurs in soils where there is seasonal soil freezing and supply of water; and in the active layers of permafrost soils in cold regions (Andersland & Ladanyi 2004). The pore water in the ground freezes as the temperature of atmosphere decreases and heat is transmitted from the ground to the atmosphere. Frost heave is the result of ice segregation during the freezing process and of the formation of alternating bands of soil and ice (ice lenses). During the freezing process, soil water flows to the freezing front and ice lensing takes place at water potentials less than atmospheric (suctions) to which the water is attracted (Konrad 1994). These lenses are generally oriented normal to the direction of heat flow.

There are currently several frost-heave models in which temperature, and soil hydraulic and thermal properties are used as input in calculations to predict frost heave. Following sections review current frost-heave theories.

2.4.1 Frost Heave Process

Frost heave involves heat and mass transfer and can be described by thermodynamics principles. The formation of ice lenses requires unsteady heat flow near the ground surface, combined with conditions of crystal ice growth (Andersland & Ladanyi 2004). The unsteady heat flow through the ground can lead to the flow of heat from the unfrozen to the freezing front (to remove the latent heat needed for freezing to occur), increase of frost penetration in unfrozen ground, and migration of water to the freezing front and formation of ice lenses. The volume of the soil-water system increases with ice forming. It is necessary for the formation of ice lenses that the rate of heat extraction exceeds the rate of heat supply (water flow) to the freezing front.

The temperature curve (Figure 2.26) shows the non-uniform heat flow situation near the ground surface, represented by temperature gradients with different slopes (Andersland & Ladanyi 2004) (Nixon 1991). The temperature gradients show the rate of heat extraction above the frost line to be greater than the rate of heat supply below the frost line. Ice growth occurs at the frost line, with temperature below 0°C.

Studies by (Konrad & Morgenstern 1980), and (Nixon 1991) and (Nixon 1992) indicate that ice lenses form in soil higher than the 0°C isotherm and that there is a frozen fringe between the ice lens and the unfrozen soil. Figure 2.26 illustrates a homogeneous fine-grained soil column with a zone of frozen soil, an active ice lens, a frozen fringe, and an underlying zone of unfrozen soil (Nixon 1991). The frozen fringe is a thin zone at the freezing front where ice has penetrated pores that contain no ice lenses and has a very low hydraulic conductivity which can impede water flow by partial filling of soil pores by ice. In the frozen fringe, liquid water exists in equilibrium with ice at a temperature below the normal freezing point of water, with the segregation freezing temperature (T_s) located at the base of the growing ice lens. The thickness of the frozen fringe depends on the temperature gradient, overburden pressure, and the soil properties (Henry 1998).

The curved interface in the soil pores between the two phases indicates that there is a pressure difference between the ice and water in soil pores ((O'Neill & Miller 1985), Figure 2.27). (Henry 1998) described the ice pressure as positive and the water pressure as negative, therefore the total pore pressure consists of the total sum of the ice and water pressures. The soil particles separate within the frozen fringe and the ice lenses form when the total pore pressure in the ice exceeds the overburden pressure. The ice lens thickness and spacing between lenses depend upon various factors such as soil type (amount of unfrozen water), overburden pressure, and freezing conditions (Konrad 1994). In general, clay soils present thin

34

ice lenses that are relatively closely spaced and often curved, whereas soils with more silt content display thicker ice lenses that are more uniformly spaced and fairly planar.

2.4.2 Soil Freezing Characteristics

Frost-heave models usually assume equilibrium at differentially small scale between phases of water in the soil pores. For equilibrium, the Clausius–Clapeyron equation describes the thermal dependency of soil ice and pore water in the soil pores (Andersland & Ladanyi 2004)

Equation 2.3 $$\frac{P_i}{\rho_i} - \frac{P_w}{\rho_w} = -L\left(\frac{\Delta T}{T_0}\right)$$

where ρ_i and ρ_w are the densities (in Mg/m^3) of ice and water, respectively; P_i is the ice pressure (Pa), P_w is the total soil water potential (Pa), L is the latent heat of fusion of water (334J/g), T_o is the temperature of the freezing point of pure water (273K), and $\Delta T = T - T_o$ is the temperature difference of the water phase in K.

Equation 2.4 relates the difference between water and ice pressure when there is a curved interface between the two phases (Henry 1998):

Equation 2.4 $$P_i - P_w = \psi_{iw}\, k$$

where ψ_{iw} is the interfacial tension between the ice and water (N/m), and k is the mean curvature of interface (m^{-1}). For freezing soils, k=2/r where r is the pore radius.

The difference between ice and water pressure is also a function of the water content, which is a function of the temperature (T) (Henry 1998):

Equation 2.5 $\qquad P_i - P_w = f(v_w) = h(T)$

Models have been developed by researchers to predict the frost heave ((O'Neill & Miller 1982), (O'Neill & Miller 1985), (Black 1995), (Sheng 1994), (Konrad & Morgenstern 1981) and (Konrad & Morgenstern 1982)). Most of the frost heave models use soil physical, thermal, and hydraulic properties and thermal conditions to predict frost heave.

Frost heave models solve the basic equations of mass and heat transfer applied to the frozen fringe, bounded by the unfrozen zone and the frozen zone (Henry 1998) (Figure 2.26). In soil that heaves during freezing, coupled flow between water and heat occurs when the temperature gradient that leads to heat flow (phase change) results in the transport of water, which is a critical factor in determining the growth of ice lens. There are significant differences among the existing frost heave models in how they simulate this flow. In contrast, heat and mass transfer in the unfrozen zone and heat transfer in the fully frozen zones of a freezing soil are treated similarly

by most models. The following two sections discuss the theory of mass and energy (heat) transfer.

2.4.3 Mass Balance

The water mass balance for the frozen fringe is given by (Henry 1998)

Equation 2.6
$$\frac{d}{dt}(\rho_w \vartheta_w + \rho_i \vartheta_i) = \nabla(\rho_w v_w + \rho_w v_l)$$

where ρ_i and ρ_w are the densities of ice and water (Mg/m^3), ϑ_i and ϑ_w are the volumetric ice and water content, v_l and v_w are the velocities of ice flow and water flow (m/s). In a problem with vertical one-dimensional (1-D) heat flow, the value of v_l is in fact the rate of frost heave. Darcy's law is assumed in Equation 2.6 for the water flow. Applying it to the frozen fringe for 1-D freezing in the vertical z-direction results in:

Equation 2.7
$$\frac{d}{dt}(\rho_w \vartheta_w + \rho_i \vartheta_i) = \frac{d}{dz}\left(\rho_w K \frac{dh}{dz} + \rho_w v_l\right)$$

where K is the hydraulic conductivity of the soil (m/s) and h is the total head of water (m). Different models have different expressions for K and h in the frozen fringe as well as in whether they model the growth (flux) of ice out of the frozen fringe.

2.4.4 Energy Balance

Latent heat L is released when water freezes. L is a significant heat source in the frozen fringe and the following Equation 2.8 models the heat transfer (Henry 1998):

Equation 2.8
$$C\frac{dT}{dt} + \nabla(\lambda\nabla T) + \nabla(v_w TC_w + v_i TC_i) = L\rho_i\left(\frac{d\vartheta_i}{dt} + \nabla v_l\right)$$

where C is the volumetric heat capacity of the soil (J/m^3K), λ is the thermal conductivity of the soil (W/mK), T is the temperature (K), v_i is the flux of ice (m/s) defined as $v_i = v_l\vartheta_i$, where ϑ_i is the volumetric ice content, C_w and C_i are the volumetric heat capacities of the soil water and ice respectively.

Fourier's law is used to describe the conductive heat flux. Convective heat transfer (heat transferred via fluid velocities) is modeled by the terms in Equation 2.8 involving water and ice flow (v_w and v_i). The sensible heat transfer (the heat transfer due to temperature change) is modeled by the first term on the left side of Equation 2.8, which can be rewritten:

Equation 2.9
$$C\frac{dT}{dt} - \frac{d}{dz}\left(\lambda\frac{dT}{dz}\right) + \frac{d}{dz}(v_w TC_w + v_i TC_i) = L\rho_i\left(\frac{d\vartheta_i}{dt} + \frac{dv_l}{dz}\right)$$

2.4.5 Segregation Potentials

(Konrad & Morgenstern 1980) introduced a detailed model for one-dimensional frost heave that evaluates frost susceptibility and heave. The model involves determining

38

the term segregation potential (SP). In order to do so, they conducted a series of

freezing tests with various stepped temperatures on the cold side of specimens, but

with the warm side temperature kept constant. Their specimens were a saturated,

frost susceptible soil, Devon silt. They applied various constant cold temperatures at

the top of the specimen and a constant warm temperature at the bottom of the

specimen, and observed that the water intake flux v_w at the formation of the final ice

lens is proportional to the temperature gradient in the frozen fringe.   The

proportionality factor SP is the slope of the linear relationship between v_w and grad T

(Figure 2.28). That is:

Equation 2.10 $$SP = \frac{v_w}{gradT}$$

(Konrad & Morgenstern 1980) suggested that after an ice lens has formed, the

frozen soil above the ice lens does not participate in mass transport, but that water is

transported to the bottom of the ice lens from the unfrozen soil through the frozen

fringe (Figure 2.26).   The driving potential for the water movement develops from

suction generated at the ice-fringe interface, and from the obstruction to water flow

due to reducing permeability in the frozen fringe. Their analysis made the following

assumptions:

1- The Clausius–Clapeyron equation is valid at the base of the ice lens (Konrad

& Morgenstern 1981).

2- The water flow is continuous across the frozen fringe. When the hydraulic conductivity of the frozen fringe K_{fo} becomes so low that water cannot migrate to the ice lens, growth of that lens terminates. Water then begins to accumulate at a lower level in the soil and new ice lenses form (Konrad & Morgenstern 1981).

3- The migratory water freezes and an ice lens develops at the segregation freezing temperature T_s (Figure 2.29), which is a few tenths of a degree below the freezing temperature T_i (0°C) of bulk water at the bottom or the frozen fringe (Konrad 1994), (Freden 1965), (Hoekstra 1969), (Penner & Goodrich 1980). The temperature in the frozen fringe varies linearly between the T_s at the lens and the T_i at the bottom of the frozen fringe.

4- The hydraulic conductivity in the frozen fringe is related to the amount of unfrozen water and can be characterized by an overall permeability k_{fo} (Konrad & Morgenstern 1981) (Figure 2.30).

The formation of ice at temperature below 0°C induces a pressure deficiency (suction gradient) across the frozen fringe and in the unfrozen soil below (Konrad 1994). In accordance with Darcy's law, the velocity of water flow depends on the suction gradient, the overall hydraulic conductivities of the unfrozen soil, and the frozen fringe. (Konrad & Morgenstern 1981) proposed that the value of SP is a function of the total suction potential at the freezing front p_w, the suction potential at the frozen-unfrozen interface p_u, the segregation freezing temperature T_s, and the

overall hydraulic conductivity in the frozen fringe K_{fo}. They developed the theoretical

suction profile in the frozen fringe in response to a linear temperature profile,

obtained from the Clausius-Clapeyron equation (Equation 2.3). By assuming the ice

pressure in the ice lens to be 0, they rearrange the Clausius-Clapeyron equation to:

Equation 2.11 $$P_w = \frac{L}{V_w T_0^*} T = MT$$

where $T = T^* - T_o^*$ is the temperature of the water phase in degrees Celsius, T_o^* is

the temperature of the freezing point of pure water (273K), P_w is the suction in the

water phase, L is the latent heat of fusion of water (334J/g), V_w is the specific

volume of water (0.1019m^3/kN), and M is a constant equal to 1224kPa/°C. As

Figure 2.30b also shows, the suction profile is assumed to be linear and pass

through the origin. Studies by several researchers have shown that Equation 2.11 is

only valid for temperatures close to 0°C (between -0.001°C and -0.06°C) at an ice

lens under atmospheric pressure (Konrad 1994), (Konrad & Morgenstern 1981) and

(Nixon, Ellwood & Slusarchuk 1981). It is also important to note that there is a

considerable difference in the shape of the actual and theoretical suction profiles as

well as in their values at a given temperature warmer than T_s (Figure 2.30).

The hydraulic conductivity of the frozen fringe K_{fo} is very important, yet difficult to

measure (Konrad 1994). The accuracy of frost heave prediction depends on how

well the hydraulic conductivity of the frozen fringe is measured (or assumed) for various conditions of temperature and suction.

2.4.6 Frost Heave Predictions

In a series of papers, Konrad and Morgenstern developed their theory of frost heave prediction using the concept of segregation potentials in fine grained soils (Konrad & Morgenstern 1980), (Konrad & Morgenstern 1981), and (Konrad & Morgenstern 1982). The parameter SP is used to model frost heave by knowing or predicting the temperature gradient in the frozen fringe, then using Equation 2.10 to predict the water intake flux v_w. The rate of frost heave v_l (dh/dt) can then be obtained using the relation:

Equation 2.12
$$\frac{dh}{dt} = v_l = 1.09\, v_w + 0.09\theta\frac{dX}{dt}$$

where X is the frost depth, θ is the volumetric water content (the porosity reduced to account for the percentage of in situ pore water that will not freeze), and 0.09 is the volumetric expansion that occurs when water is frozen. In Equation 2.12, (Konrad & Morgenstern 1982) predict the frost heave resulting from two components, the water arriving at the freezing front (effect of suction and SP) and the freezing of in-situ pore water.

2.4.7 Other Factors Affecting the Segregation Potential

Several studies with various tests have shown that the segregation potential is also influenced by overburden pressure (Konrad & Morgenstern 1982), and by thermal conditions such as the rate of cooling (Konrad 1984) (Konrad 1989a) and freeze-thaw cycling (Konrad 1989).

(Konrad & Morgenstern 1982) found the following relationship between applied pressure and SP:

Equation 2.13 $$SP = SP_0 \exp(-aP_e)$$

where SP_0 is the value of SP obtained for zero applied pressure, P_e is the applied pressure (effective overburden pressure), and a is a soil constant. Figure 2.31 shows the results of a literature survey on well-documented cases of frost heave data conducted by (Konrad & Morgenstern 1983). As the results show, the segregation potential of a given freezing soil decreases with increasing overburden pressure. In general, the segregation potentials of soils with low unfrozen water contents (silty sands) are more sensitive to small changes in overburden pressure than soils with higher unfrozen water contents such as clays.

Equation 2.10 and Equation 2.12 indicate that frost heave is proportional to the temperature gradient when the final ice lens is forming. (Konrad 1984) presented experimental results on Devon silt with no applied pressure and showed that the rate of frost heave is a function of the net rate of heat extraction (Figure 2.32). (Penner 1972) also reported similar results in Figure 2.33 which shows the frost heave rate of a saturated gravelly sand tested under an applied pressure of 3.4kPa. The figure shows that the frost heave rate is a function of the frost penetration rate. The frost heave rate increases with increased penetration rate to a maximum, then decreases at higher penetration rates.

(Konrad 1989) studied the effects of freeze-thaw cycling on the structure of a clayey silt. He conducted a test on each of a series of specimens which consisted of three or four cycles of ramped freezing and thawing under an applied pressure of 50kPa. In the first freezing run, the specimens were frozen to about half their initial height, whereas in subsequent freezing the frost front penetrated to the same depth or deeper and created zones in a single specimen with various freeze-thaw histories. In the final freezing cycle, the frost front was allowed to penetrate into unfrozen soil that was never previously subjected to freezing. Figure 2.34 shows the results from one specimen. The value of SP is lower when the temperature is lower than the segregation freezing temperature, that is, the lowest temperature the specimen experienced in the first cycle. This confirmed that the test procedure produced changes in the micro-structure of specimen. No structural changes occurred in the

frozen soil when the temperature was higher than the segregation freezing temperature. This illustrates that the soil structure will be altered as the pore ice content increases in response to decreasing temperatures in the frozen fringe.

2.5 Justification for Research

Although many studies have been completed on the effects of temperature on soil behaviour, there is still a lack of agreement as to how the consolidation and shearing properties of clays are affected by the change of temperature. In the literature, the majority of studies focused on the effects of increasing temperatures (above general laboratory temperatures) on soil behaviour. In contrast, the focus of this research was to examine the effects of temperatures close to freezing on the consolidation and shearing properties of soil.

The most recent geotechnical site investigation at the test site on PR391 showed no ice in the foundation of the road embankment. (Previous investigations confirmed the presence of ice in the foundation). Therefore, the foundation material is currently classified as "thawed (or 'degraded') permafrost". The purpose of this research is to investigate and understand the performance of highway embankments on thawed permafrost.

The research on PR391 consisted of (1) a detailed geotechnical site investigation, (2) field instrumentation, (3) data collection, (4) laboratory testing, (5) constitutive analysis and (6) numerical simulations. This research provides new insights into the nature and cause of embankment deformations and the mechanism producing functional failure (serviceability limit state). It also provides an improved ability to identify sections 'at risk' that require immediate remedial attention and evaluates suitable remedial measure for constructing of highways and road embankments, and the treatment of existing highways on thawed permafrost. In doing so, the study addresses the hypotheses listed at the end of Chapter 1.

Most researchers have studied the freezing behaviour of specimens under controlled laboratory conditions. Fewer projects have studied frost heaving of natural ground under field conditions. The focus of this research is to study the application of the current SP frost heave approach to field conditions. The objective is to use the SP method to back-calculate segregation potentials from the site observations and collected frost heave data. Results will be compared with the limited number of results in the research literature.

West Sector	Central Sector	East Sector
2020s A1B Annual: +1.1°C	2020s A1B Annual: +1.4°C	2020s A1B Annual: +1.3°C
2050s A1B Annual: +3.0°C	2050s A1B Annual: +3.2°C	2050s A1B Annual: +3.0°C
2080s A1B Annual: +4.5°C	2080s A1B Annual: +4.4°C	2080s A1B Annual: +4.5°C
2020s A2 Annual: +1.4°C	2020s A2 Annual: +1.6°C	2020s A2 Annual: +1.4°C
2050s A2 Annual: +3.0°C	2050s A2 Annual: +3.4°C	2050s A2 Annual: +3.0°C
2080s A2 Annual: +5.4°C	2080s A2 Annual: +6.1°C	2080s A2 Annual: +5.6°C

Table 2.1: Mean annual temperature change results from the 'best four models' for

each sector (Revised from CCCSN 2009)

Reference	Soil	LL & PI	Temp. Range	Cons.	Type of Shearing	Strength after Heating
(Murayama 1969)	Osaka clay			UH	UU	Down
(Sherif & Burrous 1969)	Kaolin clay			UH	UU	Down
(Laguros 1969)	3 clay types	29-47%		UH	UU	Down
(Ctori 1989)	Brick clay		6-35°C		UU	Down
(Towhata et al 1993)	Kaolin & Bentonite	70%, 29%	Up to 200°C		UU	Unchanged
(Noble & Demirel 1969)	Iowa clay	89%, 59%				Down
(Mitchell 1964)	San Francisco Bay mud			NC, DH	IU	Down
(Houston et al 1985)	Illite Smectite	88%, 47%	4-200°C	NC, DH	IU	Up
(Hueckel & Baldi 1990)	Pontida clay		18-115°C	OC, DH	ID	Down
(Burghignoli, Desideri & Miliziano 1992)	Todi clay	52%, 30%	15-60°C	NC, Cyclic DH	IU	Unchanged
Lingnau et al (1995)	Sand Bentonite	250%, 200%	26-100°C	NC, DH	IU	Down
(Moritz 1995)	Linkoping clay	65-90%	Up to 70°C	NC, UH	IU	Down
(Kuntiwattanakul et al. 1995)	MC Kaolin	70%, 29%	20-90°C	NC, DH	IU	Up
				OC, DH	IU	Unchanged
(Chiu 1996)	Kaolin C1C		22-100°C	NC, DH	IU	Unchanged
					ID	Up
(Tanaka et al 1997)	Illitic shale	30%, 21%	28-100°C	NC, DH	IU	Down

Table 2.2: Review of temperature effects on shear strength of soils (Redrawn from

Ghahremannejad 2003)
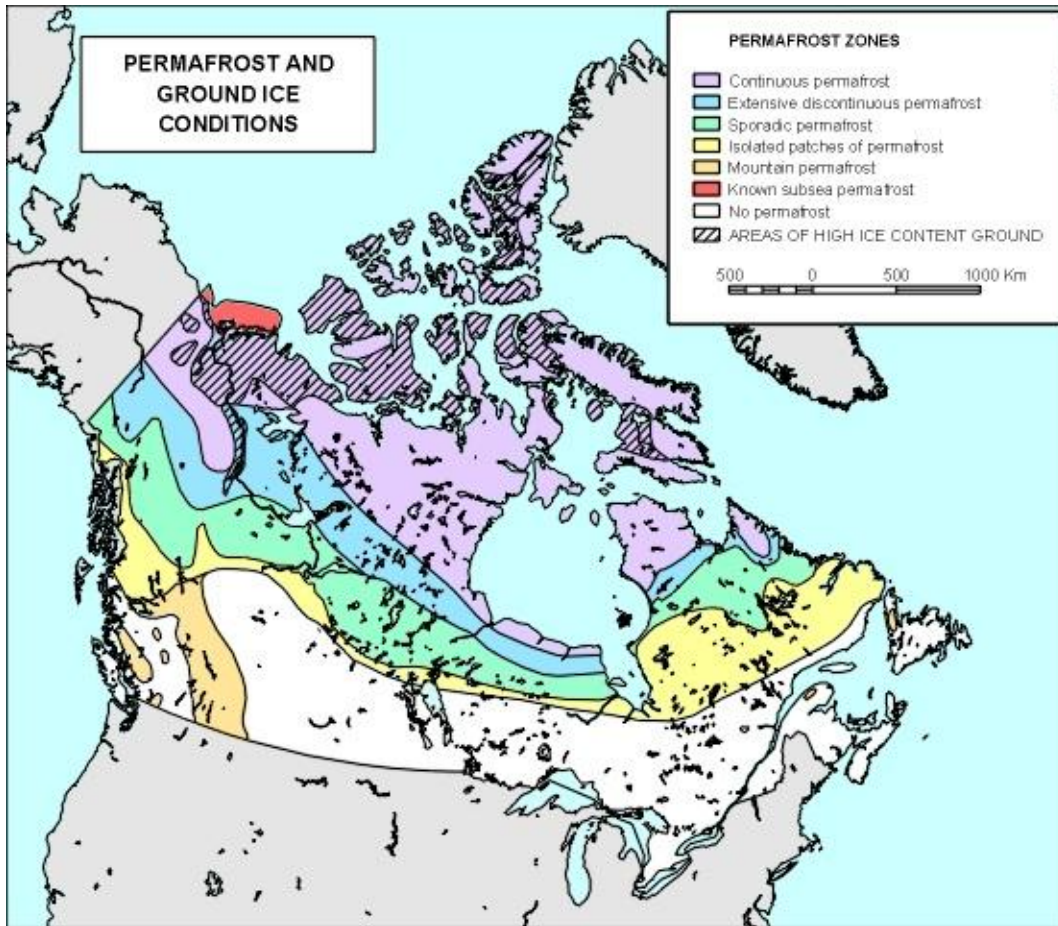
Figure 2.1: Distribution of permafrost in Canada

(http://www.nrcan.gc.ca/sites/www.nrcan.gc.ca.earth-

sciences/files/jpg/permafrost/images/wheredoes1.jpg, reproduced with the

permission of Natural Resources Canada, January 2012)
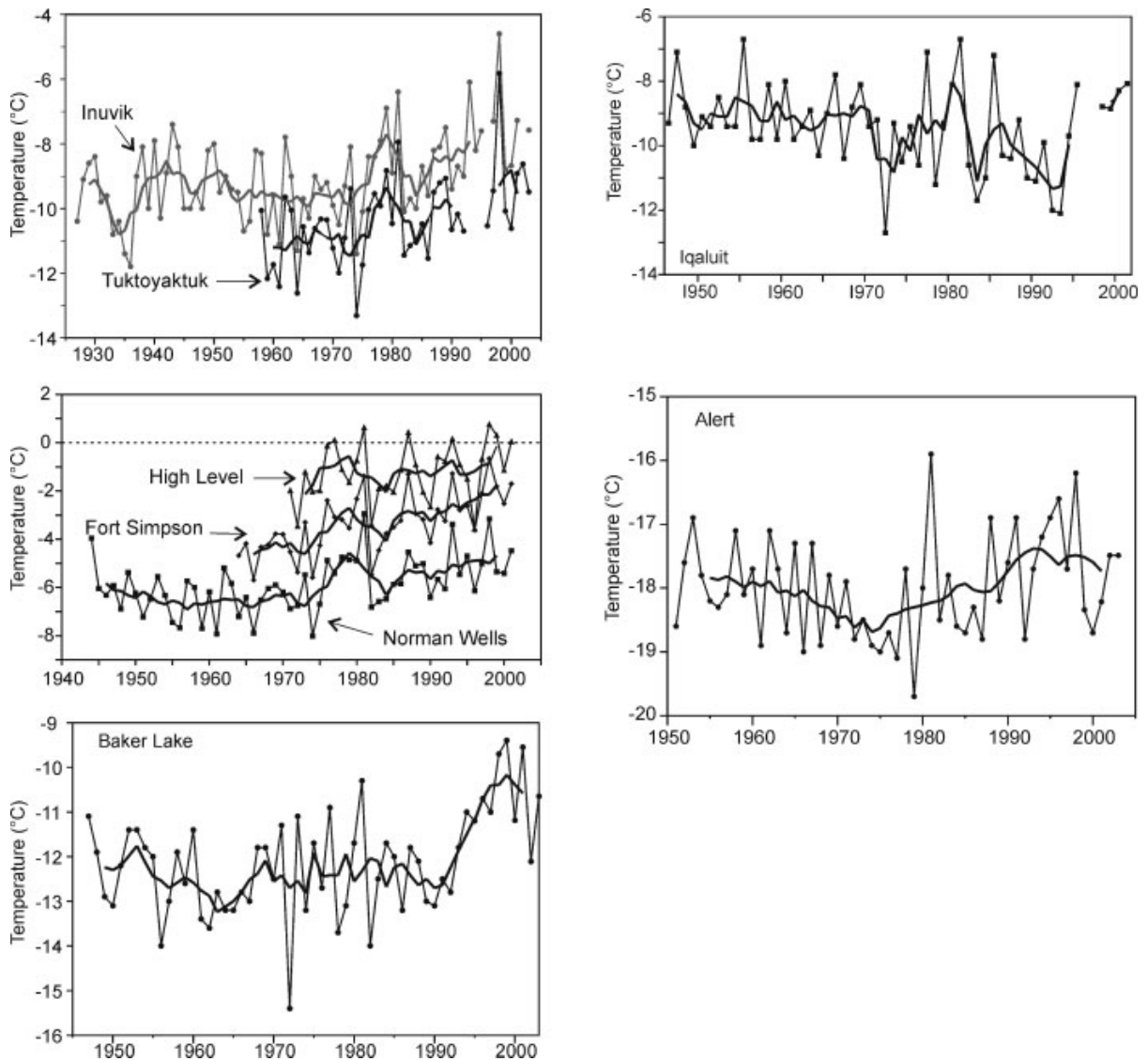
Figure 2.2: Mean annual air temperature and 5-year running mean (thick line) for Environment Canada stations in the Mackenzie region (Tuktoyaktuk, Inuvik, Norman Wells, Fort Simpson and High Level), Baker Lake, Alert and Iqaluit. Data are from Environment Canada (2000) and Environment Canada's web-based monthly climate summaries (Smith et al. 2005)
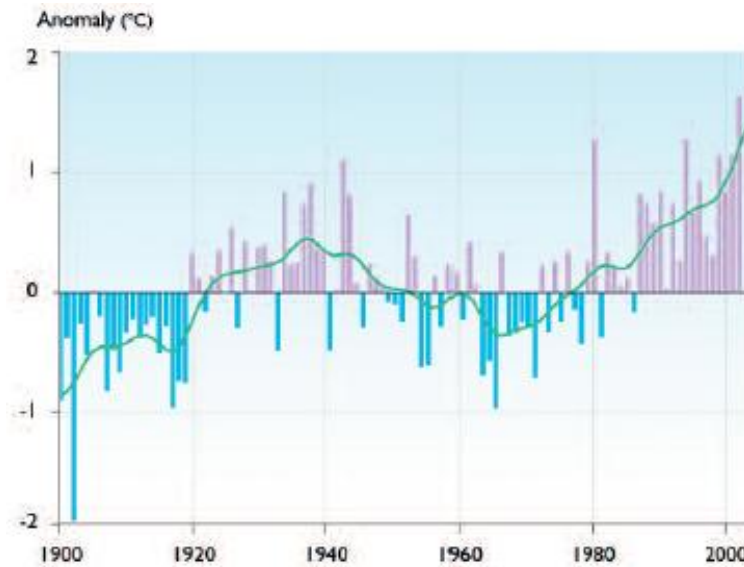
Figure 2.3: Annual anomalies of land-surface air temperature in the Arctic (60º to 90º

N) for the period 1900 to 2003. Anomalies are calculated relative to the 1961–1990

average. The smoothed curve was created using a 21-point binomial filter, which

approximates a 10-year running mean. (McBean et al. 2005, Reprinted with

permission of Cambridge University Press)
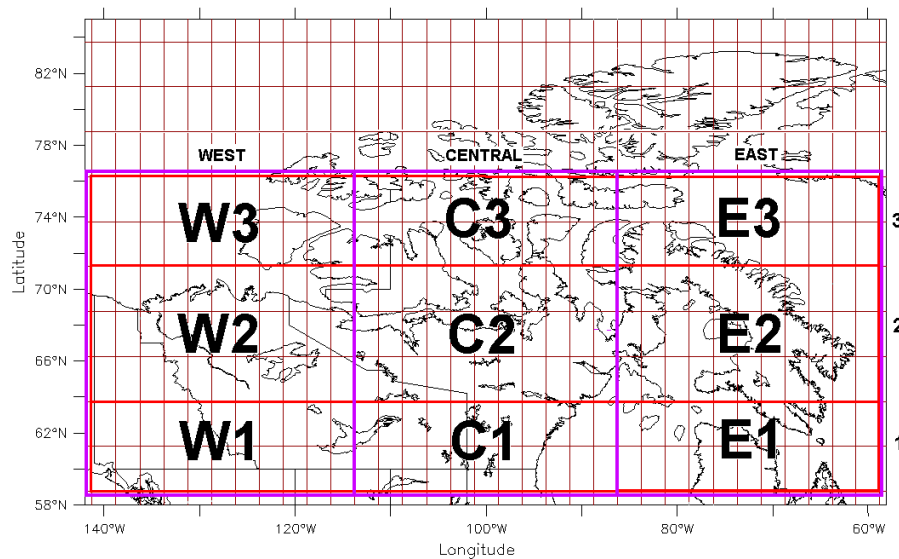
Figure 2.4: Location of Three Arctic Sectors and Nine Zones. (CCCSN 2009)
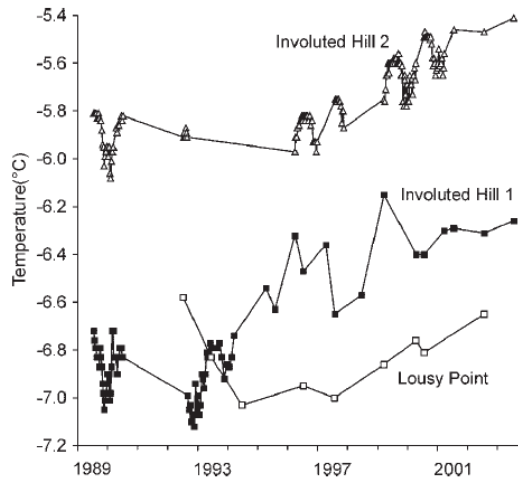
Figure 2.5: Permafrost temperature for three sites in the Mackenzie Delta region between 1989 and 2003. Temperature is given at depths of 24m, 28m and 29m for Lousy Point, Involuted Hill 1 and Involuted Hill 2 respectively. (Smith et al. 2005)
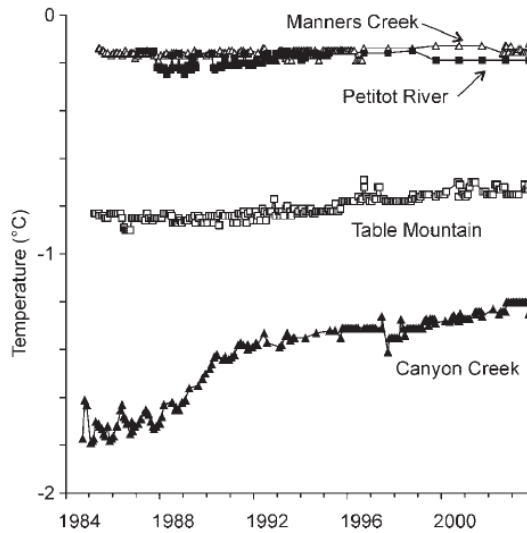
Figure 2.6: Ground temperatures between 1984 and 2003 at depths near 10m in the Mackenzie valley south of Norman Wells. Temperature at 10m depth is given for all sites except Table Mountain where the temperature at 12m depth is provided. (Smith et al. 2005)
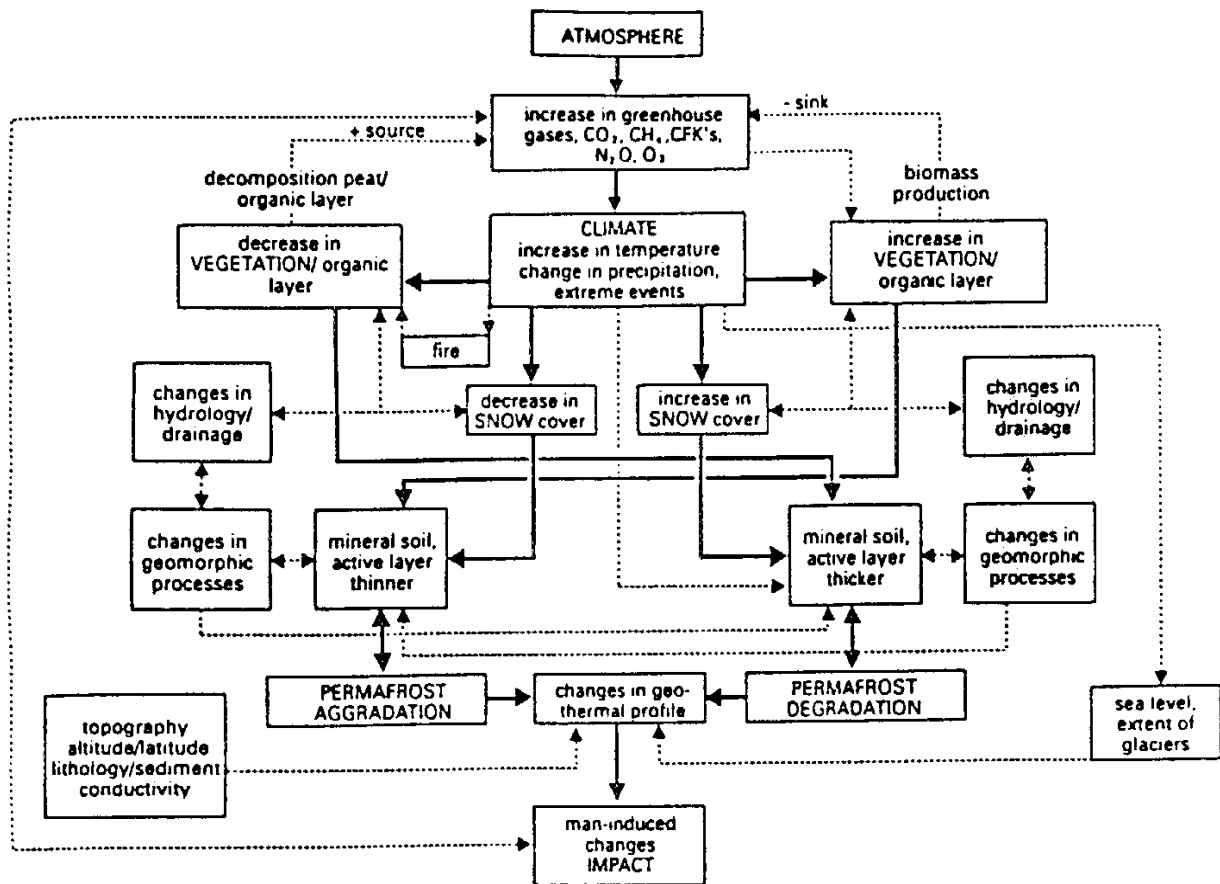
Figure 2.7: Complex interactions of the active layer and permafrost with the

atmosphere and biological, hydrological and geomorphic processes (Brown 1997)

(with kind permission of Springer Science and Business Media)
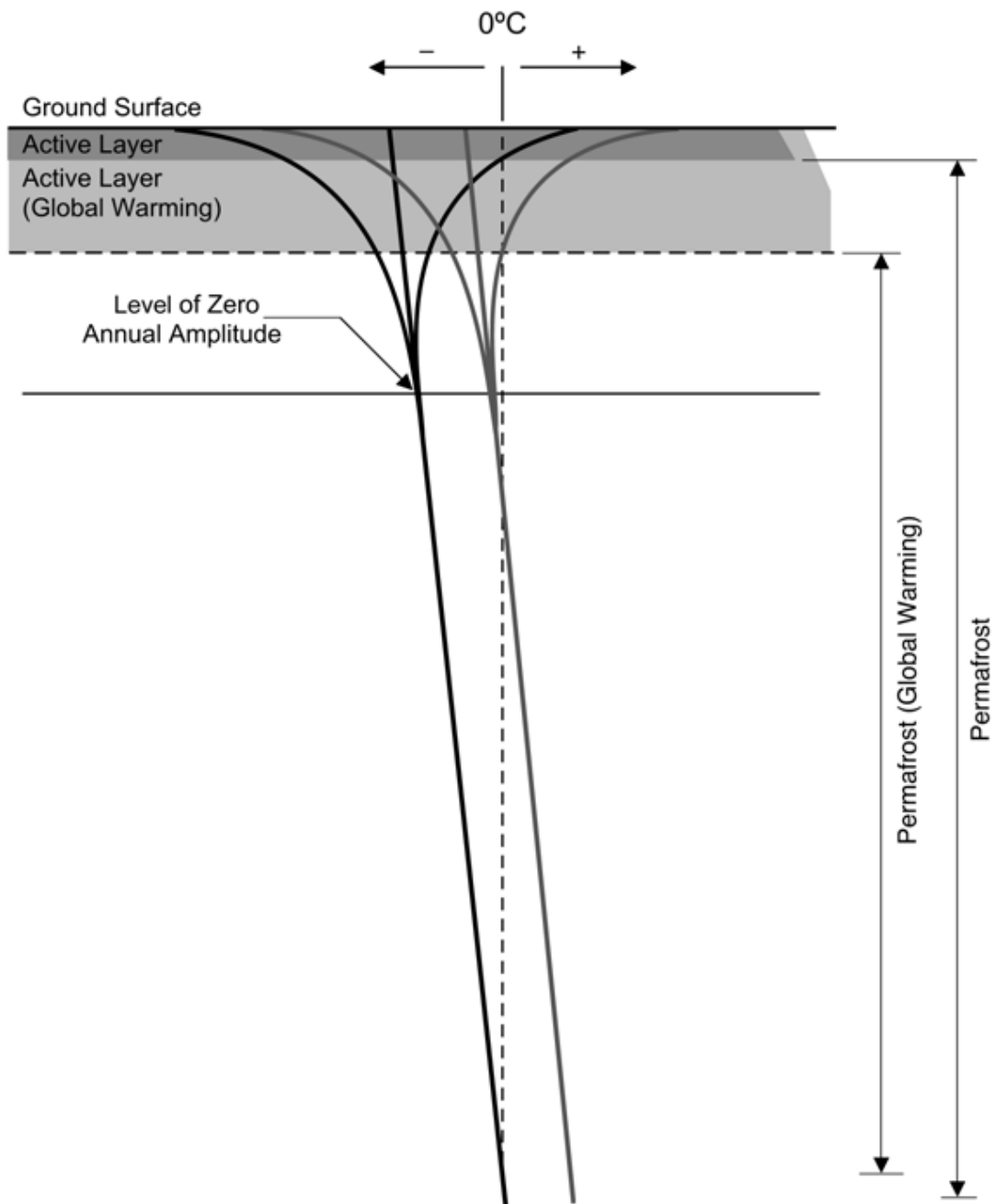
Figure 2.8: Typical ground temperature regime in permafrost (Hinkel et al. 2003)

(Author's note: The thickness of permafrost for the Global Warming case is shown incorrectly in this widely published figure.)

Figure 2.9: Flat Loop Thermosyphon foundations at Inuvik Regional Hospital in

Inuvik, NWT, Canada (photo by author)

Figure 2.10: Trans-Alaska Pipe-line System (Hinkel et al. 2003)

Figure 2.11: Buildings above original ground level, Inuvik, NWT, Canada (photo by author)
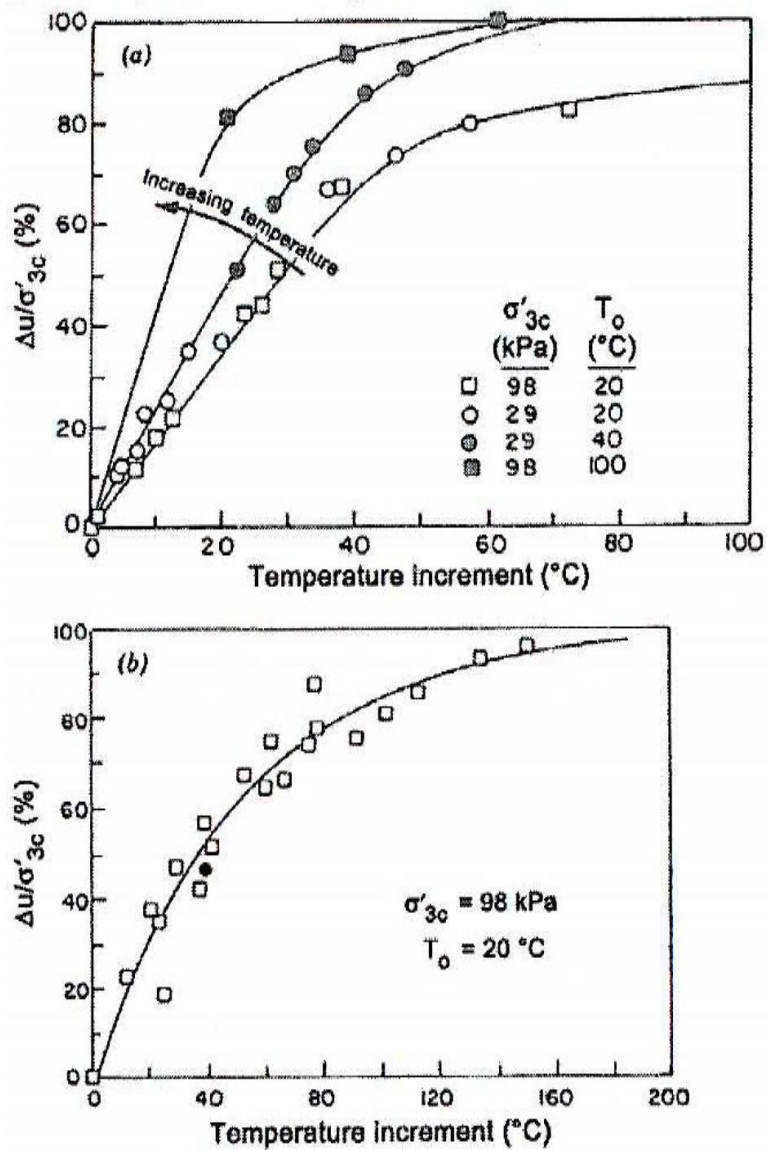
Figure 2.12: Normalized pore water pressure change with temperature increase for

a) undisturbed Pacific illite and b) undisturbed Pacific smectite-rich samples

(Houston et al. 1985)
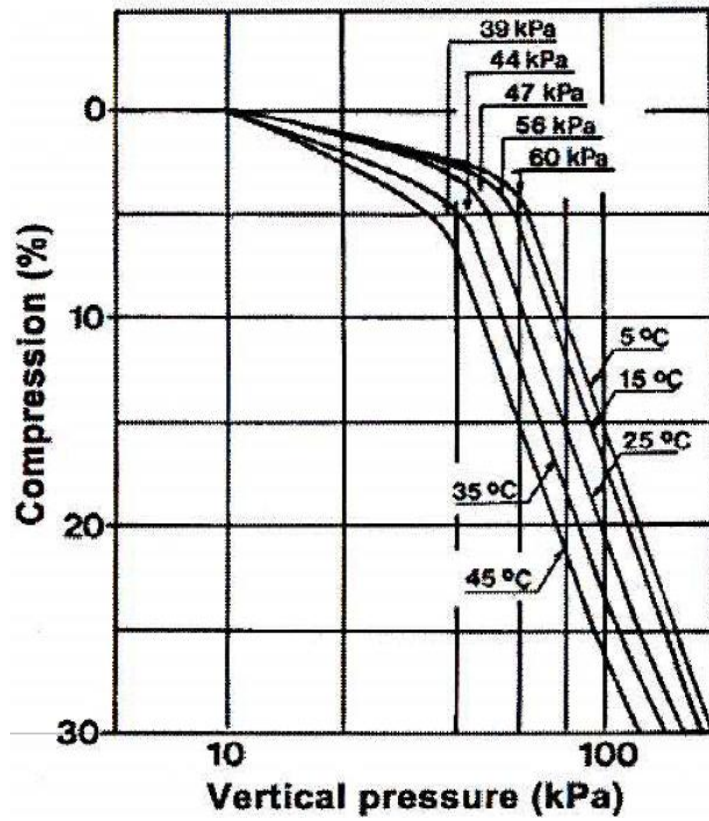
Figure 2.13: Oedometer tests at different temperatures (Eriksson 1989)
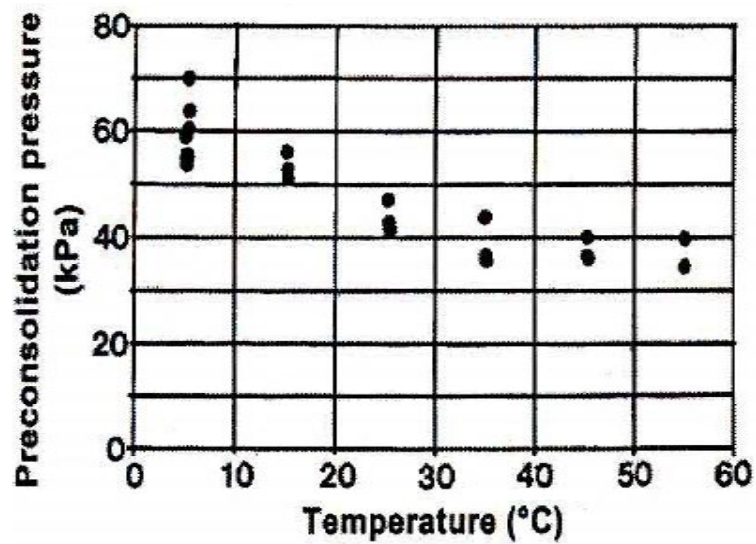
Figure 2.14: Effect of temperature on preconsolidation pressure (Eriksson 1989)
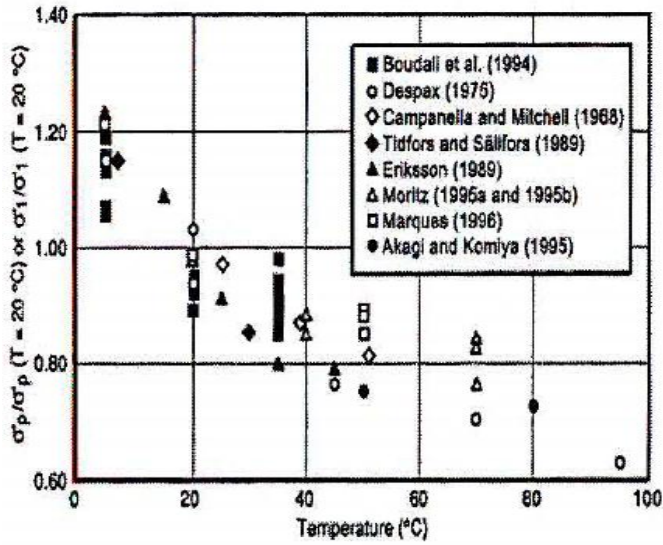
Figure 2.15: Variation of normalized preconsolidation pressure versus temperature

(Leroueil and Marques 1996)
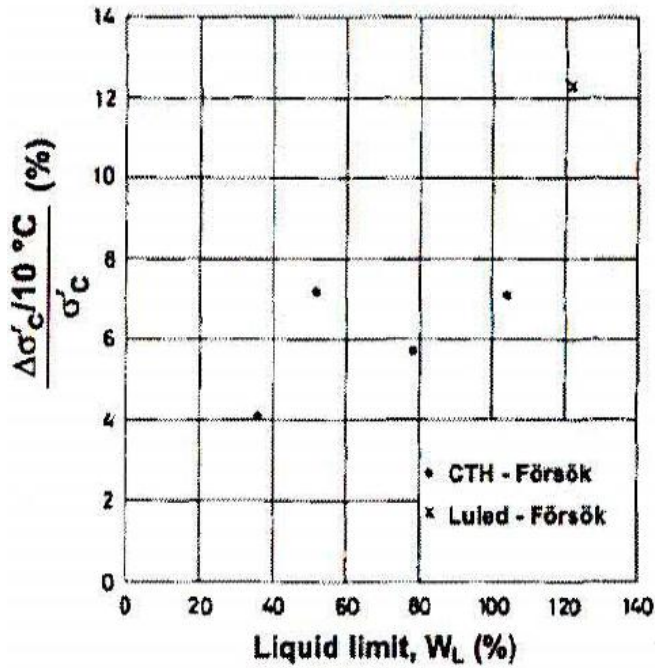
Figure 2.16: Change in preconsolidation pressure versus liquid limit (Tidfors and

Sällfors 1989)

60
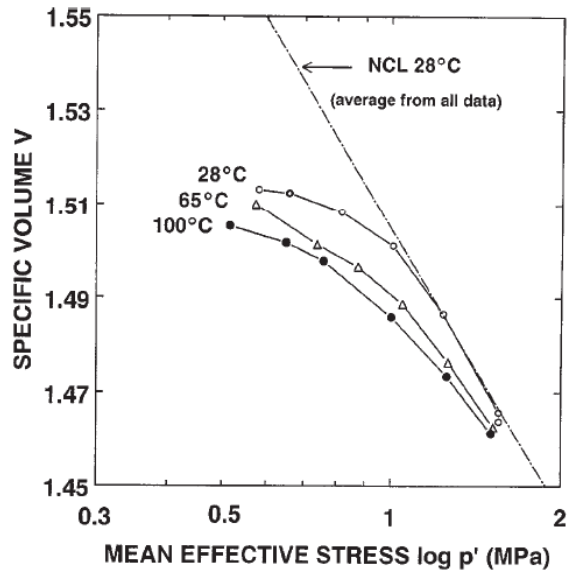
Figure 2.17: Variation of isotropic hardening lines V versus log(p') with temperature.

NCL, normal consolidation line (Graham et al. 2001).
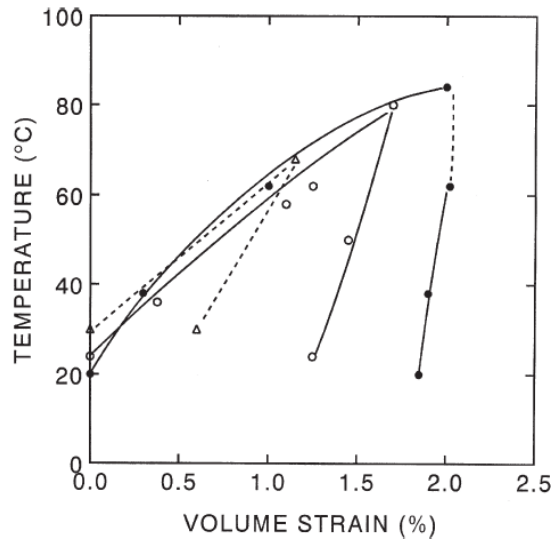
Figure 2.18: Volumetric strain versus temperature at constant isotropic effective

stress, drained tests. ○, test at 2 MPa on Pontida clay; ●, test at 6 MPa on Boom

clay (after Hueckel and Pellegrini 1989); Δ, data from (Tanaka 1995) (Graham et al.

2001).

61
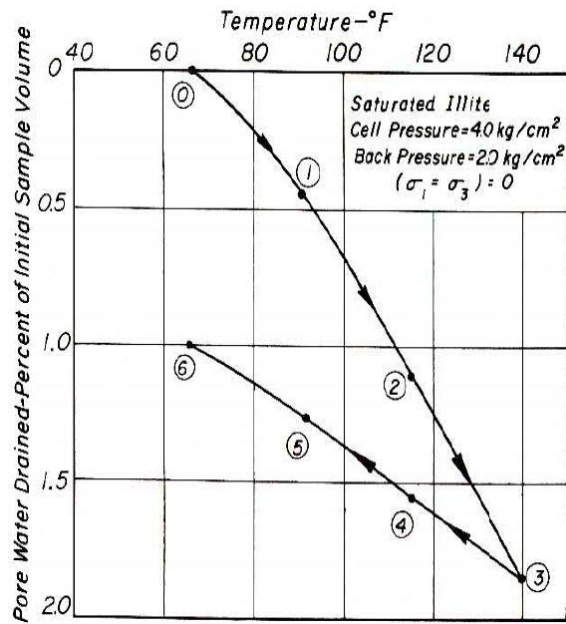
Figure 2.19: Effect of temperature variations on volume under drained conditions

(Campanella and Mitchell 1968).
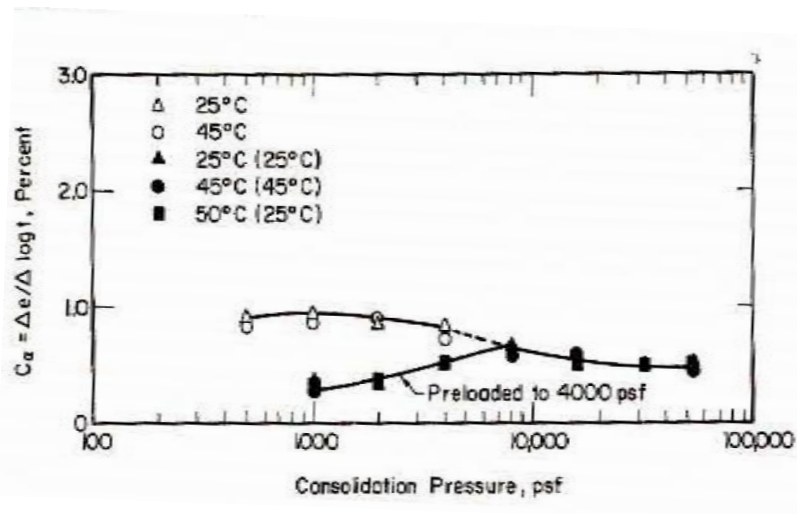
Figure 2.20: Coefficient of secondary compression for inorganic Plaudings clay at

different temperatures (Mesri 1973).
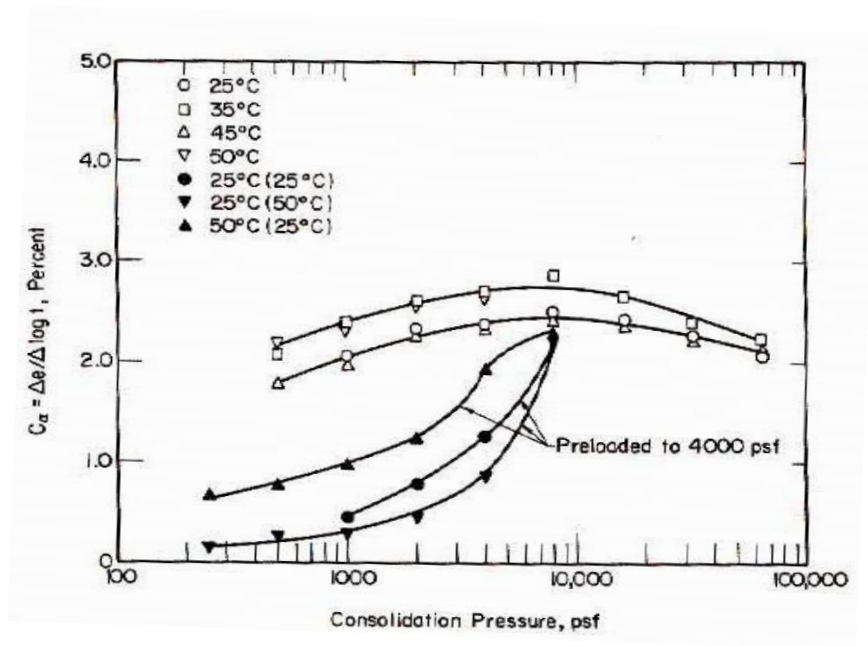
Figure 2.21: Coefficient of secondary compression for organic Plaudings clay at

different temperatures (Mesri 1973).
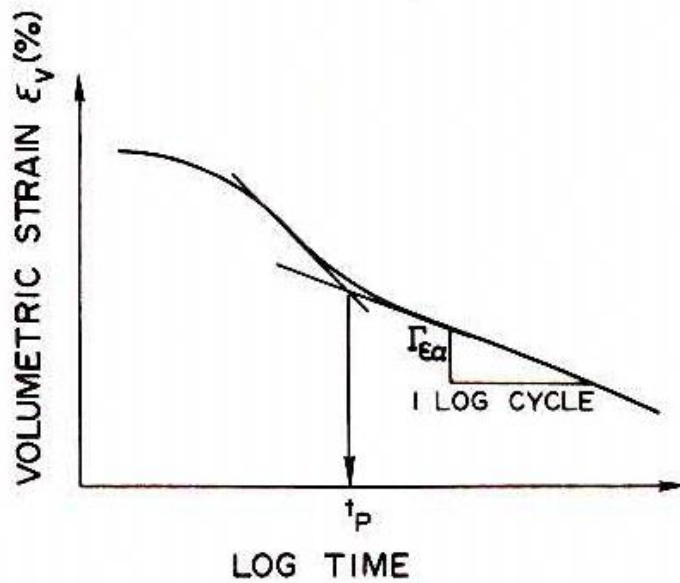
Figure 2.22: Definition of thermal coefficient of Secondary Compression, $\Gamma_{\alpha e}$

(Houston et al. 1985)
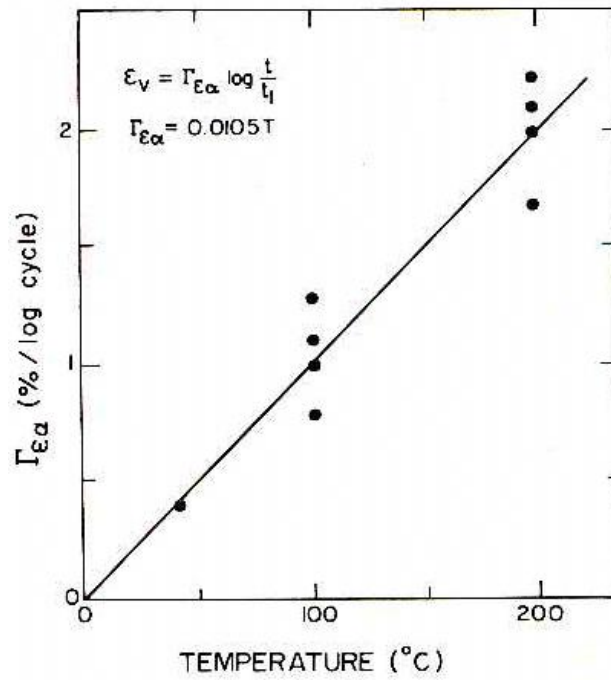
Figure 2.23: Coefficient of thermal secondary compression for undisturbed Pacific

illite (Houston et al. 1985)
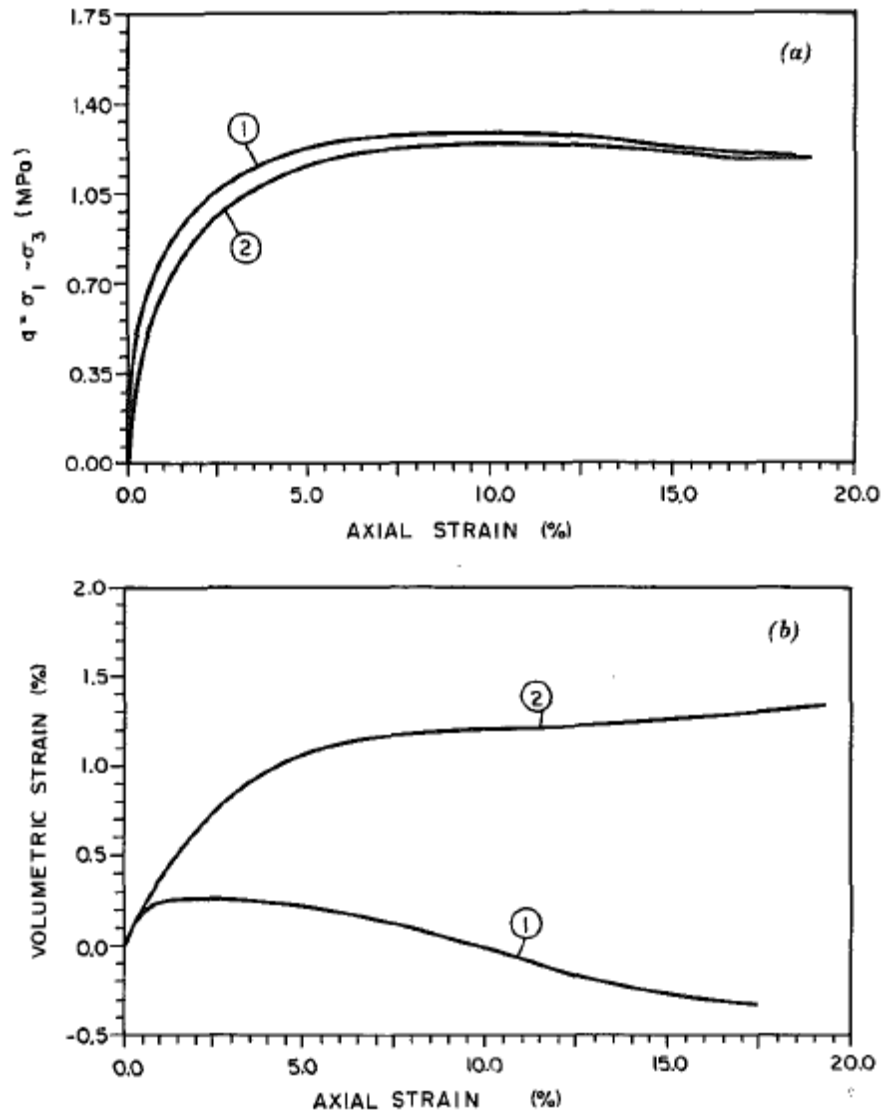
Figure 2.24: Drained Triaxial Compression Tests on Pontida Silty Clay at 18 °C and 115 °C at Confining Stress of 0.5 MPa; 1 at 23° C, 2 at 98° C: (a) Deviatoric Stress versus Axial Strain; and (b) Volumetric Strain versus Axial Strain (Hueckel and Baldi 1990)

65
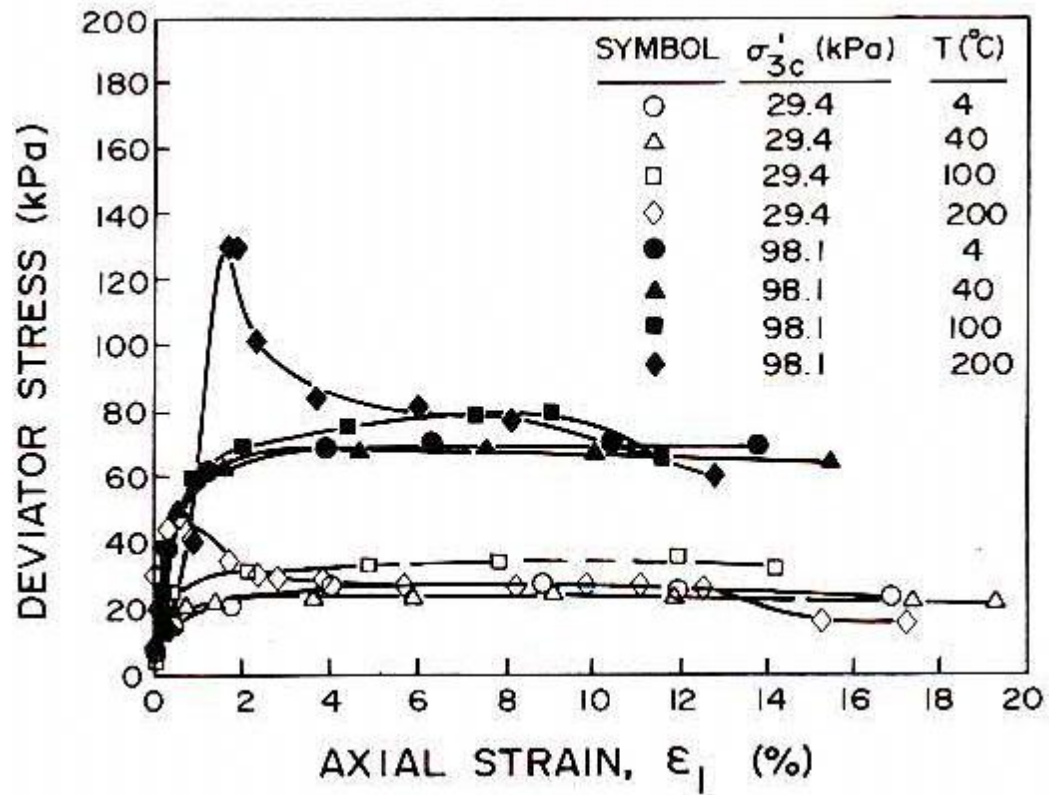
Figure 2.25: Stress-Strain behaviour of undisturbed illite at various temperature and effective stress levels (Houston et al. 1985)
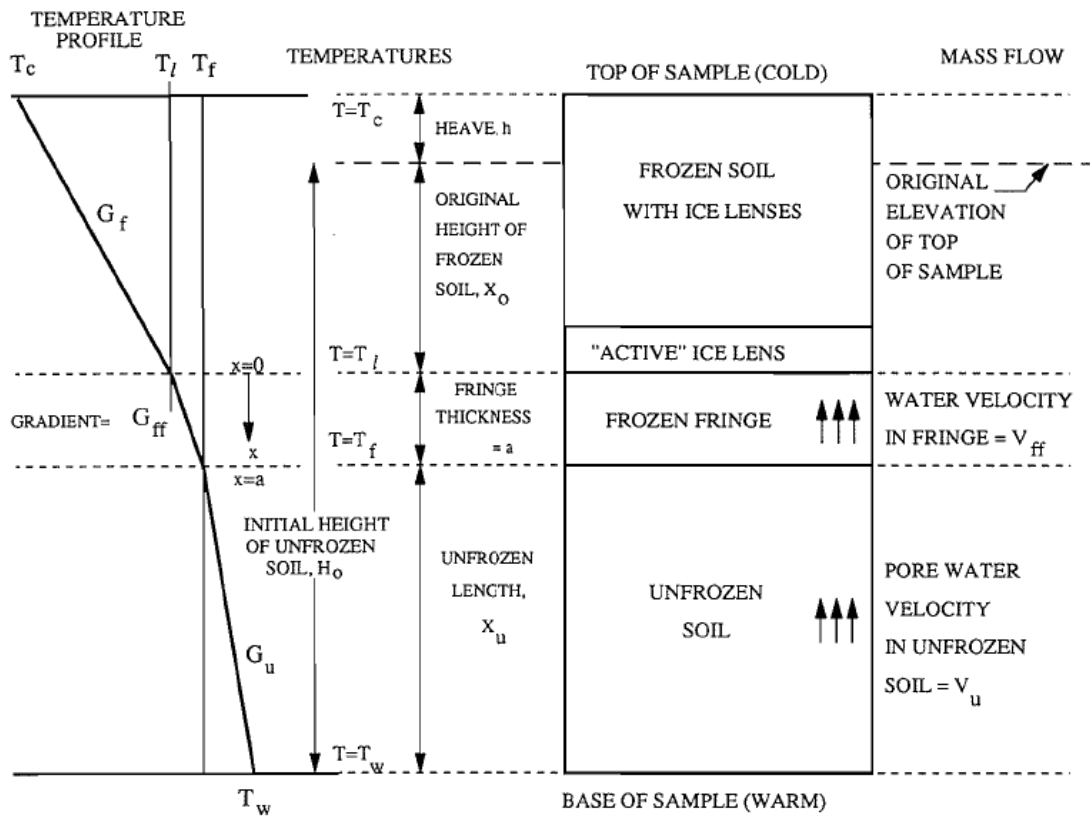
Figure 2.26: Frost heave in an idealized one-dimensional soil column (Nixon 1991)

(Author's note: Vertical axis is not to scale)
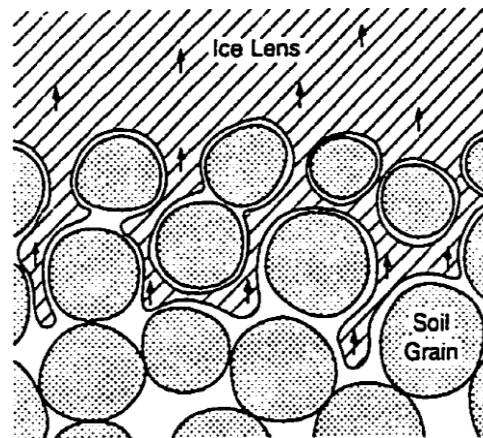
Figure 2.27: The frozen fringe with ice lens (O'Neil and Miller 1985). Arrows in

direction of heat flow
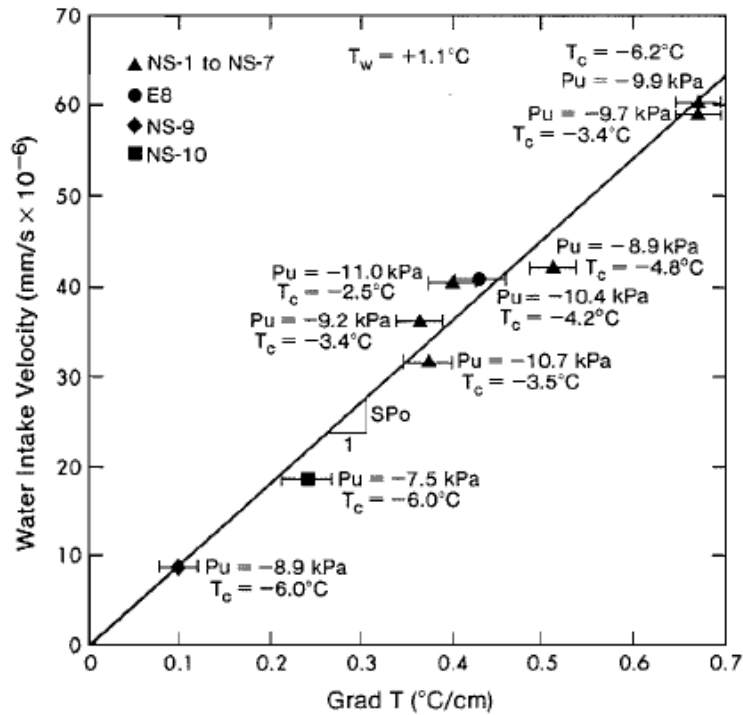
Figure 2.28: Relation between water intake velocity and temperature gradient across the active system at the formation of the final ice lens. (Konrad and Morgenstern 1981)
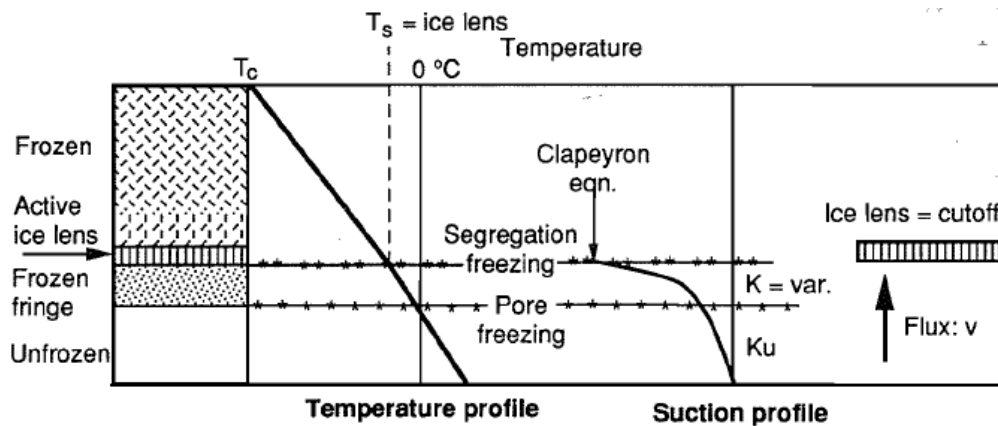
Figure 2.29: Schematic of freezing in soils Schematic of freezing in soils. Hydraulic conductivity of frozen soil (K); hydraulic conductivity of unfrozen soil (K_u) (Konrad 1994)
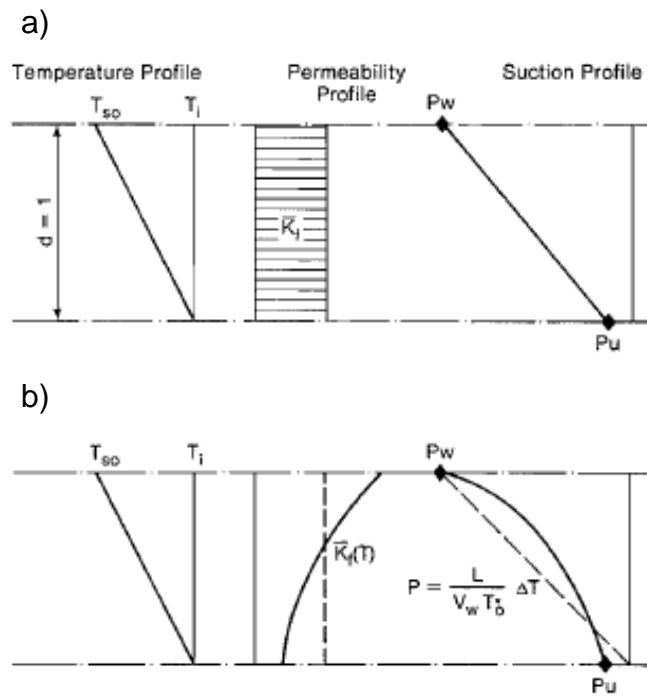
Figure 2.30: Characteristics of the frozen fringe: (a) simplified and (b) actual shape

(Konrad and Morgenstern 1981)
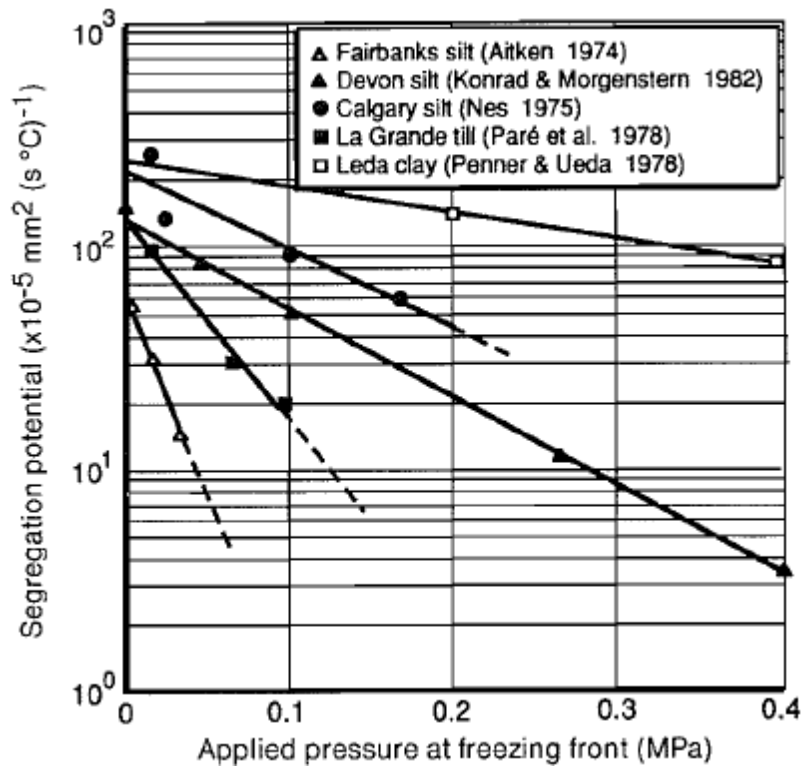
Figure 2.31: The segregation potential-pressure relationship for various soils.

(Konrad and Morgenstern 1983)
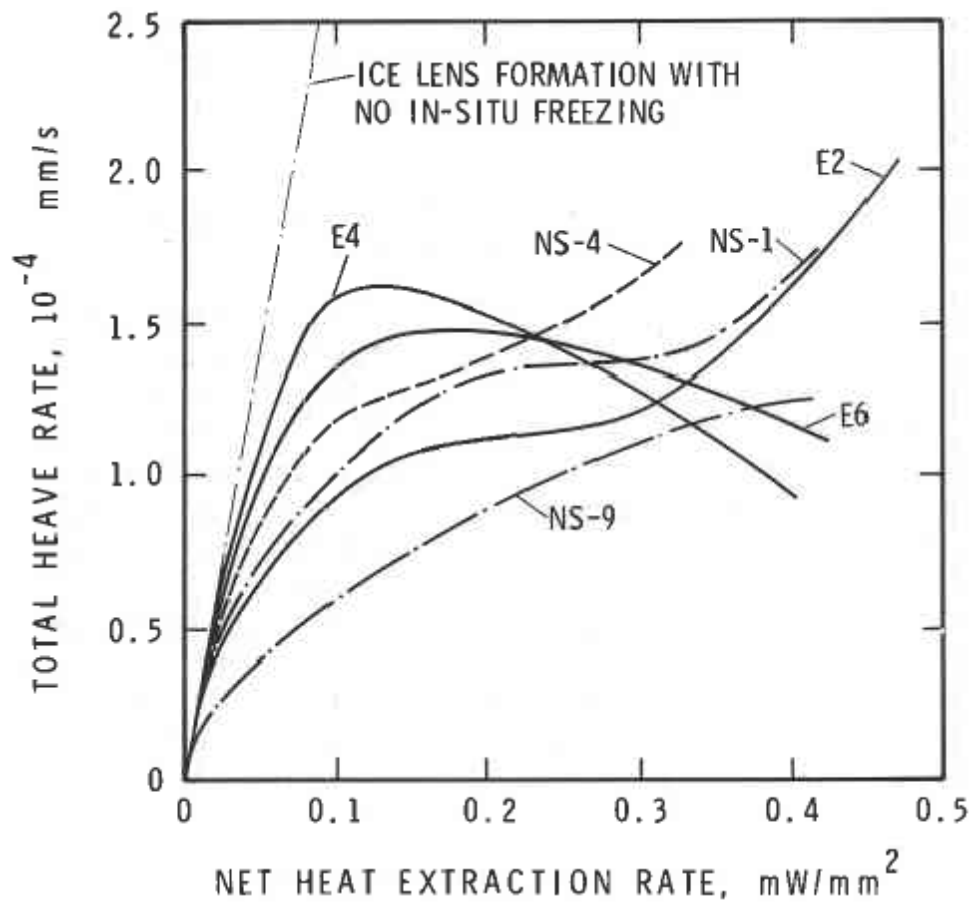
Figure 2.32: Total heave rate versus net heat extraction for Devon silt. (Konrad 1984)
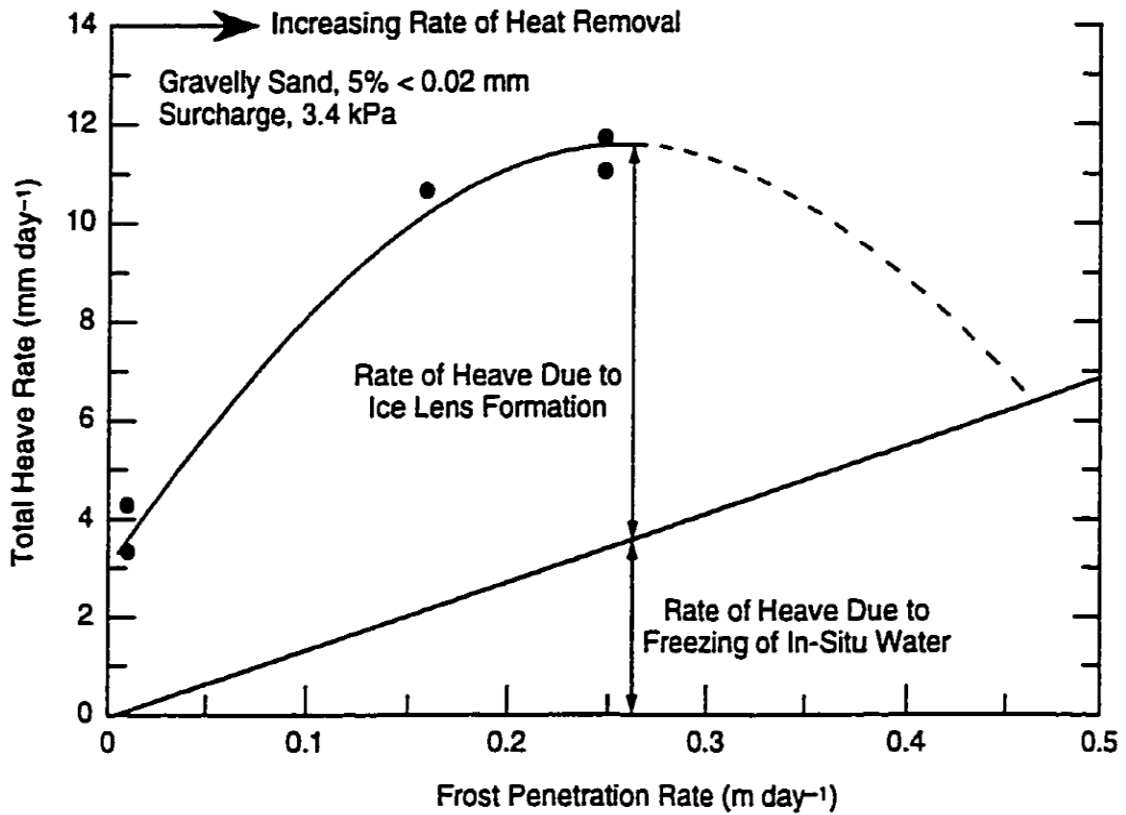
Figure 2.33: Frost heave as a function of frost penetration rate for gravelly sand with

an applied surcharge or 3.4 kPa (From Penner, E. Influence of Freezing Rate on

Frost Heaving. In Transportation Research Record 393, Figure 4, p. 60. Copyright,

National Academy of Sciences, Washington, D.C., 1972. Reproduced with

permission of the Transportation Research Board.)

a)
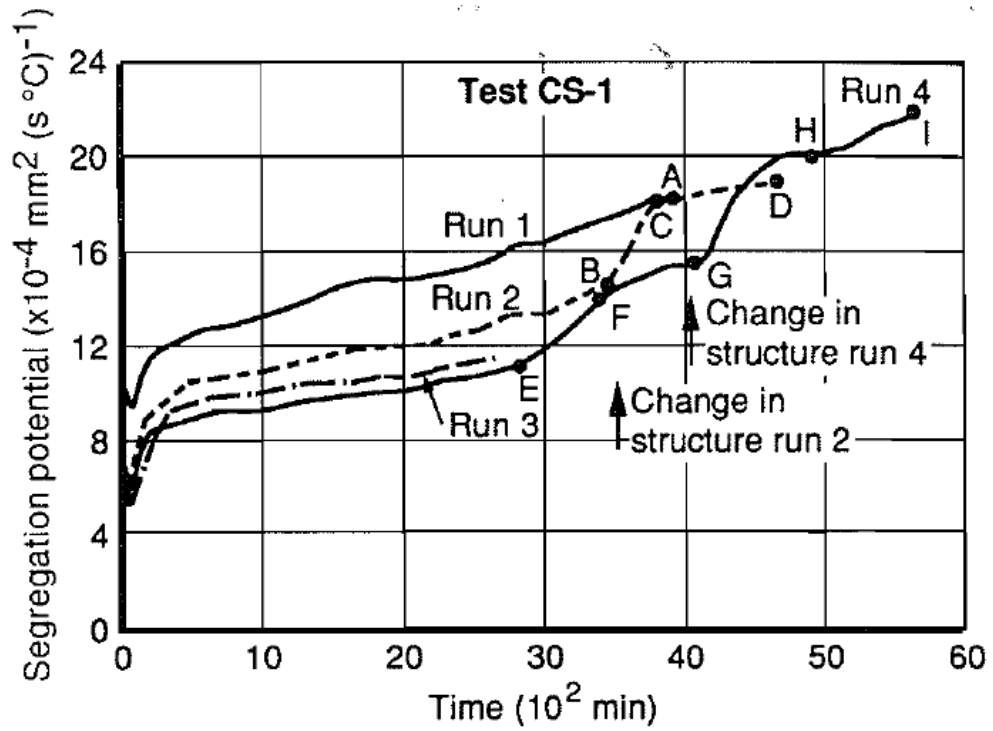
b)
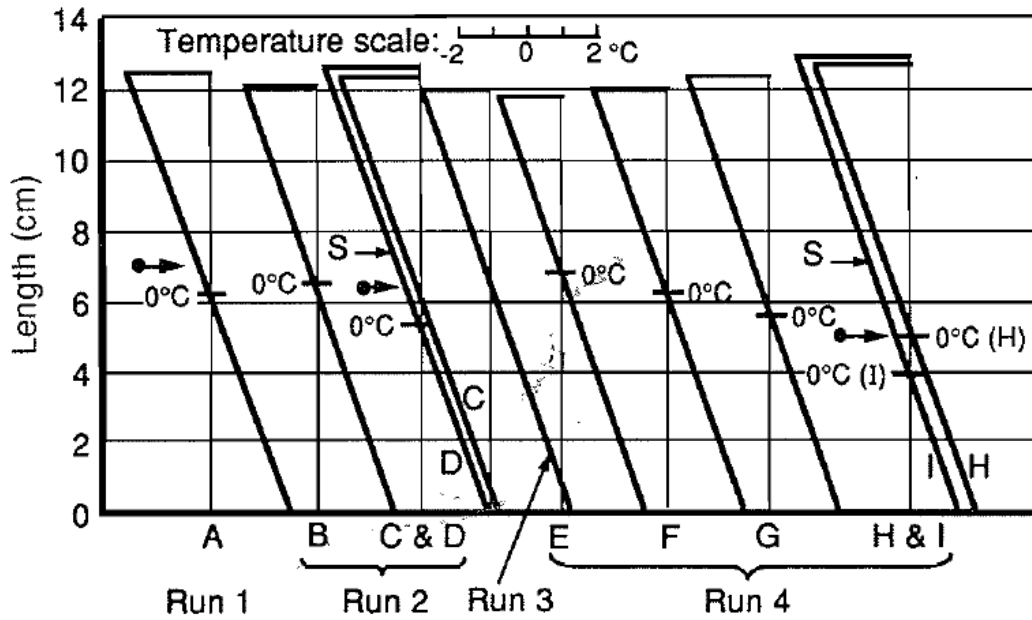
Figure 2.34: Typical results of repeated freeze-thaw runs on a clayey silt. (a) Time

vs. segregation potential (b). Temperature profiles (Konrad 1989b).

CHAPTER 3:   Site Investigation and Instrumentation

The following chapter discusses the characteristics of the research site and immediate surroundings, the geotechnical site investigation performed on the site, the site stratigraphy, the instrumentation installed on the site, and the data monitoring.

3.1 Background

More than half of the area of Manitoba is in the discontinuous permafrost zone. Figure 3.1 shows that Manitoba has discontinuous permafrost north of the isotherm for a current mean annual air temperature of about 0ºC (about 2500ºC-days of frost). The permafrost becomes continuous further north near the Hudson Bay coast. The research site examined in this doctoral project is on Provincial Road (PR) 391 which is located 18 km northwest of Thompson, Manitoba at approximately N55°50' latitude and W98°01' longitude (Figure 3.1). The PR391 is an all-weather road constructed in the region of discontinuous permafrost and the only road connecting Thompson to northern mining towns, hydroelectric generating stations, and First Nations communities in North-western Manitoba.

The PR391 was initially constructed as a compacted earthen road on discontinuous permafrost in the mid-1960s and then converted to a gravel road in the early 1970s.

In the early 1980s, it was upgraded with a bituminous pavement surface. Since construction, changes in heat transfer have melted permafrost that had been detected earlier, particularly under embankments. Thawing led to large ongoing irregular deformations and dangerous traffic issues.

The chosen research site is typical of many other problematic road embankments in the discontinuous permafrost zone. Responses by Manitoba Infrastructure and Transportation (MIT) included construction of stabilizing berms and insulating peat berms beside the embankment in the early 1990s. Over the next few years, the berms settled into the foundation soil and essentially disappeared. They currently provide no additional support to the original embankment. Regular maintenance has added several metres of gravel fill since initial construction. Where extra maintenance is required, the wearing surface has been returned to gravel from asphalt: the asphalt pavement from the early 1980s has not been replaced. Figure 3.2 and Figure 3.3 are photographs of the section of the PR391 chosen for the research project. In 1991, drilling encountered frozen soil at depths from 1.9m to 10.5m below the toe of the embankment. Later drilling in 2005, detected frozen soil at depths from 4.6m to 10.7m. As will be discussed in the next section, no frozen soil was identified in the recent drilling program for this project in late 2008 using continuous flight, solid stem augers. Considerable maintenance was required at the site. However, records outlining maintenance procedures and annual application of gravel were not made available to the author.

3.2 Provincial Road (PR) 391 Site Description

The author's research involved site investigation, field instrumentation, laboratory testing, and numerical modelling. Information about this stage of the project was published by (Alfaro et al. 2009), (Batenipour et al. 2009), (Batenipour et al. 2010), and (Batenipour et al. 2011). Geotechnical site investigation is the first step in any geotechnical analysis. The investigation of the geotechnical conditions performed by the author and the crew from the University of Manitoba and MIT in October 2008 involved drilling boreholes, sampling soil, and a site survey followed by the installation of instrumentation. Paddock Drilling Ltd. was contracted to provide drilling services. Figure 3.4 shows the 5inches Solid Stem auger on track mounted CME 850 drill rig that was used for the borehole drilling.

Boreholes were drilled at the mid-slope and toe of two cross-sections of the embankment to examine the stratigraphy, collect samples for laboratory testing, and install instruments to record the behaviour of the foundation soils over several years. One section was designated as 'stable' and the other as 'unstable'. Figure 3.5 shows the layout of the cross-section locations at PR391. The two sections are about 40m apart from each other. The 'stable' section is only about 2m high and has not deformed significantly. The 'unstable' section is also about 2m high above the surrounding natural ground. However, it settled considerably and is assumed to now contain about 5m - 6m of gravel (Figure 3.6). The gravel is partly from the original construction and partly from ongoing re-grading. The 'zero' depth in Figure

3.6 and in subsequent figures is referenced to the level of the original ground surface and of the surrounding undisturbed land. The terms 'stable' and 'unstable' are here used in the sense of a serviceability limit state and not an ultimate limit state. There are no indications of deep-seated rotational movements at the site.

Figure 3.6 shows that soil conditions below the original ground level (at depth '0' in the figure) at the two sections are considerably different. The stable section consists of approximately 4.0m of soft-to-firm clayey silt/silty clay with peat intrusions that vary from thin stratifications to pockets near the toe. At the mid-slope, the soil is primarily silt to clayey silt. The toe of the unstable section consists of 1.0m of clayey peat-silt, 1.0m of fine gravel, followed by a layer of highly plastic clay. This clay is firm, brown, silty clay at upper levels and becomes very soft and grey to a depth approaching 18m. The mid-slope of the unstable section consists of almost 2.0m of clayey peat-silt, over 2.0m of loose fine gravel, followed by firm brown silty clay that transitions to grey and soft clay. No frozen soil was found in the foundation of the both sections. The foundation material at PR391 is therefore currently classified as "degraded (thawed) permafrost". Both sections are underlain by gneissic bedrock. The surrounding area is poorly drained - there is free-standing water within approximately 20m of the embankment toe when snow is not present (Figure 3.7).

3.3 Field Instrumentation

The plan for site instrumentation was developed to investigate the temperature, pore water pressure, and vertical and horizontal deformations of the PR391 embankment (Batenipour et al. 2009).   Instrument clusters installed at the PR391 site embankment comprised thermistor strings, vibrating wire (VW) piezometers and standpipes, surface settlement plates, slope inclinometers, and VW extensometers.

In selecting instrumentation, it is necessary to consider the available resources and associated limitations.   In this research project, some of the limitations included space restrictions, monitoring ability, and cost.   Figure 3.8 shows locations of the instruments in plan view, and Figure 3.9 shows them in the two cross sections. (These two figures are diagrammatic. The instruments are closer together in both horizontal directions than appear in the figures.)   The labels on the figures are the list of instruments below and will be explained in following sections:

1- surface settlement plate

2- deep settlement gauge

3- thermistor string

4- stand pipe piezometer

5- slope inclinometer

6- vibrating wire piezometer

7- vibrating wire extensometer

All instruments were calibrated at their respective manufacturers prior to shipment and calibration certificates were provided. Calibrations of the thermistor strings, VW piezometers and VW extensometers were verified at the Geotechnical laboratory at the University of Manitoba before the installation.

3.3.1 Temperature Monitoring Instruments

The thermistor strings were installed at the toe and mid slope of both the stable and unstable sections to determine the temperature profile of the ground and depth of frost/thaw in the foundation soils below the embankment. The thermistor strings used for the study were manufactured by RST Instruments (Figure 3.10) and consist of individual thermistor sensors at 1m spacing. The RST thermistor string can measure temperature between -80°C and 75°C which is well beyond the expected temperature range for this research project (RST 2008). The thermistor strings were installed in vertical holes (Figure 3.11) and the holes were backfilled with a cement-bentonite grout after the sensors were placed. The mix design of the cement-bentonite grout generally followed the recommendations of (Mikkelsen 2002).

3.3.2 Water Pressure Monitoring Instruments

The VW piezometers were installed at the toes of both the stable and unstable sections to monitor pore-water pressures at two different depths beneath the embankment. The multi-level VW piezometers used for the study were manufactured by DGE Slope Indicator and consist of VW piezometers in multi-level housings (Figure 3.12), assembled in-line with the PVC pipe and installed down hole (DGE Slope Indicator 2004). The holes were backfilled with the cement-bentonite grout after VW piezometers were placed.

Casagrande-type standpipe piezometers were installed at the toe of both the stable and unstable sections to monitor the water level in ground. Tips for the Casagrande standpipe piezometers used for the study were manufactured by RST Instruments and consist of a slotted PVC body that encloses a porous plastic filter element, which allows the groundwater to permeate into the standpipe (RST 2008) (Figure 3.13). The water level indicator provided by DGE Slope Indicator was used to measure water levels in the standpipes. The indicator consists of a probe, a cable with laser-marked graduations, and a cable reel (DGE Slope Indicator 2004). The operator lowers the probe into the standpipe. When the probe contacts the surface of the water, the LED illuminates and the beeper sounds. The operator then reads the depth-to-water measurement from graduations on the cable.

3.3.3 Displacement Monitoring Instruments

Surface settlement plates were installed on the ground surface at the toe and mid slope of both the stable and unstable sections to monitor the settlement and heave of the ground surface. The surface settlement plates consist of upper and lower steel plates connected by a 15cm steel rod (Figure 3.14), and were inserted in a hole excavated at the ground surface. At the shoulder of the road, bearing in mind that the road would be subject to re-grading and snow removal, simple 15cm steel rebar pins were used to monitor surface settlements and heaves. The tops of the surface settlement plates and rebar pins were used as the survey points for topographical surveying using total station instruments.

Deep settlement gauges were installed at the toe and mid slope of both the stable and unstable sections to monitor vertical settlements at different depths in the foundation soil under the embankment. The deep settlement gauges consist of a 15cm auger base attached to a steel rod (Figure 3.15). These were anchored into the boreholes prior to backfilling the hole. The tops of the metal rods were used as survey points.

Slope inclinometers (SI) casings were installed beneath the toes of the embankment at both sections to monitor the lateral movements. Inclinometer casing is a special purpose, grooved pipe used in inclinometer installations. All slope inclinometer casings were 70mm in diameter and purchased from DGE Slope Indicator (Figure

3.16). The casings were installed in boreholes drilled through the clay into the bedrock.   A traversing Digitilt inclinometer probe manufactured by DGE Slope Indicator was the standard device used for surveying SI casings (Figure 3.17). The probe measures local slopes in the SI casing as the embankment and foundation soil deform. These slopes are then integrated over the length of the casing to provide estimates of lateral displacements. The Digitilt inclinometer probe was calibrated frequently during the data collection period.

There are installation corrections and error corrections that have to be applied to inclinometer readings.   The installation corrections can account for casing orientation, casing spiral or changes in the casing height. Figure 3.18 shows the measurements of the compass orientation of the SI casings axis and the height of the casings installed at PR391. All inclinometer data have been corrected for orientation, with the A^+ direction being in the downslope direction of the embankment, and thus perpendicular to the centreline of the road. Corrections to the data have been done using DigiPro for Windows (DGE Slope Indicator 2006). Error corrections account for bias, or inaccurate readings. Many errors cannot be reliably corrected without comparing a survey with the surveys taken before and after the one in question. If an error is identified in the field, it is usually best to re-do the survey. The SI casings were also susceptible to freezing and ice clogging during winter because the water level was too high (almost to the ground level) at PR391 and was present in the casings.   On a number of occasions during the data

collection, ice had to be thawed with the aid of a steamer in order to let the probe into the casings.

Vibrating wire (VW) extensometers with a gauge-length of 1.0m were installed horizontally at the toe of both test sections at a depth of 0.8m (Figure 3.19). The instruments were intended to monitor lateral deformations at shallow depths and hopefully to relate movements at the toe to lateral spreading and longitudinal cracking of the road surface. The VW extensometers used for the study were manufactured by RST instruments and consist of a VW displacement sensor encased in a sealed body (RST 2008). The body contains a telescopic PVC pipe fitted with two flanges and an inner stainless steel rod. One end of the rod is attached to the flange, while its other end is connected to a displacement sensor attached to other flange. As deformation occurs, the telescopic pipe moves with the soil and causes the rod to operate the displacement sensor. The initial reading of the instrument was used as a datum. Subsequent readings were compared to the datum to calculate the horizontal strain. The RST VW extensometer can function at the temperature range between -20°C and 80°C which is well beyond the expected temperature range at the depth of 0.8m for this research project. Unfortunately, the extensometer at the stable section failed shortly after installation. It is believed that this may have been caused during recompaction or settling of fill material following placement.

83

3.3.4 Data Collection

Data from the instruments have been collected during just over two years of operation. A Campbell Scientific CR3000 data acquisition (DA) system and two AM16/32B channel relay mutiplexers (Figure 3.20) were used to collect data from the thermistor strings, VW piezometers and VW extensometers. The DA was custom-programmed by a code prepared by RST Instruments for the instrumentation and related calibration factors used in the research study. The DA was brought to the site on a monthly basis at the same time that survey data were collected from the surface pins. At those times, the data from the instruments were collected by the DA. The data were then downloaded manually to a personal computer using LoggerNet software provided by Campbell Scientific. Telephone access was not available at reasonable cost at the relatively remote site. Remote-sensing was not therefore possible. In any case, the surface settlement pins needed to be read using on-site topographical surveying.

As mentioned previously, the slope inclinometers were monitored by the SI probe, the standpipes were monitored by the water level indicator, and the surface settlement plates and deep settlement gauges were monitored by surveying. Arrangements were made by Manitoba Infrastructure and Transportation so that all instruments were read monthly by the staff of Bindle Engineering staff in Thompson, Manitoba. The data collection by the DA was started just after the installation of

instruments in November 2008. Monitoring of the SI probes, standpipes, and surveying were started in June 2009. Both were terminated in April 2011.
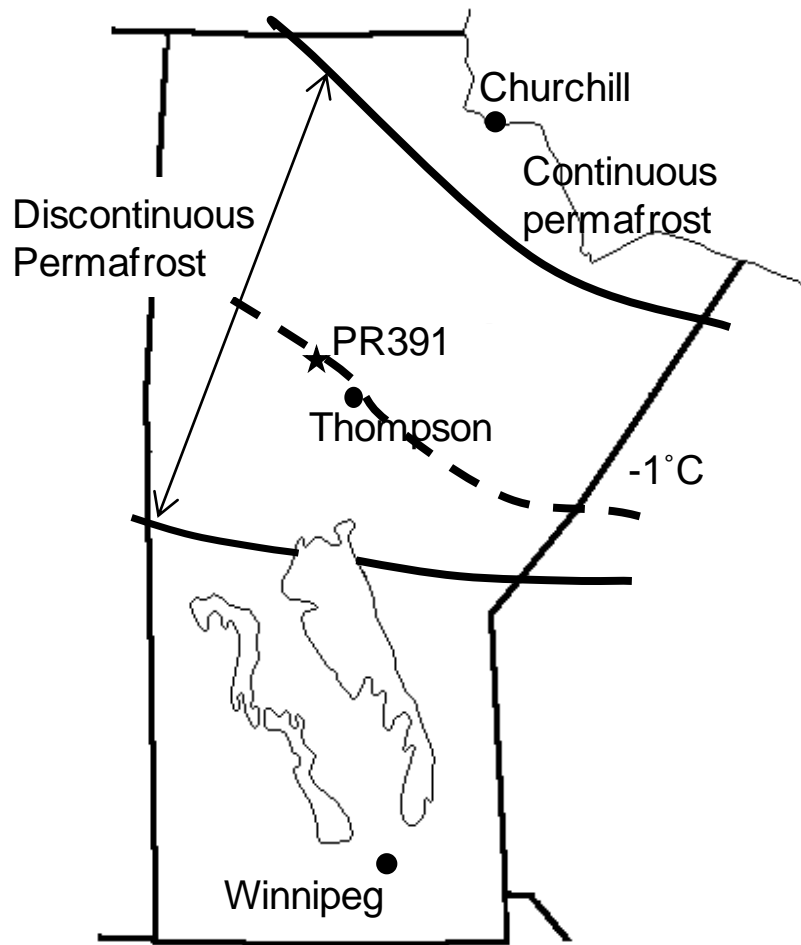
Figure 3.1: Location of permafrost in Manitoba and test site (Batenipour et al. 2009)

Figure 3.2: PR391 research site – road to Thompson

Figure 3.3: PR391 research site – road from Thompson
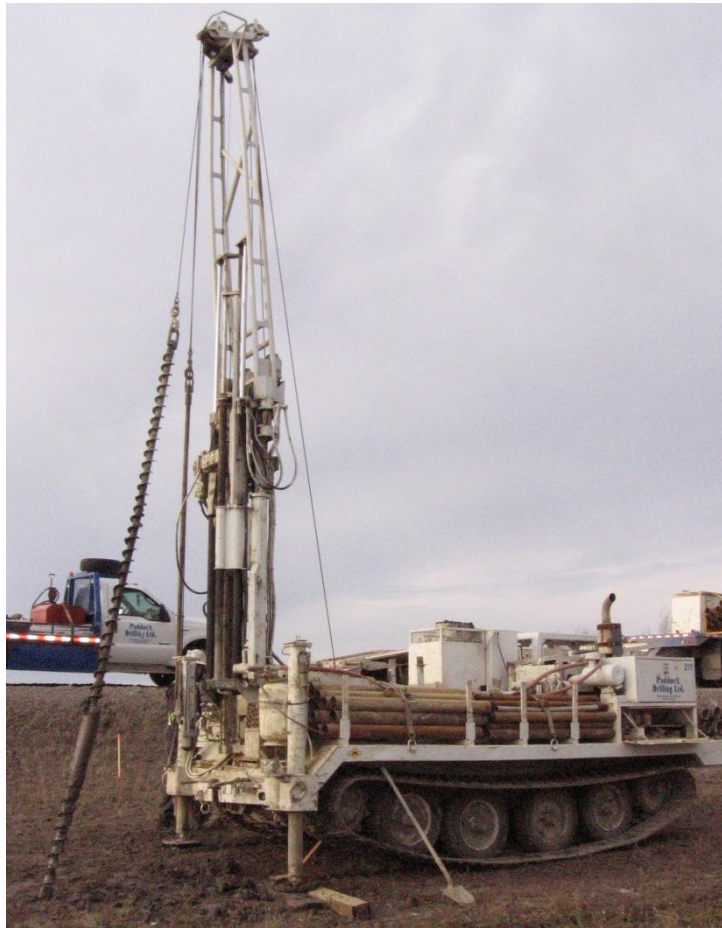
Figure 3.4: 5inches Solid Stem auger on track mounted CME 850 drill rig during

installation of instruments, October 2008.
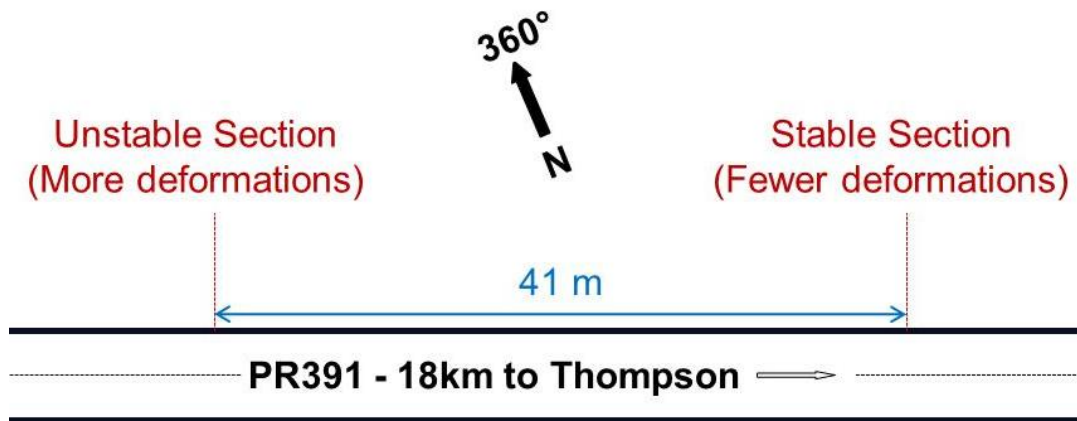
Figure 3.5: Location of cross sections at PR391
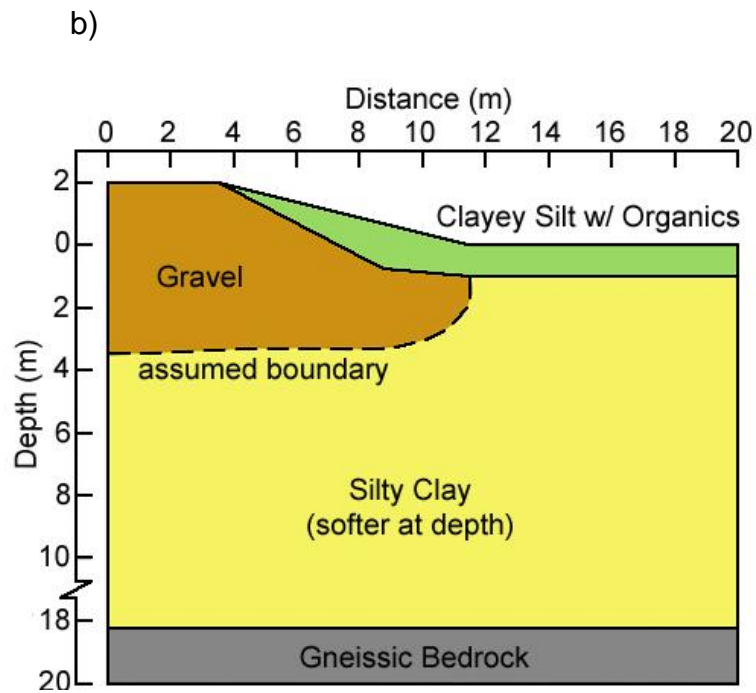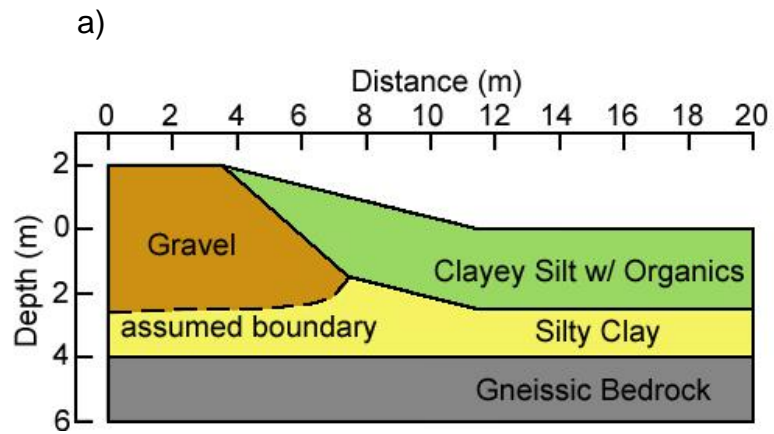
Figure 3.6: a) 'stable section'; b) 'unstable' section (Batenipour et al. 2010)

Figure 3.7: PR391, August 2008
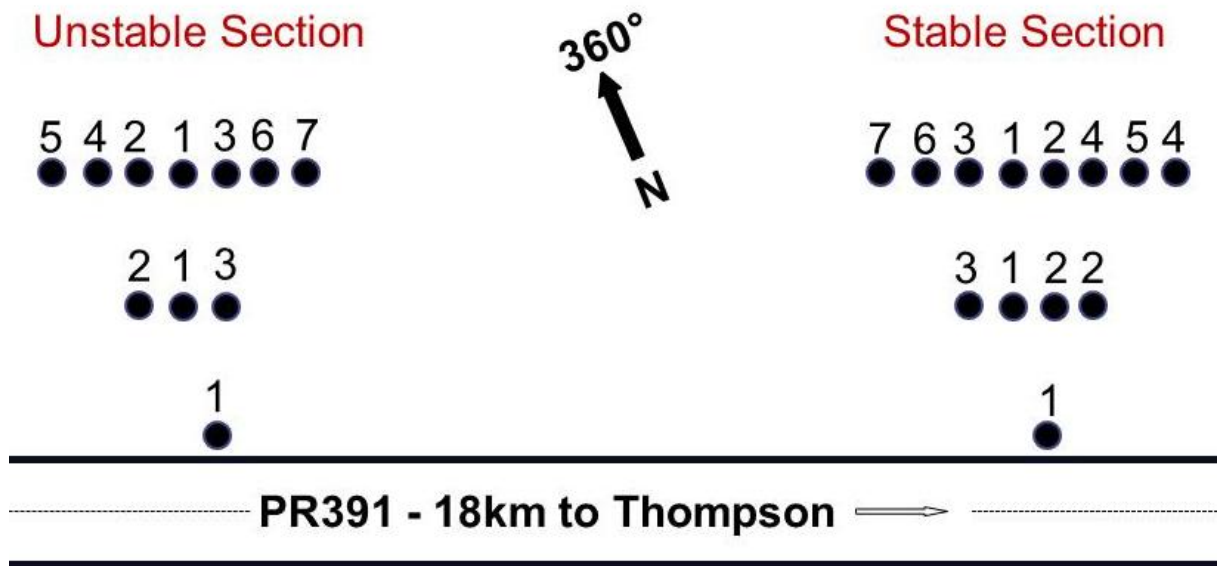
Figure 3.8: Instrumentation layout at PR391
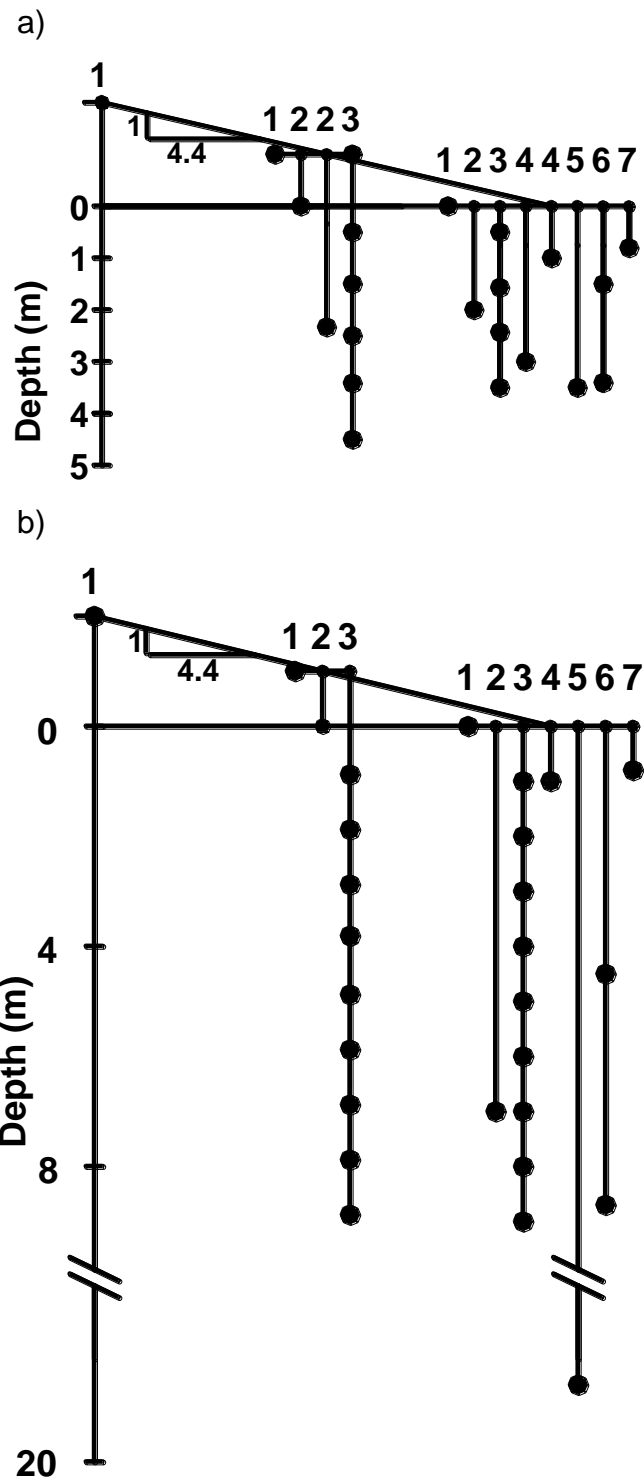
Figure 3.9: Instrumentations cross section of PR391 at a) stable; b) unstable section

(Batenipour et al. 2010)

Figure 3.10: Thermistor string

Figure 3.11: Instrument installation into the hole

Figure 3.12: Multi-level vibrating wire piezometer

Figure 3.13: Casagrande standpipe piezometer

Figure 3.14: Surface settlement plate

Figure 3.15: Deep settlement gauge

Figure 3.16: Slope inclinometer casings

Figure 3.17: Inclinometer probe
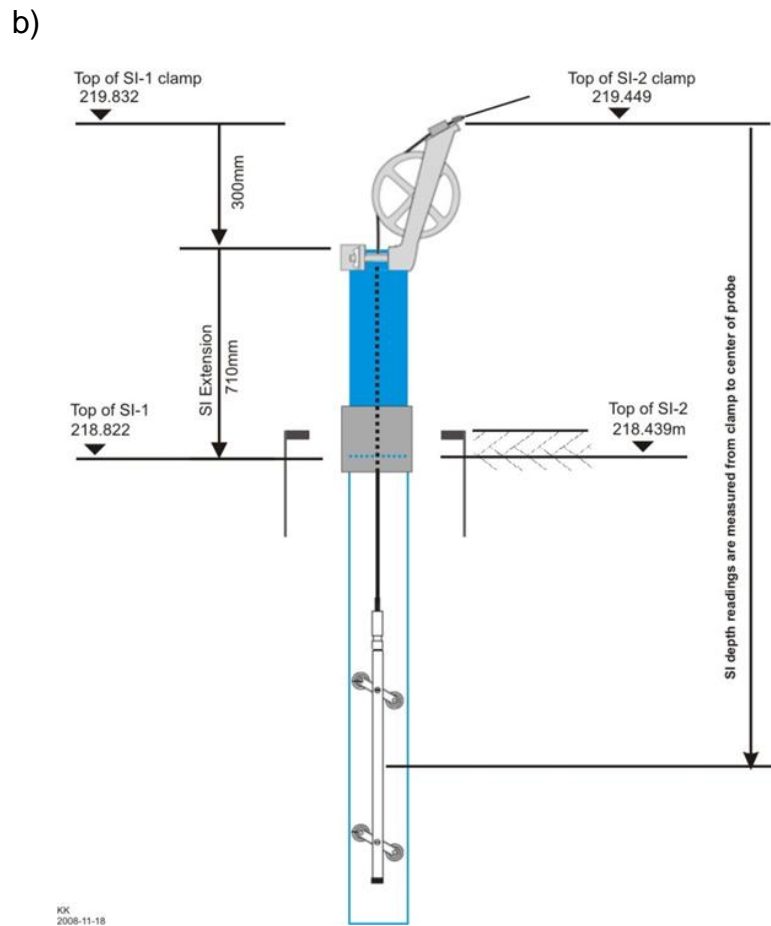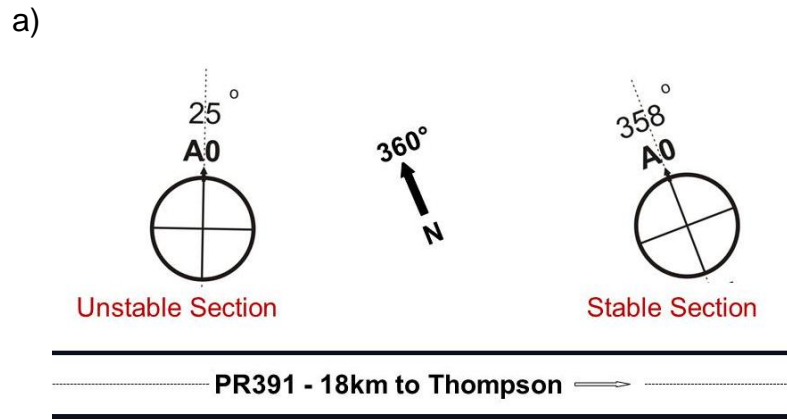
Figure 3.18: a) Compass orientation of SI casings b) height of SI casings (Redrawn from unpublished figure by Ken Kalynuk, MIT)

Figure 3.19: Vibrating wire extensometer

Figure 3.20: Campbell Scientific CR3000 and multiplexers

CHAPTER 4:   Laboratory Test Program

In order to understand thoroughly the properties of the foundation soil underneath the PR391 embankment, and to investigate the behaviour of the soil at various temperatures, a number of different tests were carried out at the geotechnical laboratory at the University of Manitoba on soil samples extracted from the PR391 test site. Shelby tube samples (71mm diameter) were extracted from the boreholes drilled for the installation of slope inclinometers at the toes of both sections. (The holes are called SI1 and SI2 for stable and unstable sections respectively). For classification purposes, index properties of the soil, including the natural gravimetric water content, Atterberg limits and hydrometer analysis, were measured. These index properties provide information on the general nature and variability of the foundation material beneath the PR391 embankment. Mechanical properties, including the consolidation and shearing properties of the soils, were investigated at temperatures of 3°C and 21°C by performing one-dimensional consolidation (oedometer) tests and consolidated undrained triaxial tests with pore pressure measurement (CIŪ tests). The purpose of this work was to identify if properties measured at the usual temperature in the laboratory (21°C) were different from those in the ground at about 3°C.

This chapter explains the laboratory testing procedures and analysis of results. The interpretation of the results will be discussed in Chapter 7. All the laboratory testing data, including the related documentations, calculations and spreadsheets, are included on the CD attached to this thesis (see Appendix A).

4.1 Natural Water Content, Atterberg Limits and Hydrometer Analysis

The natural gravimetric water contents and Atterberg limits (plastic and liquid limits) were determined for samples from boreholes SI1 and SI2 using the test procedures described in (ASTM D2216-10) and (ASTM D4318-05). Atterberg limits are measured only in clays and silty clays.

Natural gravimetric water content (w) describes the quantity of water contained in a soil sample (Budhu 2007). Technically, it is the ratio of the weight of water to the weight of dry soil in the tested specimen. The plastic limit (w_P) is the water content where soil transitions between semi-solid and plastic behaviour, and the liquid limit (w_L) is the water content at which a soil changes from plastic to liquid behaviour. Both tests are performed under carefully defined conditions. The water contents, liquid and plastic limits are useful for classifying soils into groupings with widely understood, though approximate properties. Their principal usefulness is in establishing the natural variability of soils at a site. They are not immediately useful for design or analysis.

The plasticity index (I_P) is a measure of the plasticity of a soil. The plasticity index is the range of water contents over which the soil deforms plastically.

Equation 4.1 $I_P = w_L - w_P$

Above the liquid limit, the soil has low shear strength and behaves broadly like a liquid. Below the plastic limit, the soil behaves like a stiff, brittle solid. The plasticity index depends on the proportion of clay-size particles in the soil.

Values of natural water contents, Atterberg limits, and plasticity indices measured at PR391 are shown in Table 4.1. Values of measured natural water content and Atterberg limits for both the stable and unstable sections are shown in Figure 4.1 and Figure 4.2, with the current ground surface taken as zero depth. Test results are shown as range bars surrounding water content data points.

For tests on soil samples from the stable section, the maximum and minimum measured plasticity indices were 40% and 10% respectively while the maximum and minimum plasticity indices for unstable section were 32% and 17%, respectively. Note however that the results are systematic, not random, with higher values near the surface and lower values at greater depths.

102

The liquidity index (I_L) provides a quantitative measure of the current state of a soil sample. It depends on the natural gravimetric water content with respect to the Atterberg limits and is defined as shown in Equation 4.2. It also gives a qualitative estimate of undrained shear strength.

Equation 4.2 $\qquad I_L = \dfrac{w - w_P}{I_P}$

The results show the values of liquidity indices increases with depth increases (see values of I_L of in Table 4.1). This can also be observed on Figure 4.1 and Figure 4.2 in which the water contents get closer to the liquid limit (the right side of the Atterberg limits bar) with increasing depth. This represents the soil becoming generally softer as depth increases. Weathering processes such as freezing-thawing and wetting-drying produce lower water contents at shallow depths, and higher shear strengths.

Hydrometer analyses were done for samples from boreholes SI1 and SI2 according to (ASTM D422-63). Hydrometer analysis is the process by which fine-grained silts and clays, are graded by their particle size distribution. Table 4.1 shows the percentage of silt and clay present in the fine grained portion of the samples. Figure 4.1 and Figure 4.2 shows the percentage of clay present – known as the clay fraction – at the both stable and unstable sections. The results of the hydrometer

analyses show that the clay fraction is lower at greater depths and the ratio of clay/silt particles is around 50:50 for depths greater than about 8m at the unstable section.

4.2 One-Dimensional Consolidation at Two Different Temperatures

Samples from boreholes SI1 and SI2 were tested to examine the compression behaviour of soil with changes of temperature in one-dimensional consolidation using incremental loading. The tests were performed following (ASTM D2435-96) and were conducted to determine the compression and re-compression indices, C_c and C_r respectively, the secondary compression index $C_{\alpha e}$, and the preconsolidation pressure σ'_{zc} at two different temperatures. A total of fourteen ASTM standard consolidation tests was carried out at 3°C and 21°C. For the 3°C tests, the oedometer frames were placed in an environmental chamber which could control temperatures to within ±1°C.

4.2.1 Oedometer Test Setup and Procedures

Standard lever-arm consolidation frames (oedometers) with cells fitted with 64mm diameter by 19mm high consolidation rings were used for the one-dimensional compression tests carried out in this program (Figure 4.3). The cells include two porous stones: a larger stone that is placed beneath the specimen and a smaller

stone that is screwed on to the loading cap and placed on top of the specimen. Filter paper is placed between the porous stones and the specimen to ensure that no soil particles infiltrate the stones. The cell is mounted to the apparatus on the fixed machine plate. The cross beam can then be lowered, bringing the load assembly into contact with the seating of the cell loading cap. As the beam hanger is loaded, it applies vertical force to the load assembly and the cell loading cap which in turn applies pressure to the sample. The dial gauge (or Linear Variable Differential Transducer, LVDT) moves as the load assembly lowers or rises. The gauge can be adjusted to any height along the top of the bar immediately above the centre of the loading plate. Rotations on the gauge are used to measure the height/consolidation of the specimen. The loading beam was adjusted as necessary during the test so that it remained horizontal.

To inhibit swelling and reduce consequent destructuring, the first increment of applied pressure on specimens was set at 13kPa. Loads on the specimens were increased using a load increment ratio of about 1 (that is, approximately doubling the applied load with each increment). Each of the early loads was applied for 24 hours. Following loading to the maximum applied stress (about 700kPa), the specimens were unloaded in stages and then reloaded again to the maximum applied stress (about 1400kPa). This final vertical stress was then maintained for five to seven days in order to measure the secondary compression behaviour of the clay.

4.2.2 Oedometer Test Results

When a soil is loaded one-dimensionally under a constant normal total stress, its compression has two components. One, primary consolidation, is associated with the hydrodynamic expulsion of water, increasing effective stress, and consequent reorganization of the soil structure. Two, the clay continues to settle even after excess pore water pressures have dissipated and effective stresses are constant. This section discusses the primary and secondary compression behaviour of the soil samples from PR391 and the effect of temperature changes on them.

The values of void ratio (e) were measured for each loading and unloading increment of the tests as (Budhu 2007):

Equation 4.3 $$e = \frac{G_s \cdot \rho_w - \rho_d}{\rho_d}$$

where G_s is the specific gravity of the soil (assumed to be 2.70), ρ_w is the density of water (1.0 Mg/m^3 used in these calculations), and ρ_d is the dry density (mass of dry soil divided by the volume) for each increment. The height of the specimen after 24 hours was used to calculate the volume of the specimen for each loading and unloading increment.

Primary consolidation is the change in volume of soil caused by the expulsion of water from the voids and transfer of loading from initial excess pore water pressures

to the soil particles. The primary consolidation stage is characterized by the compression index C_c (in the normally consolidated range). The C_c is the average slope of loading curves in plots of void ratio (e) versus log applied normal stress (σ'_z) and can be obtained as (Budhu 2007):

Equation 4.4 $$C_c = \frac{e_1 - e_2}{\log(\sigma'_{z2}/\sigma'_{z1})} = \frac{|\Delta e|}{\log(\sigma'_{z2}/\sigma'_{z1})}$$

Values of the unloading/reloading index (or recompression index) (C_r) were calculated. The C_r is the average slope of unloading/reloading curves in plots of void ratio (e) versus log normal stress (σ'_z). Preconsolidation pressures (σ'_{zc}) were also evaluated using the Casagrande procedure (Budhu 2007). The σ'_{zc} is the maximum vertical overburden stress that a particular soil specimen has sustained in the past. Figure 4.4 shows an example of a plot of void ratio (e) versus log normal stress (σ'_z) and calculations of C_c, C_r and σ'_{zc}. Table 4.2 includes the summary of all the results, and the proportional change for each measured parameter at two temperatures of 3°C and 21°C, based on the following equation:

Equation 4.5 $$\Delta_{value}(\%) = \frac{\text{value at } 21°C - \text{value at } 3°C}{\text{value at } 21°C} \times 100$$

The preconsolidation pressures were not well-defined in any of the tested samples (see Figure 4.4 as an example), despite initially loading the specimens to 13kPa to inhibit swelling. This is to some extent due to disturbance of the tube samples,

which were 71mm diameter, but may also be a result of the original locations of the samples beneath the embankment which has been subjected to a wide range of stress and weathering conditions. The measured preconsolidation pressures were unlikely to have been caused by previous higher loading from proglacial Lake Agassiz. They are more likely to have been caused by weathering processes such as freezing-thawing or drying-wetting which also cause destructuring of the original clay fabric. Reduced weathering with depth explains the decrease in the apparent preconsolidation pressures at lower elevations in both the stable and unstable sections as shown in Figure 4.1 and Figure 4.2 respectively. The results also showed that values of preconsolidation pressure decrease with increasing temperature. This observation is consistent with the results reported by researchers in the literature review presented in Chapter 2.

Figure 4.5 shows plots of void ratio versus log normal effective stress for the tests carried out at 21°C at both stable and unstable sections. As the figure shows, the slope of the normal consolidation curve becomes less steep with increasing depth at both sections (that is, lower C_c at greater depths, see Table 4.2). This illustrates that soil specimens are less compressible at deeper locations. This correlates with the lower plasticity indices and lower clay fractions at depth (Figure 4.1 and Figure 4.2). Comparison of Figure 4.5a and b also shows that the normal consolidation curves for specimens from the unstable section have a slightly steeper slope than the curves for the stable section (higher C_c values for the unstable section). The

specimens from the unstable section are more compressible than the specimens from the stable section. This could be as a result of a weaker soil structure in the unstable section.

Figure 4.6 and Figure 4.7 compare plots of void ratio versus log normal stress and Table 4.2 includes the values of C_c and C_r for specimens from the stable section and unstable section at different temperatures. The results show that tests from the stable section and unstable section generally have a similar slope on the loading path (value of C_c) and unload/reload path (value of C_r) at both temperatures (3°C and 21°C). The only exceptions are for specimens from greater depths at the unstable section. The similarity of the values of C_c and C_r shows that the change of temperature in these tests does not have a significant effect on the values of compression index and unload/reload index. The deeper locations beneath the unstable section show larger differences. Comparison of Figure 4.6 and Figure 4.7 also shows that the range of the void ratios in the tests is much higher in the unstable section than the stable section, probably as a result of the higher liquidity indices.

Secondary compression (creep) is the change in volume of soil associated with viscoplastic reorganization of diffuse double layers (DDLs) around clay particles (Kelln et al. 2008). Secondary compression is usually characterized by the index $C_{\alpha e}$, defined as the slope of the curve obtained by plotting void ratio (e) versus log

time in the normally consolidated range of loading (Yin et al. 2002, Budhu 2007, Kelln et al. 2008):

Equation 4.6
$$C_{\alpha e} = \frac{e_1 - e_2}{\log(t_2/t_1)} = \frac{|\Delta e|}{\log(t_2/t_1)} \; ; t_2 > t_1$$

In order to measure the secondary compression behaviour of the soil from the PR391 embankment, the maximum applied vertical stress (about 1400kPa) was maintained for five to seven days.   (This loading is well above the in-situ preconsolidation pressures shown in Table 4.2). Figure 4.8 shows an example of a plot of void ratio (e) versus log time and the fitted line used to calculate $C_{\alpha e}$. Table 4.2 includes values of $C_{\alpha e}$ calculated from the test results on the oedometer specimens.

Figure 4.9 shows plots of void ratio versus log time for the tests carried out at 21°C for specimens from both the stable and unstable sections, under an applied vertical stress of 1400kPa. The figure shows that viscous compression in the unstable section tests was larger than corresponding values in the stable section tests (that is, values of $C_{\alpha e}$ were higher at the unstable section, see Table 4.2). Once again, this reflects the higher plasticity of the clay at the unstable section.

Figure 4.10 and Figure 4.11 show plots of void ratio versus log time for specimens from the stable and unstable sections respectively that were tested at 21°C and 3°C.

Measured values of $C_{\alpha e}$ are included in Table 4.2 for specimens from the two sections. The secondary compression values from the tests at 21°C and 3°C illustrate that except for the specimens at greater depths in the unstable section, changes in temperature do not seem to greatly affect the creep behaviour of the specimens in the PR391 embankment.

It is noticeable, however, that all of the specimens, including those with low plasticity index, exhibit secondary compression. Primary and secondary compression indices of clays depend on the mineralogy of the clay particles and the chemistry of the pore fluid (Mitchell & Soga 2005). They have been related empirically through the ratio $C_{\alpha e}/C_c$, which can frequently be considered constant in the normally consolidated range for a given soil (Mesri & Godlewski 1997). Table 4.2 shows values of $C_{\alpha e}/C_c$ obtained from the present series of tests. The values are in the range of 0.016 to 0.056. The lower measured values are below the range of $C_{\alpha e}/C_c$ values reported by (Mesri, Feng & Shahien 1995) for the compression behaviour of clays. Their values generally remain within a narrow range of 0.04 to 0.08.

Comparing the values of $C_{\alpha e}/C_c$ for both the stable and unstable sections shows that the ratio of $C_{\alpha e}/C_c$ does not change with temperature at shallow depths. The values of $C_{\alpha e}/C_c$ increase slightly with increases of temperature at greater depths at the unstable section.

4.3 Triaxial Test Results at Two Different Temperatures

Triaxial testing was done on soil specimens from boreholes SI1 and SI2 using the consolidated undrained compression test method (CIŪ) for examining the shearing properties of soil with changes of temperature. A total of nine ASTM standard CIŪ tests were carried out at 3°C and 21°C. The tests followed (ASTM D4767). For the 3°C tests, the triaxial apparatuses were placed in the environmental chamber that could control temperatures to within ±1°C.

4.3.1 Triaxial Test Setup and Procedures

The triaxial apparatus shown in Figure 4.12 was used for determining the shearing properties of the clay at PR391 under different stress conditions and at two temperatures of 3°C and 21°C. Isotropically consolidated undrained tests with pore water pressure measurement (CIŪ tests) provide effective stress strength parameters. This type of test is currently considered to be the most useful testing procedure for many geotechnical projects.

Cylindrical specimens were trimmed to a nominal diameter of about 50mm and a nominal length of about 100mm (aspect ratio of 2.0) from Shelby tube samples taken from the SI1 and SI2 boreholes. In the test cell, the specimens were surrounded by an impermeable rubber membrane attached to the cell pedestal and to the top loading cap. A porous stone and a filter paper were placed at the top and bottom of

112

the specimens to permit drainage of pore water from the specimen and regulation of the pore water pressure. Strips of filter paper were also placed round the specimen inside the rubber membrane to facilitate drainage. Water pressure inside the cell provides the horizontal principal total stresses. The vertical pressure at the top cap is produced by a combination of the cell fluid pressure and the applied force from the ram during application of axial deformations. Tests are run under controlled axial strain.

As is normal, the tests were done in two phases, the consolidation phase and the shearing phase. During the consolidation phase, the specimens were consolidated using an all-round pressure ('cell pressure' or 'confining pressure', σ_3), a vertical pressure ($\sigma_1 = \sigma_3$), and a back pressure (u_b). A u_b of 200kPa was applied to keep the specimen and the drainage channels free of gas. Drainage was kept open during the consolidation phase of adding the confining pressure and the resulting changes of volume were monitored. The effective consolidation pressure ($\sigma'_3 = \sigma_3 - u_b$) was applied until no additional volume changes were observed (Figure 4.13). This normally took about 48 hours.

Skempton's pore pressure parameter, B is a measure of the saturation of the soil, following the equation below (Skempton 1954):

Equation 4.7 $$B = \frac{\Delta u}{\Delta \sigma_3}$$

where Δu is the change in pore water pressure as a result of change in the cell pressure ($\Delta\sigma_3$), while drainage is closed. To ensure fully saturated/consolidated conditions, the drainage lead was shut off and the confining total pressure raised by an amount $\Delta\sigma_3$ (usually about 50kPa), the resulting change in pore water pressure Δu was measured. Before the second phase of shearing the specimens, a B-value of 98 percent or higher had to be obtained.

After completing the consolidation phase, specimens were sheared by increasing the vertical pressure ($\sigma_1 > \sigma_3$) by compressing the specimen at constant rate of axial deformation (ε_1). During this second shearing phase, the cell pressure (σ_3) was kept constant while the loading ram was driven down at the axial strain rate of 5.2e-03 %/min in 100mm long specimens. This axial strain rate is slow enough to ensure that shear-generated pore water pressures are transferred properly to a pore water pressure transducer at the base of the cell. Drainage was kept closed during the shearing phase. Readings were taken of the confining pressure (σ_3), the pore water pressure (u), the axial load, and the axial deformations. Shearing was typically stopped at between 15 and 20 percent axial strain.

4.3.2 Results from Triaxial Tests

Results from the triaxial tests were plotted as graphs of deviator stress (q) vs mean principal effective stress (p') and q vs ε_1, where:

Equation 4.8 $q = \sigma_1 - \sigma_3$

 and

Equation 4.9 $p' = \dfrac{\sigma'_1 + 2\sigma'_3}{3}$

where $\sigma'_1 = \sigma_1$ - u and $\sigma'_3 = \sigma_3$ - u.

Figure 4.14 and Figure 4.15 show representative results of the shearing phase plotted as q vs p' and q vs ε_1 for nine specimens at two temperatures of 21°C and 3°C. The figures show that all the specimens are expansive (dilative) and ductile, that is strain hardening. This is usually the case when the soil is silty and initially dense or moderately dense. (The results of hydrometer tests confirmed the presence of around 50% silt in the specimens, see Table 4.1). During the shearing phase, specimens first tend to compress elastically, that is, they produce increasing pore water pressures. During this part of the test, the plot of q vs p' rises vertically and then bends slightly to the left. When the silt particles begin to interact, the specimen has to expand. This produces decreasing pore water pressures and the plot bends to the right. In Figure 4.15, deviator stresses continue to increase until shearing is terminated at between 15 and 20 percent axial strain. In cases like this, failure cannot be defined by a maximum deviator stress criterion.

Limited numbers of specimens were available at any given depth and it was not possible to develop failure envelopes from multiple specimens. Because the

specimens were strain-hardening, it was possible to identify failure from straight-line sections of q vs p' plots for single specimens. The straight lines were chosen to go through the origin in these q vs p' plots. The Mohr-Coulomb criterion was used instead to indicate failure. According to this theory, failure takes place at $(\sigma'_1/\sigma'_3)_{max}$ which in plots of q vs. p', is equivalent to (Budhu 2007):

Equation 4.10 $$M = \left(\frac{q}{p'}\right)_{max} = \frac{6\sin\varnothing'}{3 - \sin\varnothing'}$$

where $\varnothing'$ is the effective stress friction angle and c' = 0.

Table 4.3 summarizes the results of the triaxial testing. As the table shows, the values of friction angle ($\varnothing'$) for both stable and unstable sections are in the range of 32° to 42°. The relationship between $\varnothing'$ and plasticity indices is not strong as might be expected. As can be expected from references such as (Campanella & Mitchell 1968), and (Graham et al. 2001) (see literature review in Chapter 2), the results also show only small effects of temperature on the friction angle of these specimens.

Test	Section	Depth (m)	w_P (%)	w (%)	w_L (%)	I_p (%)	I_L	Clay (%)	Silt (%)
HBO12		1.5	23	40	63	40	0.4	88	12
HBO11		1.6	23	38	63	40	0.4	87	13
HBO09		1.7	24	36	62	37	0.3	83	17
HBO10	Stable Toe	1.8	25	37	60	35	0.3	86	14
HBT03		3.0	16	36	31	14	1.4	38	62
HBO18		3.4	17	25	27	10	0.7	34	66
HBO17		3.5	15	25	31	16	0.6	42	58
HBT02		3.0	16	26	33	17	0.6	51	49
HBO16		3.4	26	33	58	32	0.2	65	35
HBO15		3.5	27	36	57	31	0.3	69	31
HBT07		4.5	23	38	46	23	0.7	54	46
HBT06		4.8	32	40	54	22	0.4	59	41
HBO13		6.4	20	36	52	32	0.5	82	18
HBO14		6.6	19	32	49	30	0.4	80	20
HBO19	Unstable Toe	7.7	20	42	40	20	1.1	59	41
HBT08		7.8	19	39	39	21	1.0	63	37
HBO20		8.1	19	33	39	21	0.7	63	37
HBT09		8.2	18	36	42	23	0.8	57	43
HBT10		9.4	18	43	39	21	1.2	56	44
HBT12		10.5	20	40	40	20	1.0	57	43
HBO21		10.8	18	38	37	19	1.0	55	45
HBT11		10.9	17	39	36	18	1.2	43	57
HBO22		11.2	17	39	37	20	1.1	52	48

- w_P = plastic limit, w = gravimetric water content, w_L = liquid limit, I_P = plasticity index, I_L = liquidity index

Table 4.1: Properties of the soil of both sections at PR391

Test	Section	Depth (m)	T (°C)	σ'$_{zc}$ (kPa)	Δσ'$_{zc}$ (%)	C_c	ΔC$_c$ (%)	C_r	ΔC$_r$ (%)	$C_{\alpha e}$	ΔC$_{\alpha e}$ (%)	$C_{\alpha e}$/C_c	Δ$_{(C\alpha e/Cc)}$ (%)
HBO12		1.5	3	111	-52	0.255	-4	0.069	-10	0.005	0	0.020	4
HBO11	Stable Toe	1.6	21	73		0.246		0.063		0.005		0.020	
HBO09		1.7	21	108	-4	0.229	-6	0.065	-15	0.004	3	0.017	8
HBO10		1.8	3	112		0.242		0.075		0.004		0.016	
HBO18		3.4	3	80	-8	0.079	11	0.020	-11	0.003	28	0.037	18
HBO17		3.5	21	74		0.089		0.018		0.004		0.045	
HBO16		3.4	3	109	-49	0.354	-5	0.062	9	0.012	24	0.035	28
HBO15		3.5	21	73		0.336		0.068		0.016		0.048	
HBO13	Unstable Toe	6.4	21	50	-80	0.261	12	0.057	14	0.007	11	0.025	-2
HBO14		6.6	3	90		0.229		0.049		0.006		0.026	
HBO19		7.7	21	62	-21	0.234	9	0.039	-36	0.013	59	0.056	55
HBO20		8.1	3	75		0.213		0.053		0.005		0.025	
HBO21		10.8	21	65	23	0.135	-74	0.021	-90	0.009	28	0.067	59
HBO22		11.2	3	50		0.235		0.040		0.007		0.028	

- σ'$_{zc}$ = preconsolidation pressure, C_c = compression index, C_r = re-compression index, $C_{\alpha e}$ = secondary compression index

Table 4.2: Results of one dimensional consolidation testing

Test	Section	Depth (m)	T (°C)	M (q/p')max	ø' (°)
HBT03	Stable Toe	3.0	21	1.54	38
HBT02		3.0	21	1.38	34
HBT07		4.5	3	1.40	35
HBT06		4.8	21	1.73	42
HBT08	Unstable Toe	7.8	21	1.32	33
HBT09		8.2	3	1.10	28
HBT10		9.4	21	1.29	32
HBT12		10.5	21	1.27	32
HBT11		10.9	3	1.52	37

- ø' = effective stress friction angle

Table 4.3: Results of triaxial testing
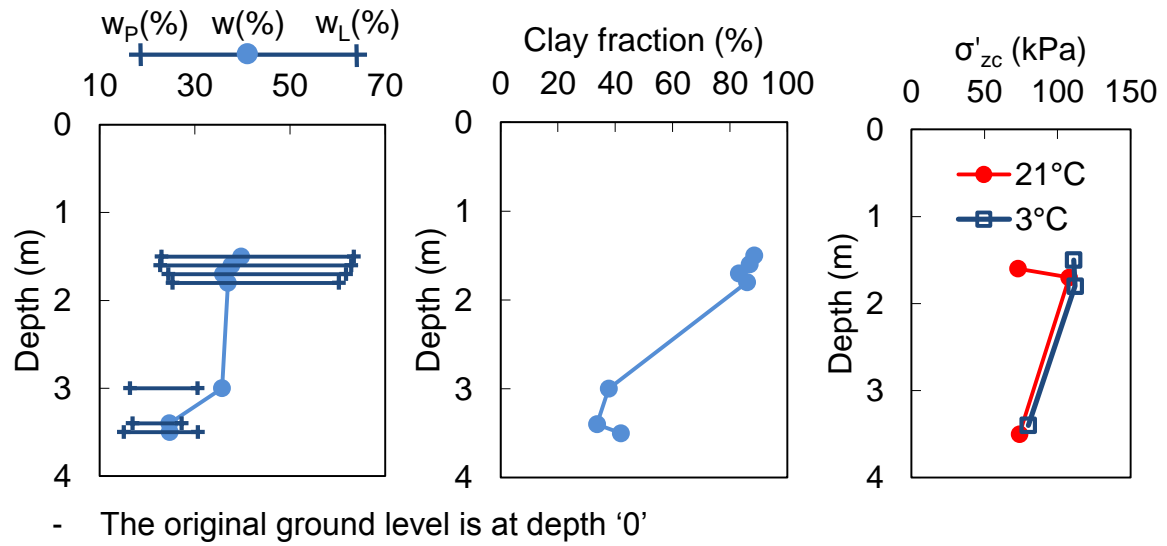
Figure 4.1: Natural gravimetric water contents, Atterberg limits, Clay fractions, and preconsolidation pressures of the specimens from the stable section
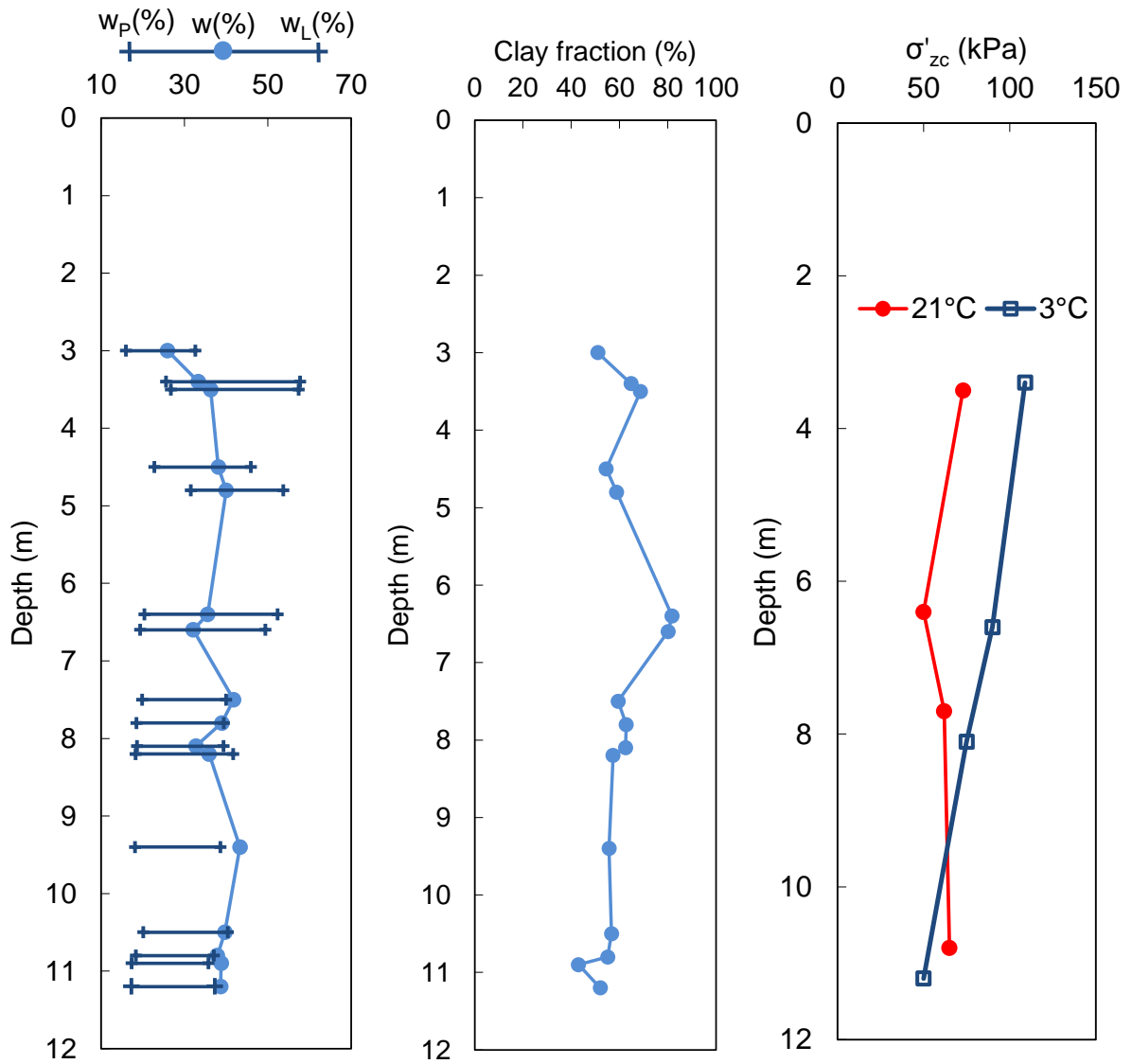
-    The original ground level is at depth '0'

Figure 4.2: Natural gravimetric water contents, Atterberg limits, Clay fractions, and preconsolidation pressures of the specimens from the unstable section

- The original ground level is at depth '0'

Figure 4.3: One dimensional consolidation machines
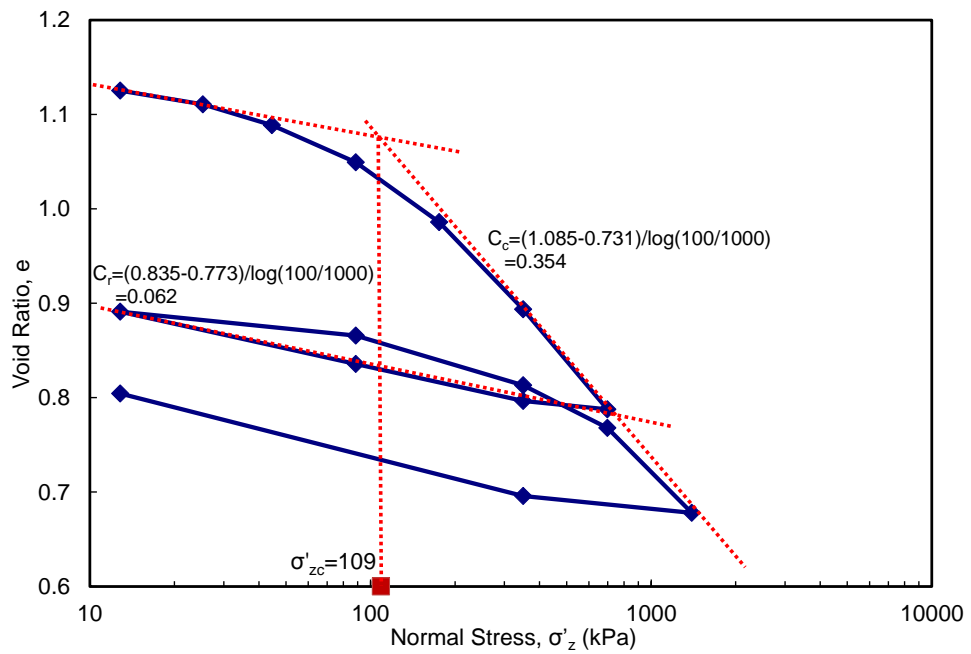
Figure 4.4: Example plot of void ratio (e) versus log normal stress (σ'_z) and

calculations of C_c, C_r and σ'_{zc} for HBO16

a) stable section
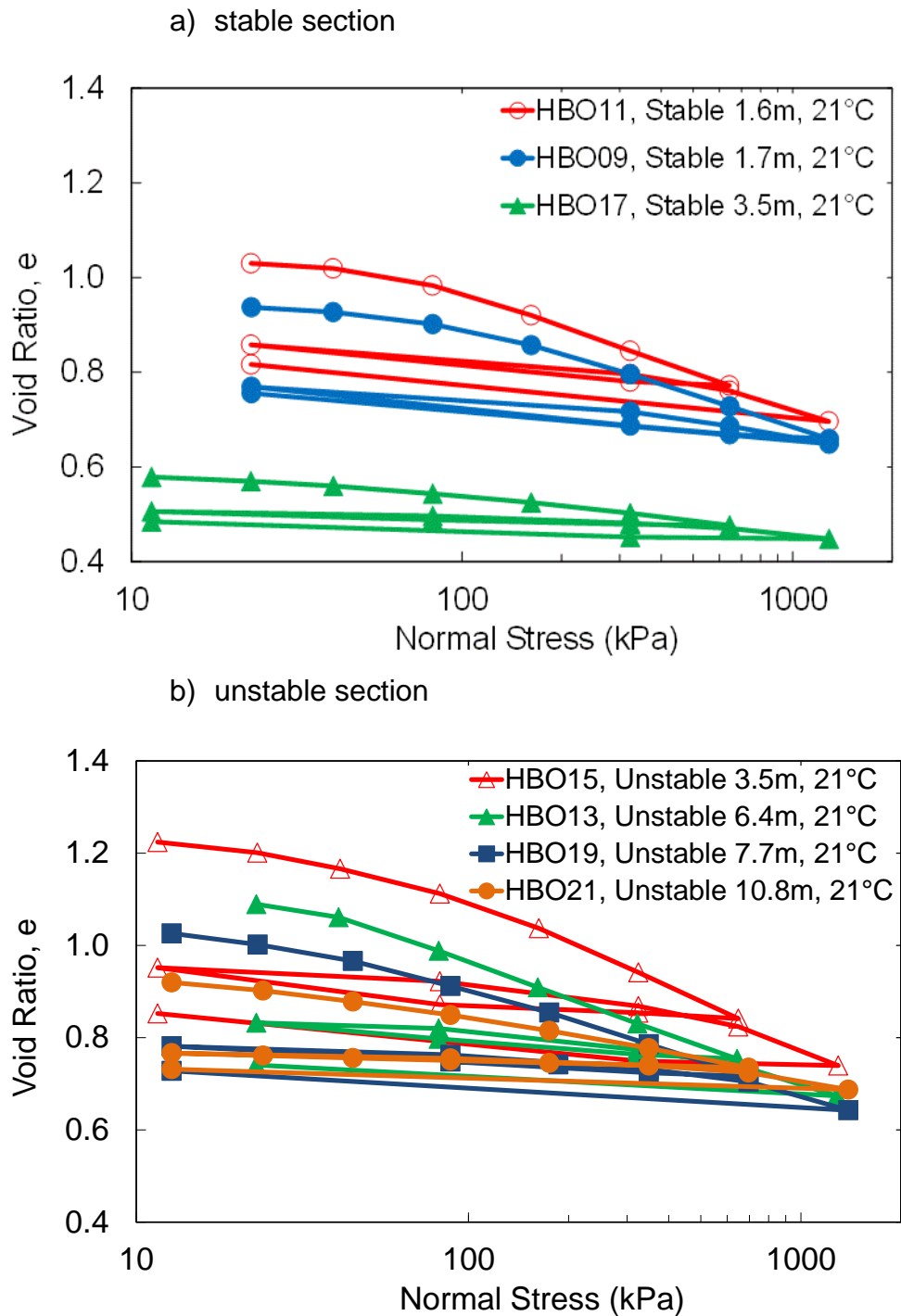
b) unstable section

Figure 4.5: Void ratio versus log normal stress for the tests carried out at 21°C on specimens from the stable and unstable sections
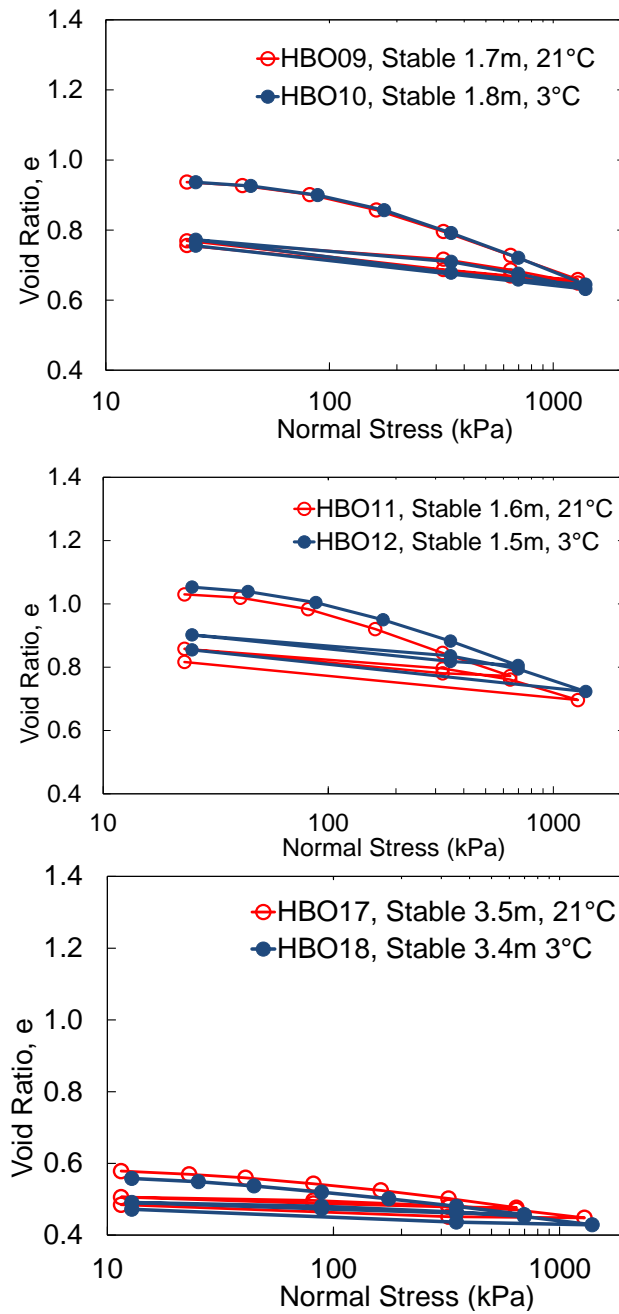
Figure 4.6: Void ratio versus log normal stress for the tests carried out at 21°C and

3°C on specimens from the stable section

124
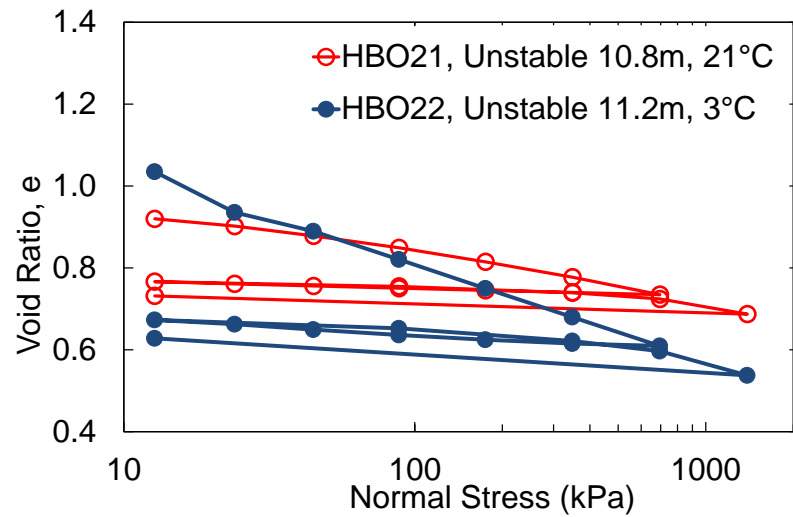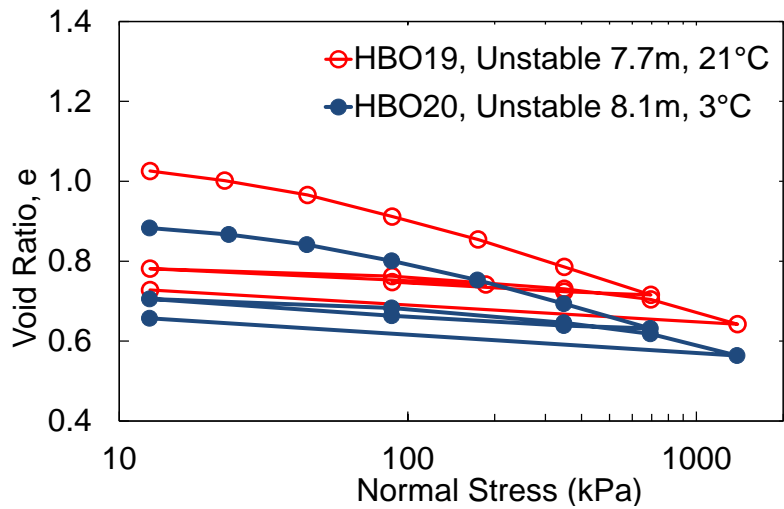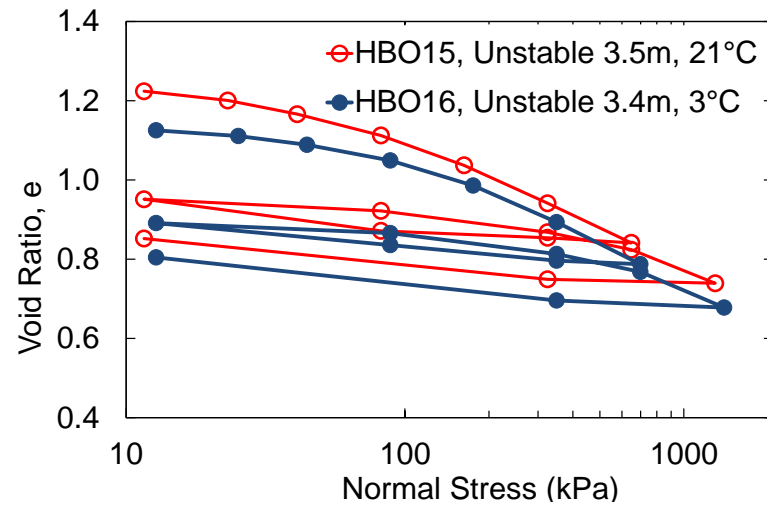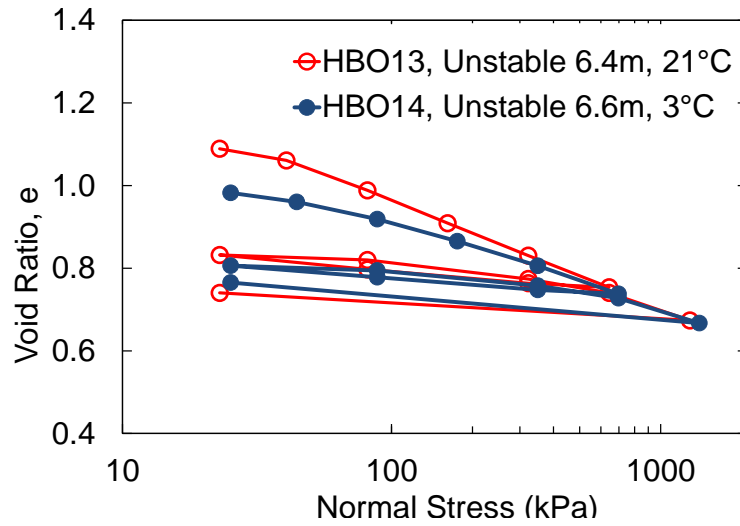
Figure 4.7: Void ratio versus log normal stress for the tests carried out at 21°C and 3°C on specimens from the unstable section

125
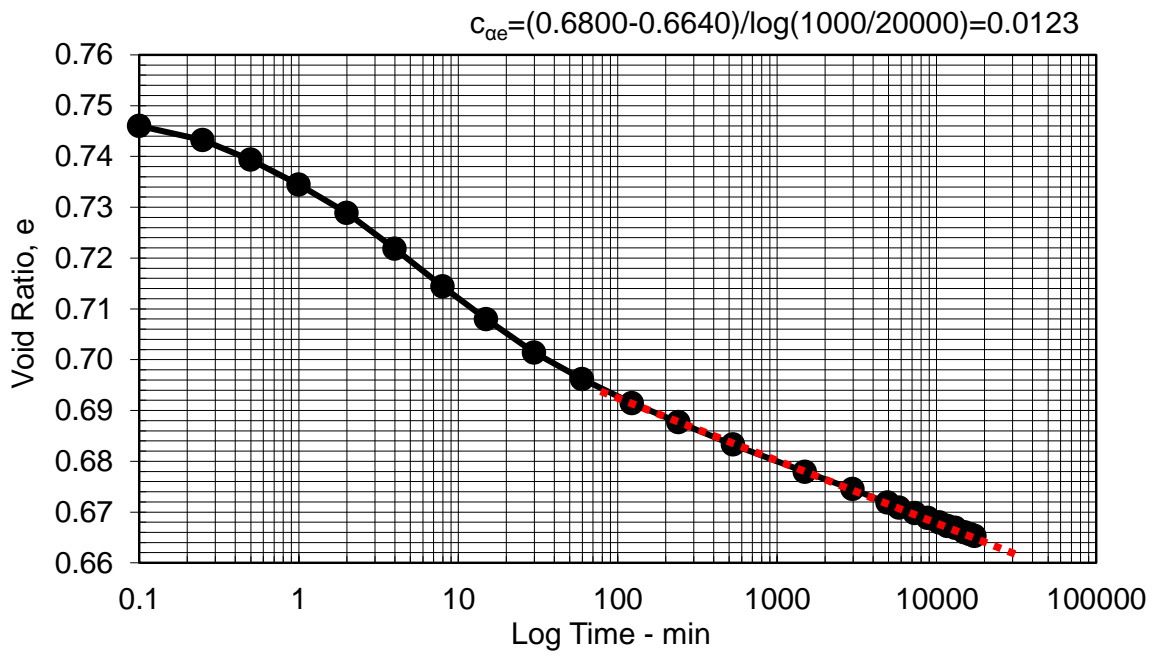
Figure 4.8: Example plot of void ratio (e) versus log normal stress (σ'$_z$) and

calculation of C$_{\alpha e}$ for HBO16, under the vertical applied stress of 1400kPa

a) stable section
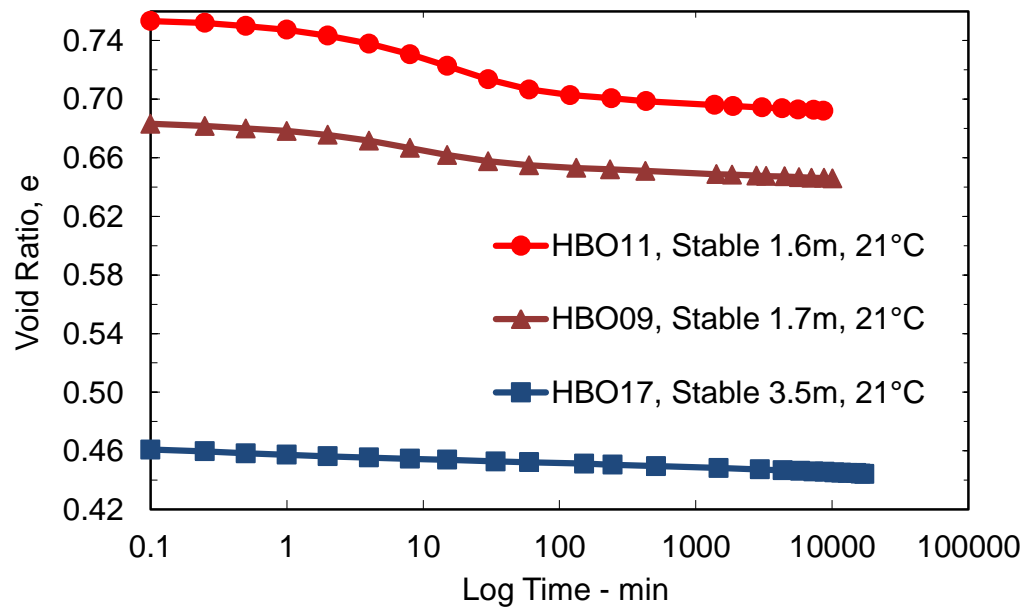
b) unstable section
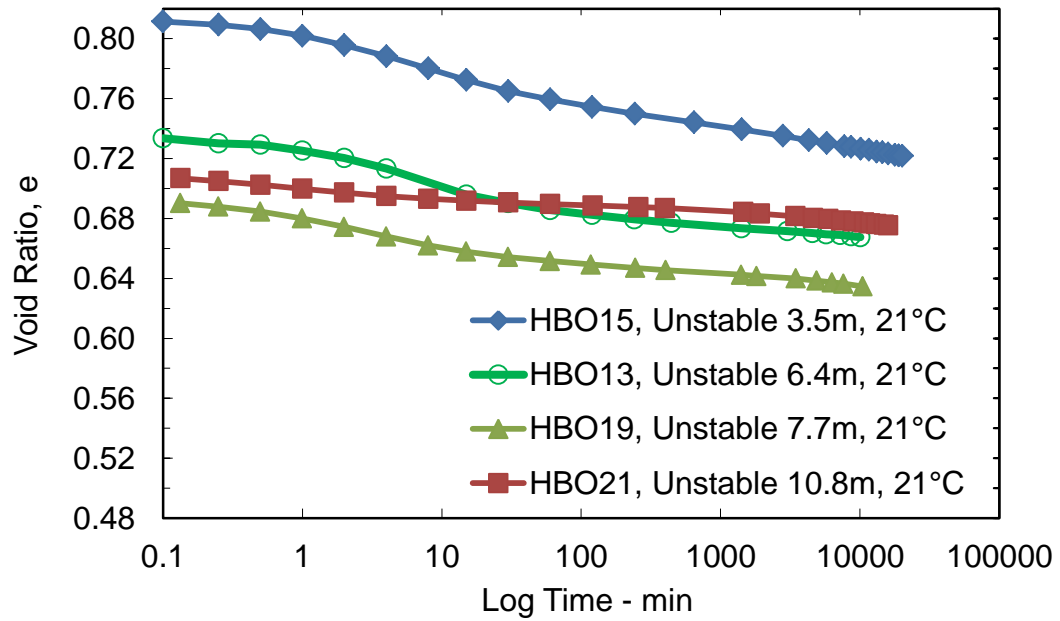
Figure 4.9: Void ratio versus log time for the tests carried out at 21°C on specimens from the stable and unstable sections, under a vertical applied stress of 1400kPa

127
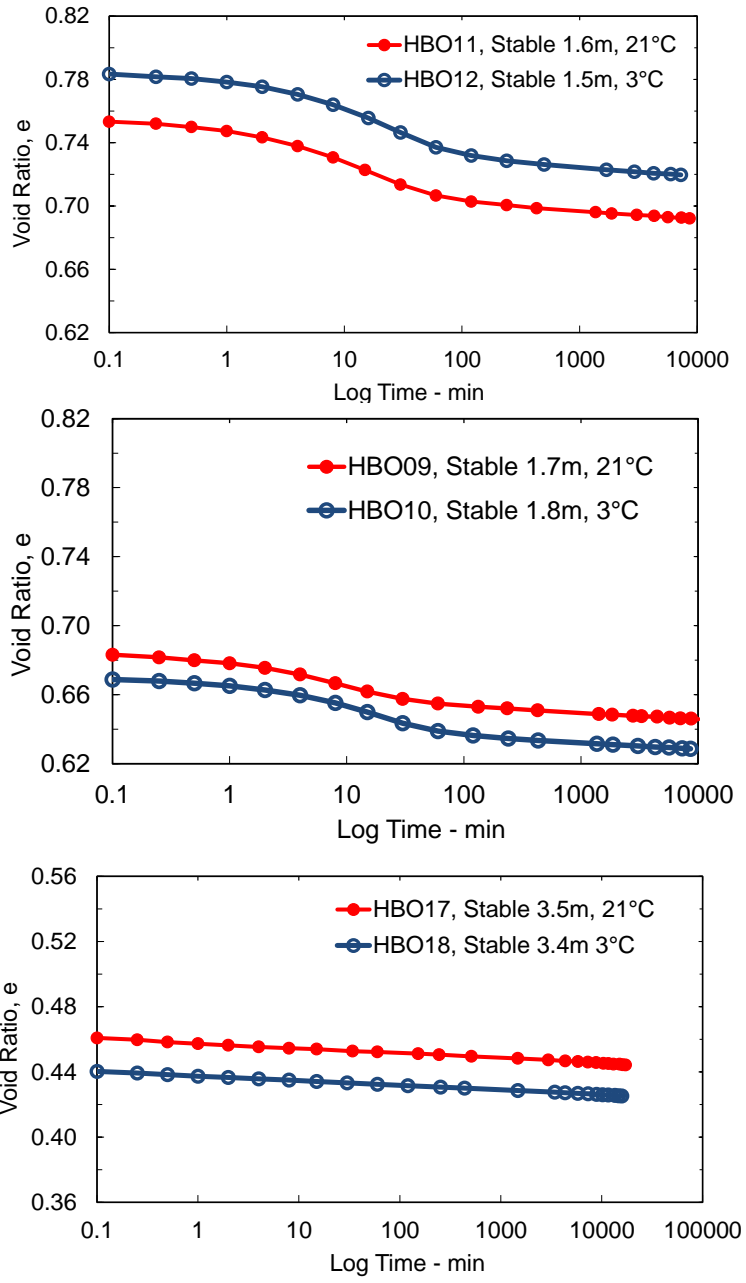
Figure 4.10: Void ratio versus log time for the tests carried out at 21°C and 3°C on specimens from the stable section, under a vertical applied stress of 1400kPa
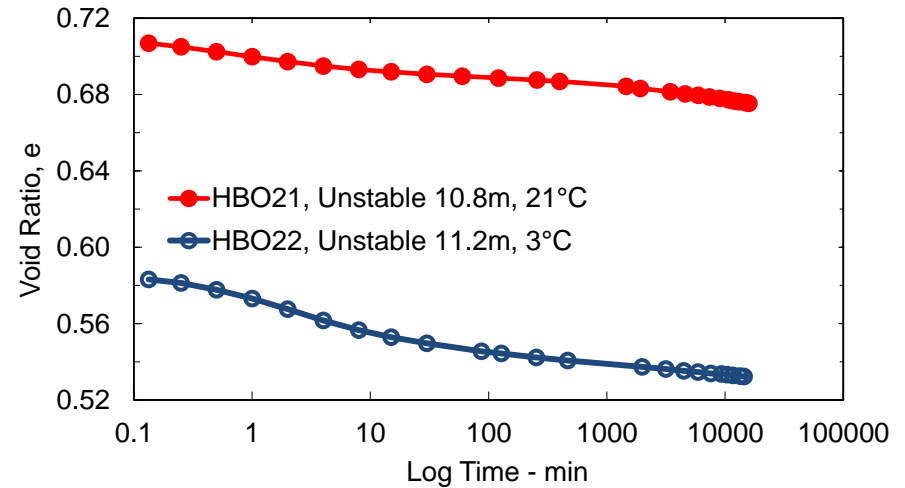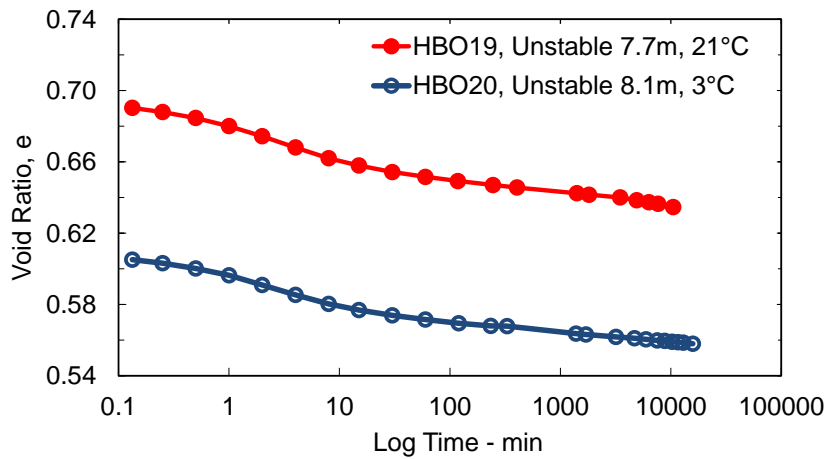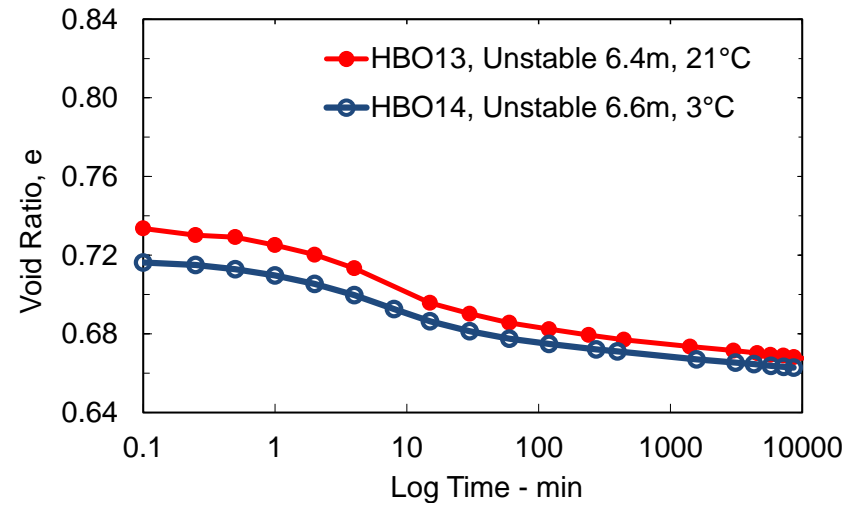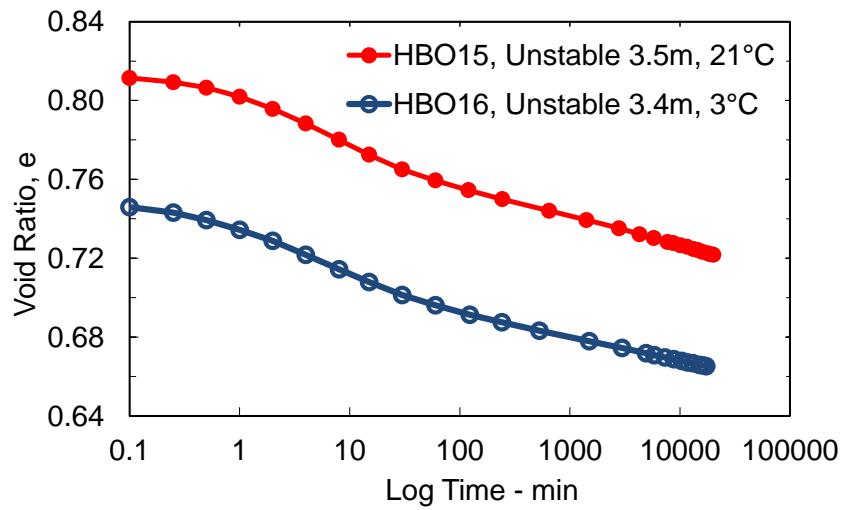
Figure 4.11: Void ratio versus log time for the tests carried out at 21°C and 3°C on specimens from the stable and

unstable sections, under a vertical applied stress of 1400kPa

Figure 4.12: Triaxial CIŪ apparatus
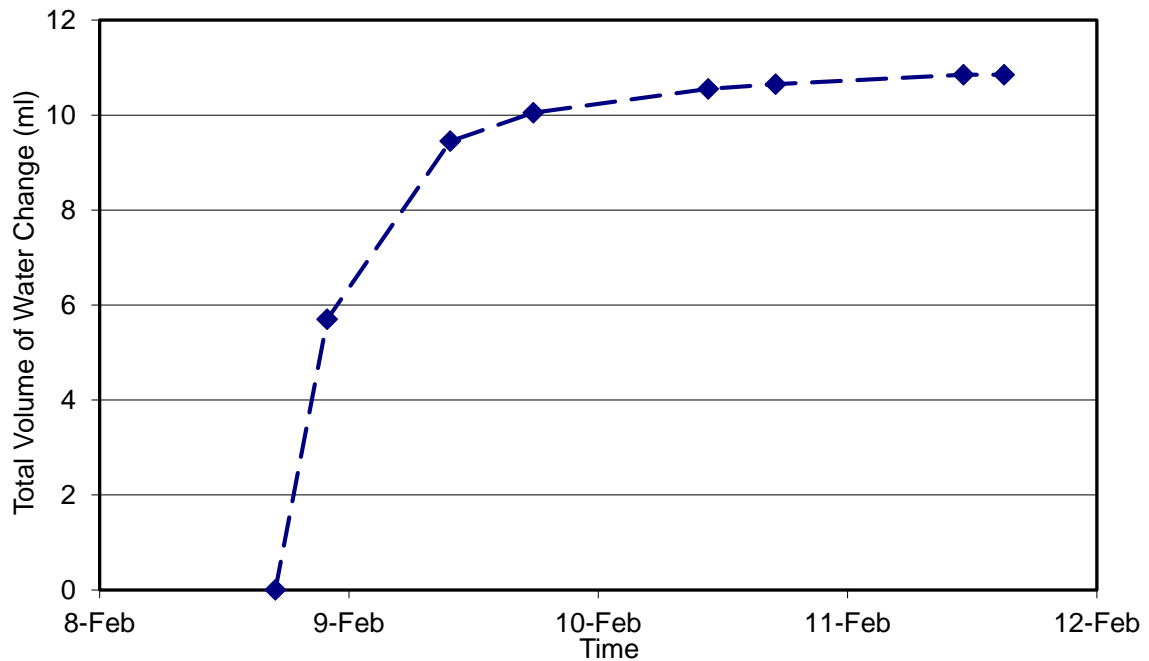
Figure 4.13: Example plot of total volume of water change versus time during

consolidation phase for HBT09
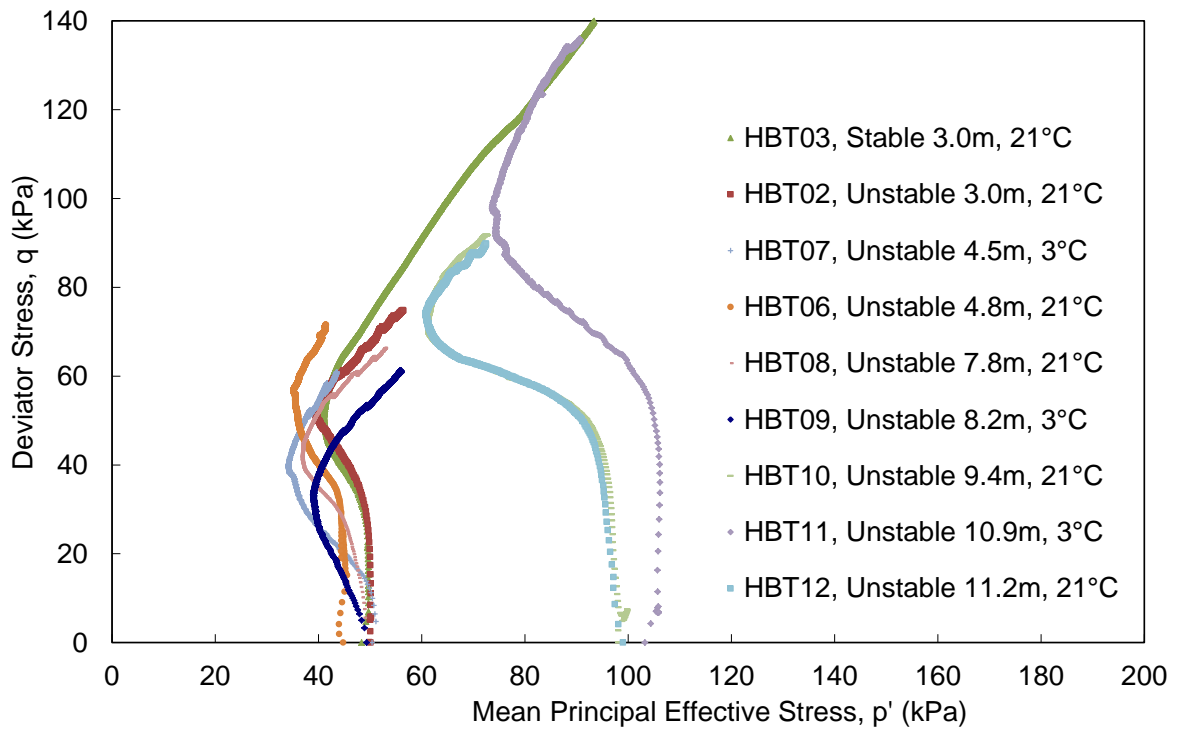
Figure 4.14: Plots of q vs p' for triaxial tests
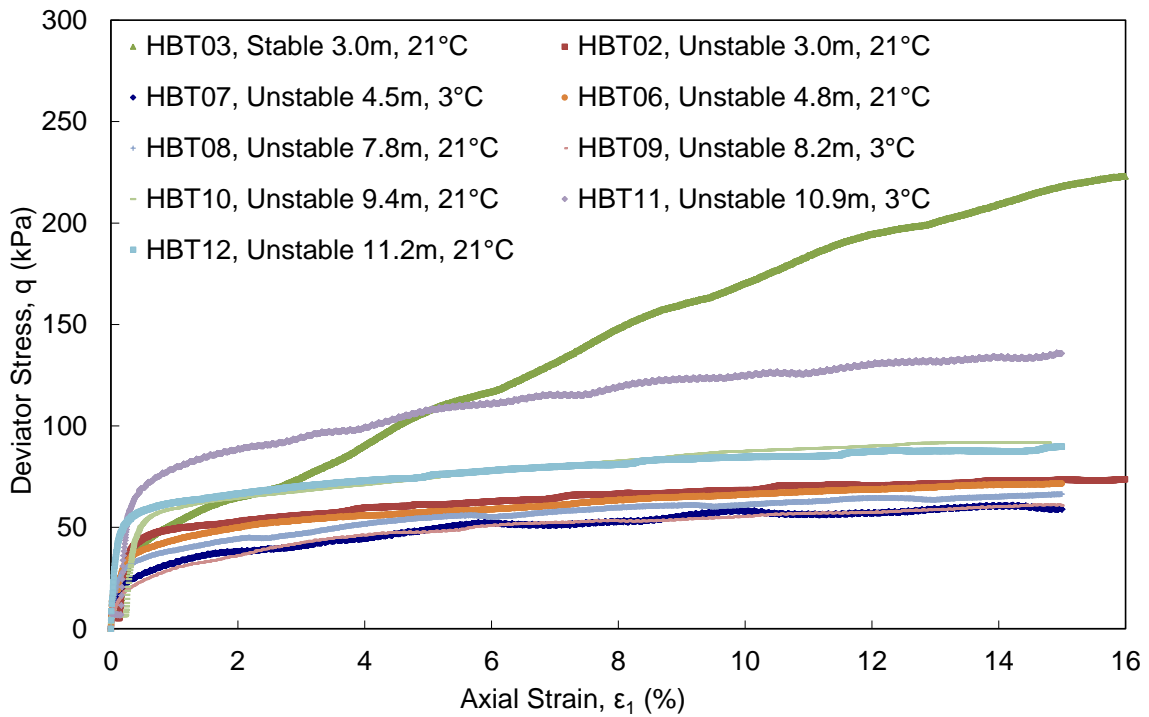
Figure 4.15: Plots of q vs ε_1 for triaxial tests

131

CHAPTER 5:   Data from Field Instrumentation

Instrument clusters were installed at the shoulder, mid-slope and toe of both the stable and unstable sections of the PR391 site embankment. (The details of instrumentations were discussed in Chapter 3.)   Data were collected from the instruments and analyzed during the first two years of operation, that is, over two freeze-thaw cycles.   The data include monthly temperatures from the thermistor strings at 1m intervals, surveyed results from the surface settlement plates and deep settlement gauges, lateral displacements measured by slope inclinometers and horizontal VW (Vibrating Wire) extensometers, and pore water pressures measured by the VW piezometers.   This chapter analyses the data and discusses the results. The results provide a better understanding of the deformations of the embankment, changes of temperature, changes of pore water pressure and flow in the ground.   A short overview of the material in this chapter was presented by (Batenipour et al. 2011).   Interpretation of the results will be discussed in Chapter 7.

5.1 Ground Temperature

Figure 5.1 and Figure 5.2 show the monthly temperature profiles for two cycles of cooling and heating between November 2008 and October 2010.   The two figures show data from thermistor strings at a) toe and b) mid-slope for the unstable and stable sections respectively.   Please note the different scales used for depths in

132

these figures. They arise from the different thicknesses of the foundation soils under the two sections, (Figure 3.6). The original ground level is at depth '0'.

The data in both figures start in early November for both years of cooling and heating cycles, when temperatures at shallow depths were already beginning to decrease with the onset of winter. Gradually, the low temperatures move deeper into the soil profile. Heating near the surface begins in mid-April and again moves slowly down the profile during summer and fall months until cooling begins again in late September.

The seasonal difference in temperature decreases with increasing depth in the ground. The depth of mean zero annual temperature amplitude (DMZAA) is the depth at which the seasonal variations of temperatures are essentially zero. Ground temperatures below this depth are not influenced by surface temperatures (Andersland & Ladanyi 2004). Figure 5.1a and b show that the depth of zero annual amplitude at the unstable section is about 8m - 9m below the ground level at the unstable section. The respective temperature profiles for the mid-slope and toe converge at about the same depth, although there is approximately a 1.6°C difference between the two values. The soil underneath the embankment is colder than soil at the same depth underneath the toe. It is believed that this can be explained by the previous presence and thawing of a frost bulb underneath the embankment or alternatively by differences in thermal conductivity between gravel in

the embankment and clay in the foundation soils. This observation could have been verified if thermistor strings had been installed under the centre of the embankment. Perhaps unfortunately, safety, snow clearing, and grading made this impossible. Cooler temperatures beneath the embankment may also be due to an insulating cover of snow beneath the toe, combined with the effects of snow clearing on the roadway. Figure 5.2a and b do not show the level of DMZAA at the stable section. The bedrock was encountered at 4m depth. Thermistor strings were not installed into the bedrock.

Figure 5.3 and Figure 5.4 show plots of temperature versus time (here shown as date) at different depths for the unstable and stable sections respectively. As expected, the figures show, perhaps more clearly than Figure 5.1 and Figure 5.2, that the seasonal variations in temperature decrease with depth. The dates of the maximum and minimum values shift towards later dates with increasing depth. The temperatures in the active layer (about 1m - 2m below the ground level) stay below 0°C for about five months from November to May.

Figure 5.5 and Figure 5.6 show minimum, average, and maximum temperature profiles with depth for the unstable and stable sections respectively, for years 2008-09 and 2009-10. As in Figure 5.1 to Figure 5.4, results are shown for the thermistor strings at both the toe and mid-slope of the two sections.

The geothermal gradient is the rate of change of temperature with depth in the ground. When average temperatures are examined in this way, the slope of the average temperature profile can be taken as an approximate indicator of net heat flow into, or out from, the ground surface over a period of one year. Figure 5.5 and Figure 5.6 include the average temperature profiles over two years at the four instrumented locations, that is at the toes and mid-slopes of the two test sections. The average temperatures at all four locations decrease with increasing depth. This indicates a net heat flux into the foundation soils and warming of the ground surface. It is important to note, however, that this observation is based on only two years of temperature readings. Future collection and analysis of temperature data will provide a better understanding of the annual temperature changes in the ground.

The minimum temperature profiles in Figure 5.5 and Figure 5.6 show that no sub-zero temperatures were observed below the active layer during 2008-09 and 2009-10. It supports the observations in an earlier section that initially frozen soil has thawed during the lifetime of the soil - there has been general warming of the embankments and their foundations.

5.2 Displacement Data

The following two sections discuss the results and analysis of the displacement data of the embankment collected during the two years of data monitoring. The displacements include the vertical and horizontal movements measured by

135

surveying the surface settlement plates and deep settlement gauges, and the lateral movements measured by slope inclinometers and VW extensometer. It will be remembered from Chapter 3 that surveying of the displacement instruments only began in June 2009.

5.2.1 Movements Measured by Settlement Plates and Gauges

Figure 5.7 and Figure 5.8 show displacements of surface settlement plates in both the stable and unstable sections at the shoulder of the road, at mid-slope, and at the toe of the embankment. Vertical movements are shown as elevation changes in Figure 5.7, and horizontal movements perpendicular to the centreline of the road in Figure 5.8.

Figure 5.7 shows the vertical movements at the shoulder, mid-slope and toe of the two sections. Both sections show seasonal movements that are largely, but not completely recoverable. The seasonal heaves seen in Figure 5.7 are believed to be frost heave. (The concept of frost heave is discussed in Chapter 2, Section 2.4.) The toe of the embankment shows the highest amount of frost heave during the freezing season, while the shoulder shows almost no frost heave, probably due to the gravel fill on the shoulder. Gravel can be considered to be a non-frost susceptible material (Koyama & Sasaki 1967). It drains freely by gravity and does not lead to upward movement of capillary moisture.

There appears to be little cumulative vertical movement at the stable section. In contrast, there has been about 0.15m of non-recoverable cumulative settlement at the shoulder of the unstable section.

The lateral movements at the ground surface (again from the surface settlement plates) in Figure 5.8 shows somewhat similar trends, though seasonal effects are perhaps only apparent at the toes of the embankments. All movements are away from the centreline of the embankment. Again, the stable section did not move much in the two years of observation – the scatter in the data is probably about equal to the precision of the observations. All three plates at the unstable section show cumulative movements, about 0.07m at the shoulder and mid-slope, and 0.03m at the toe.

Figure 5.9 shows the vertical movements of deep settlement gauges underneath the mid-slope at the original ground level, and underneath the toe of the stable and unstable sections at depths of about 4m and 7m respectively. A frost heave of about 0.04m can be seen underneath the mid-slope of the stable section. In contrast, no frost heave is observed underneath the mid-slope of the unstable section. This could be due to the existence of more gravel in the materials of the fill embankment at the unstable section (see Figure 3.6). There is also about 0.10m of nonrecoverable cumulative settlement underneath the mid-slope of the unstable

section.   No significant vertical movement (frost heave or nonrecoverable displacements) is experienced beneath the toes of the stable and unstable section.

5.2.2 Lateral Displacements

Vibrating wire (VW) extensometers with a gauge-length of 1.0m were installed at the toes of both test sections at a depth of 0.8m.   The instruments were intended to monitor lateral deformations at shallow depths and hopefully to relate movements at the toe to lateral spreading and longitudinal cracking of the road surface.   As previously mentioned in Chapter 3, the extensometer at the stable section failed shortly after installation.

Figure 5.10 shows horizontal strains at the toe of the unstable section plotted against time (here shown as date) over a 28 month period in 2008-2011.   The results show ongoing outward displacements, with about 0.80% horizontal strains at the toe of the unstable section over a period of 28 months.   Figure 5.10 indicates fairly rapid deformation rates during the first freezing season (November 2008 to June 2009).   This may be due to natural re-densification of soil around the extensometer following installation.   After the first year, from July 2009 to April 2011, the rate of horizontal straining decreased.

The slope inclinometers were installed beneath the toes of the embankment at both sections. Figure 5.11 shows cumulative displacements measured by the slope inclinometer at the toe of the stable and unstable sections. As expected, the lateral movements beneath the toe of the stable section are small. The figure shows that the inclinometer at the toe of the unstable section, experienced lateral displacements away from the centre of the embankment at depths greater than about 3m. Maximum displacement of about 0.01m occurs at a depth of 8m. At shallower depths, the slope inclinometer moved back towards the centre of the embankment. This is believed to be due to the rearwards bending of the slope indicator casing, an experience that has been observed in other local projects.

In general, the combined surface and deep measurements of displacements show that the cumulative movements of the embankment are largely downward at the shoulder and smaller at the toe. The resulting shear stresses push the lower levels of clay horizontally away from the centre of the embankment at greater depths.

5.3 Ground Water Data

The standpipe piezometers were installed at the toe of the stable and unstable sections to monitor the water level in the ground. The collected data during the summer months show that the water level at the toe of the embankment is almost at the ground surface. The groundwater levels during summer months varied by about

0.6m at the stable section and by about 0.3m at the unstable section. No readings were taken during the freezing months (from October till April) of both years of data collection because the water inside the standpipes was frozen.

Vibrating wire (VW) piezometers were installed at the toes of both the stable and unstable sections to monitor pore-water pressures at two different depths beneath the embankment. Figure 5.12 shows total heads plotted against time (indicated here as date) in the stable and unstable sections respectively. (Remember that the silty clay is much thicker beneath the unstable section, see Figure 3.6.) There is significantly more variability in total heads during summer months at the stable section than the unstable section. The variability approaches 1m and is broadly similar to what was seen in the standpipes. The differences between the pore water pressure patterns at the stable and unstable sections may be due to small differences in local drainage at the two sections. More importantly, the figures imply seasonal changes in the gradients of total head at both sections. This is most clearly seen in the data from the unstable section in Figure 5.12b. Ground water conditions appear to be broadly hydrostatic during summer months, with the ground water level approximately at the ground surface. During freezing, upwards gradients develop. These are believed to be caused by upward flow of water towards suction pressures (negative potentials) at the freezing front as it moves downwards during the winter.
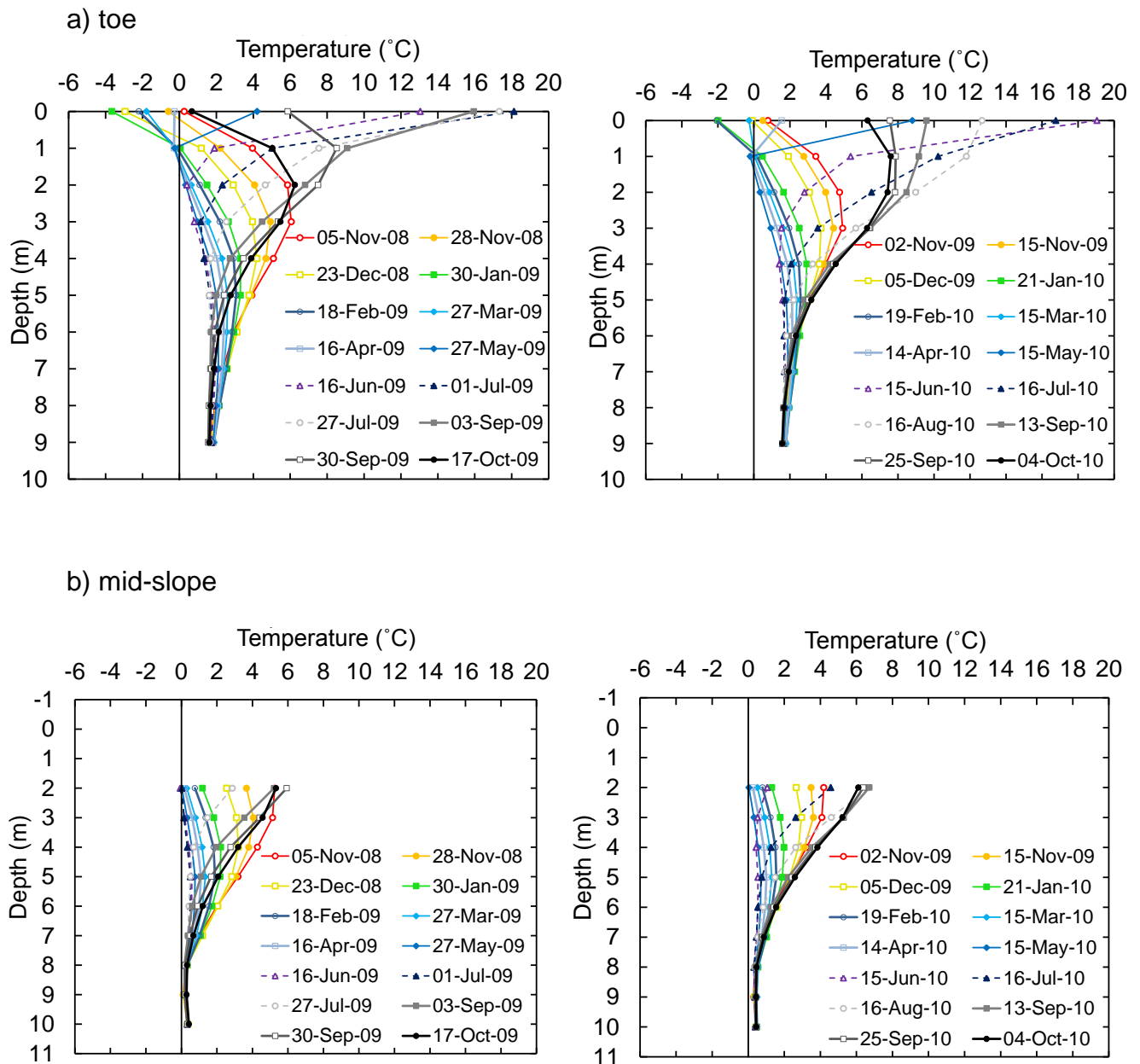
a) toe

b) mid-slope

Figure 5.1: Monthly temperature profiles between November 2008 and October 2010 for the unstable section at the a) toe; and b) mid-slope.
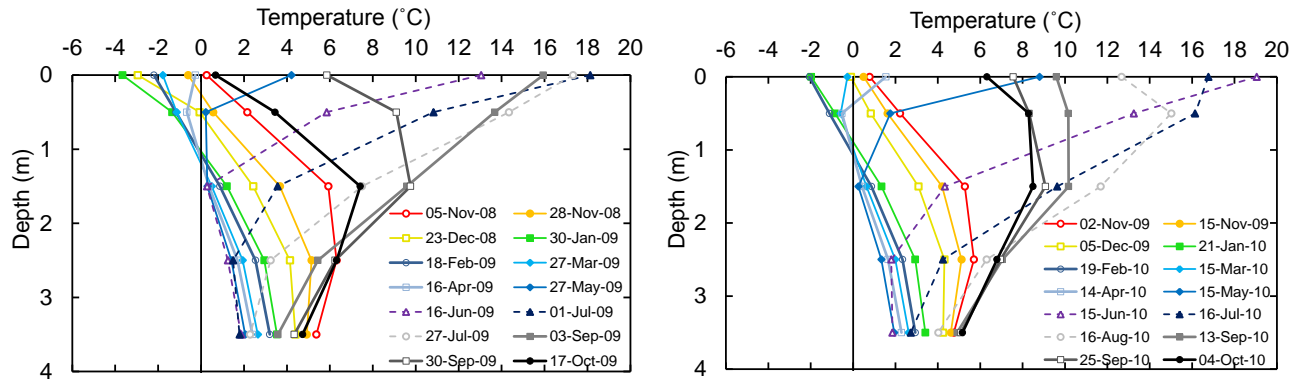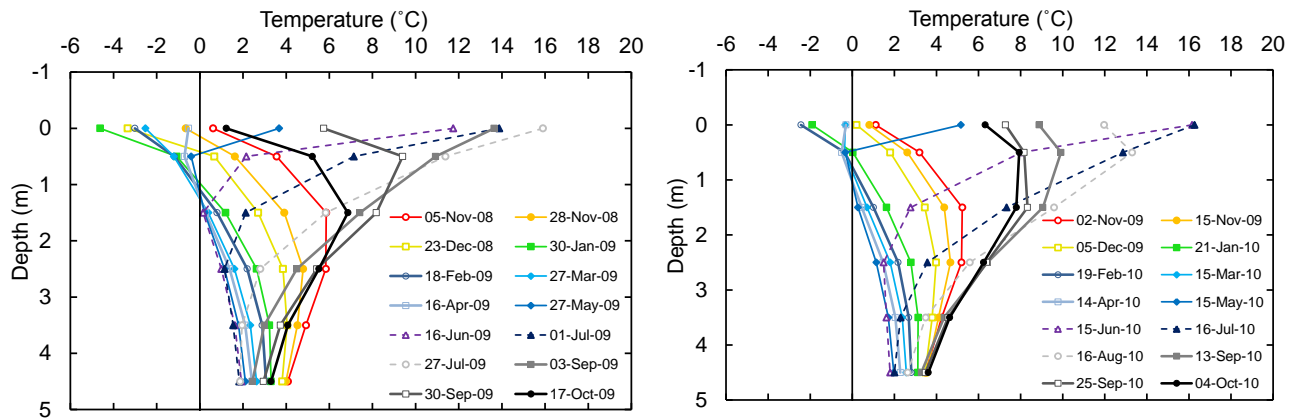
a) toe

b) mid-slope

Figure 5.2: Monthly temperature profiles between November 2008 and October 2010 for the stable section at the a) toe; and b) mid-slope.
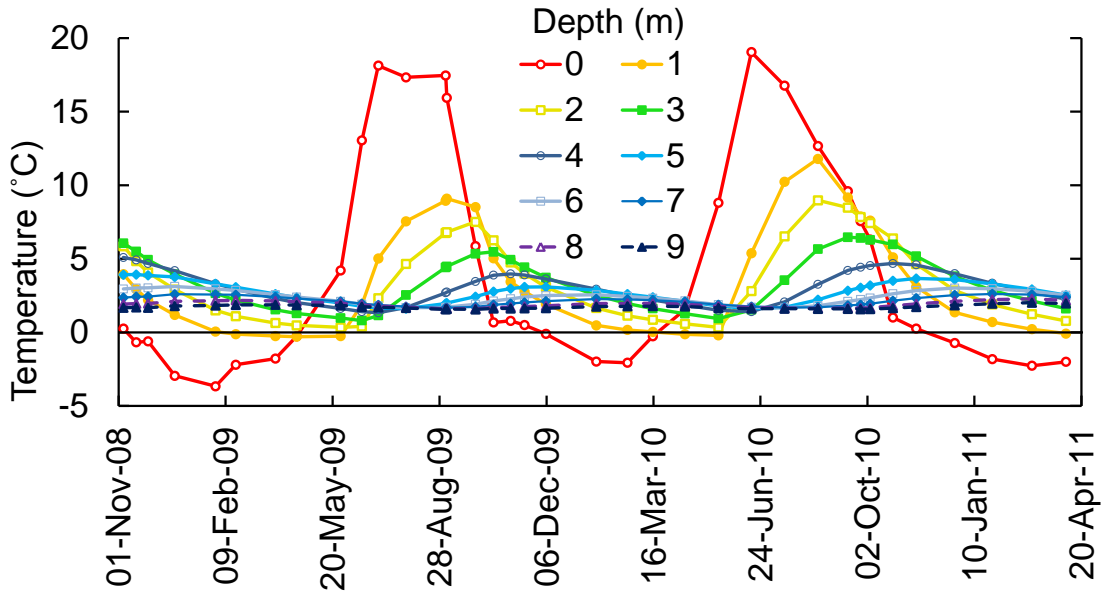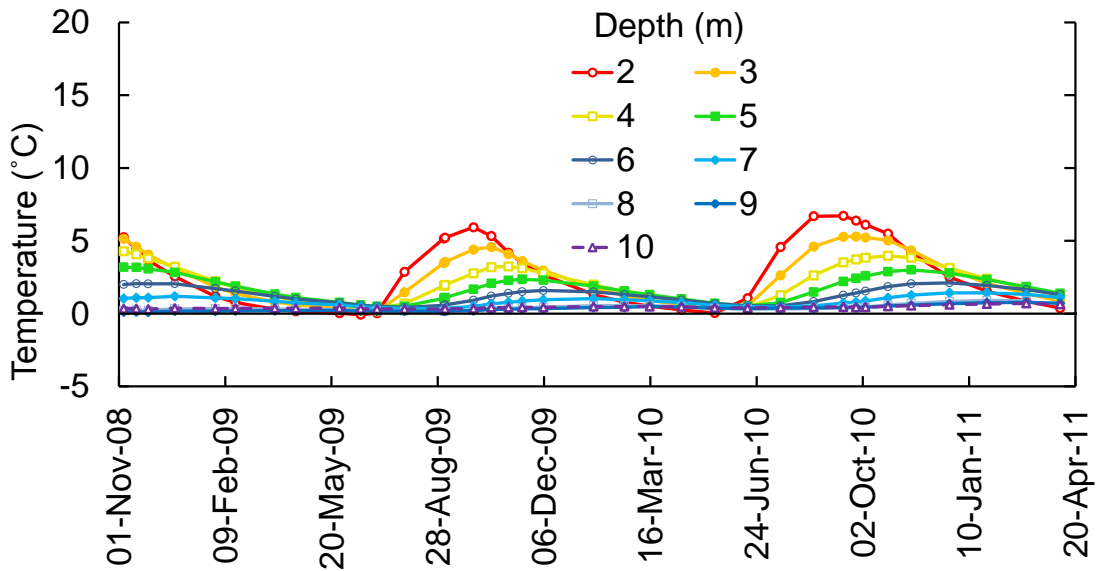
a) toe

b) mid-slope

Figure 5.3: Temperature vs. time at different depths for the unstable section at the a) toe; and b) mid-slope.
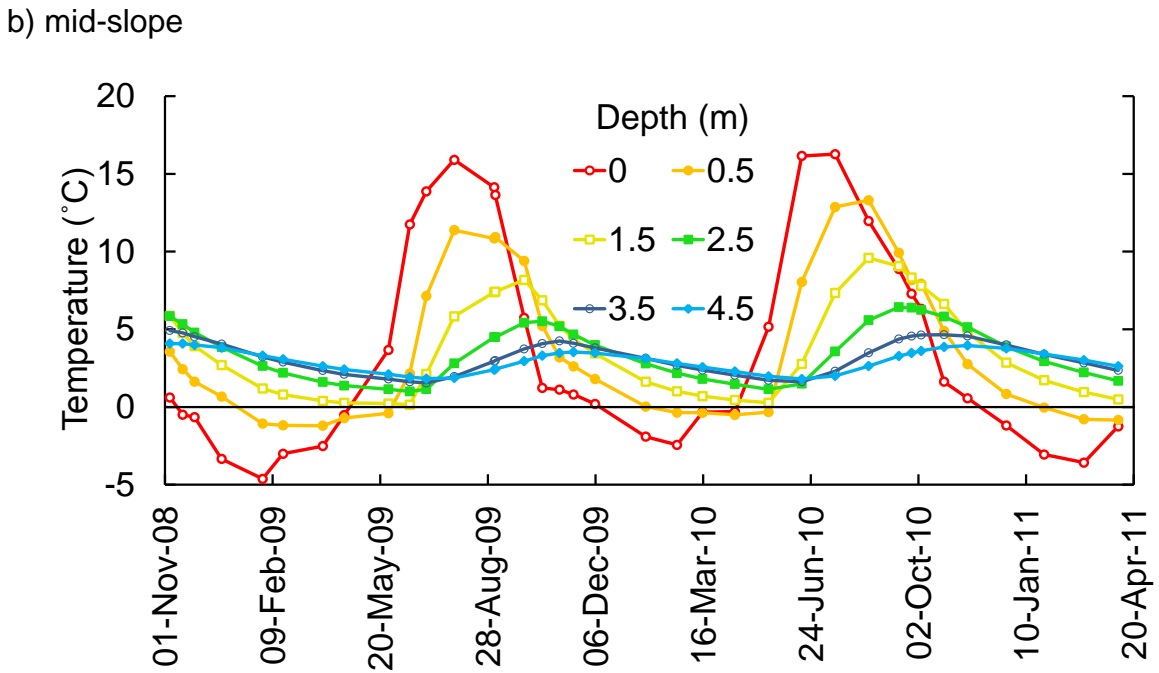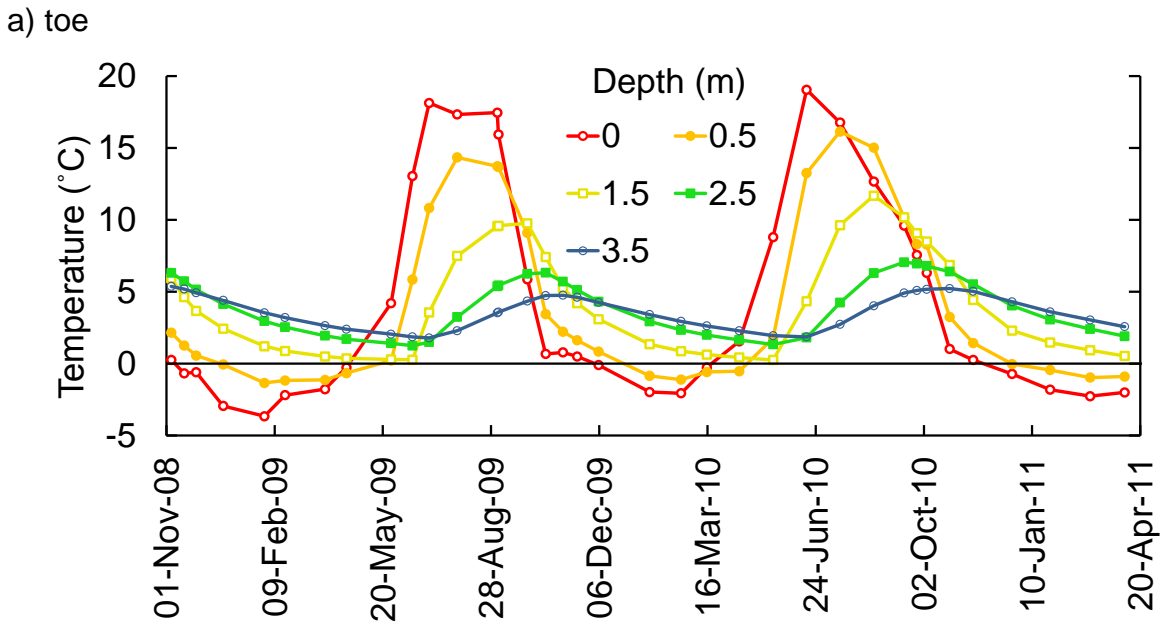
a) toe

b) mid-slope

Figure 5.4: Temperature vs. time at different depths for the stable section at the a) toe; and b) mid-slope.
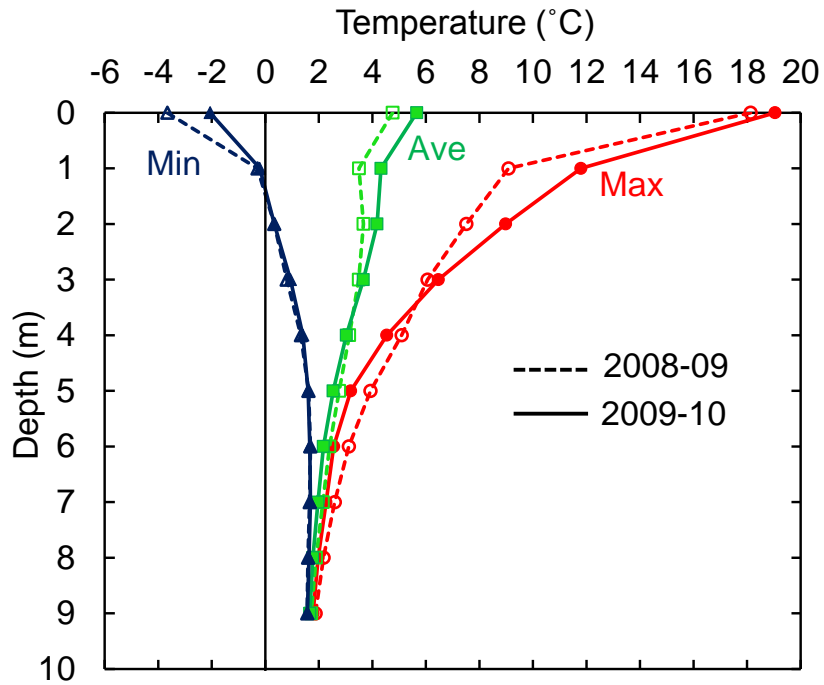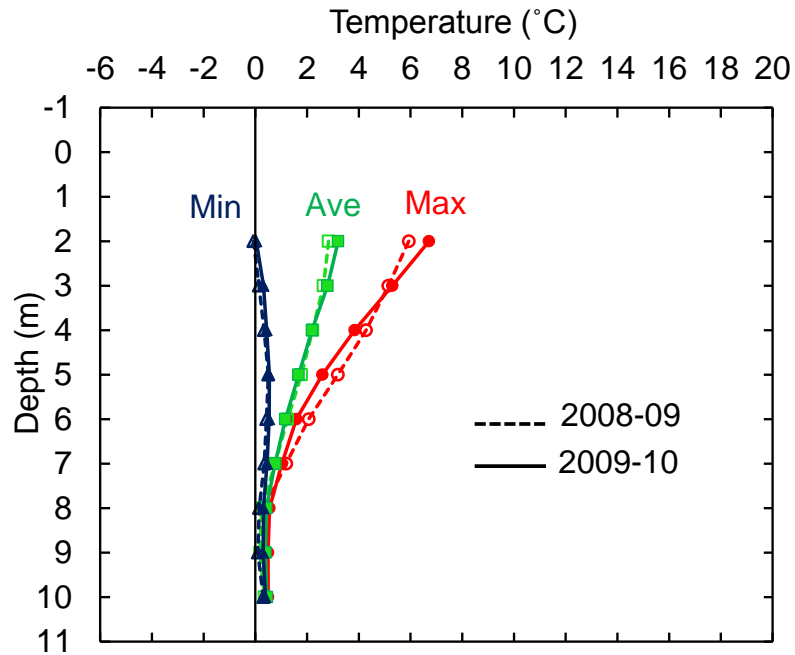
a) toe

b) mid-slope

Figure 5.5: Annual temperature envelopes between November 2008 and October 2010 for the unstable section at the a) toe; and b) mid-slope.
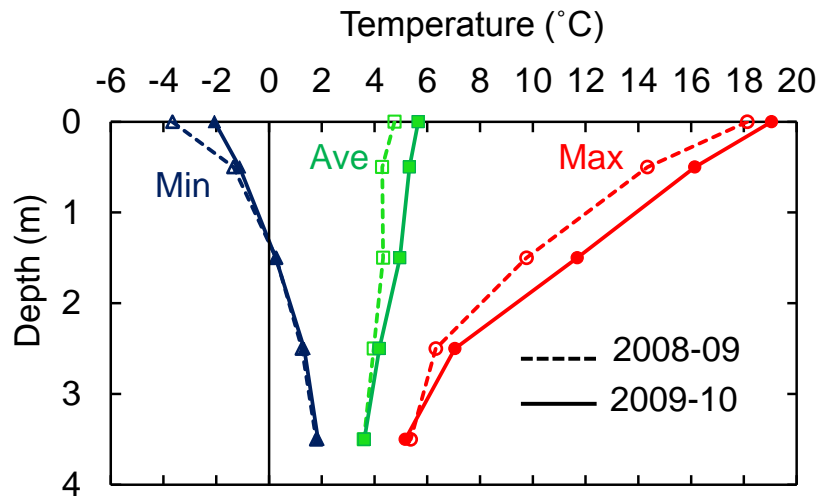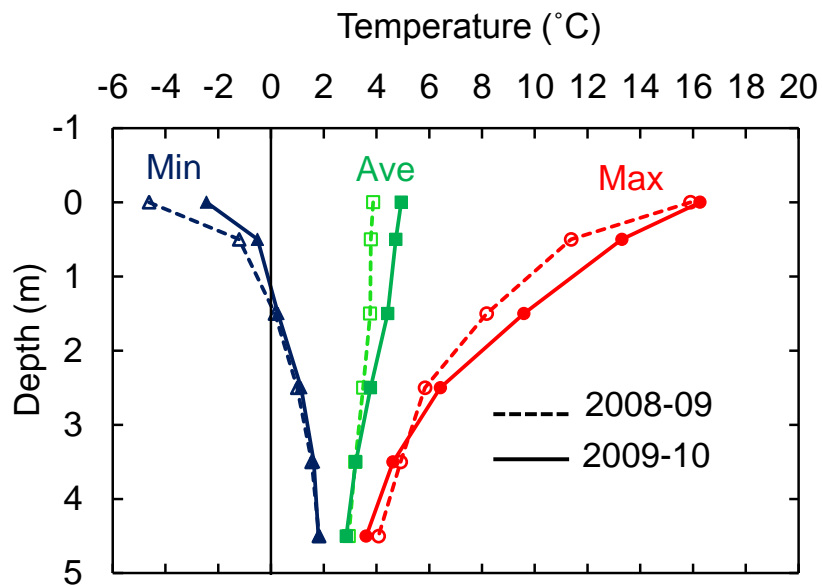
a) toe

b) mid-slope

Figure 5.6: Annual temperature envelopes between November 2008 and October 2010 for the stable section at the a) toe; and b) mid-slope.
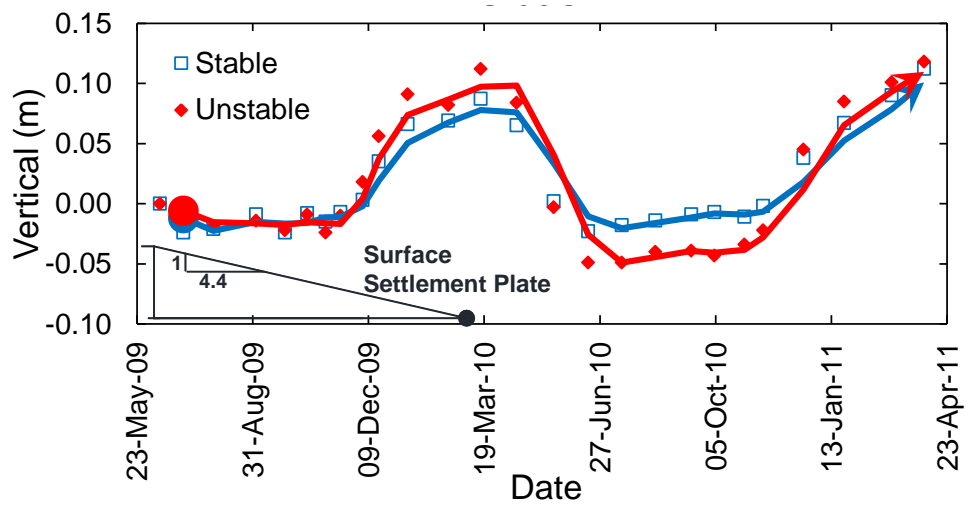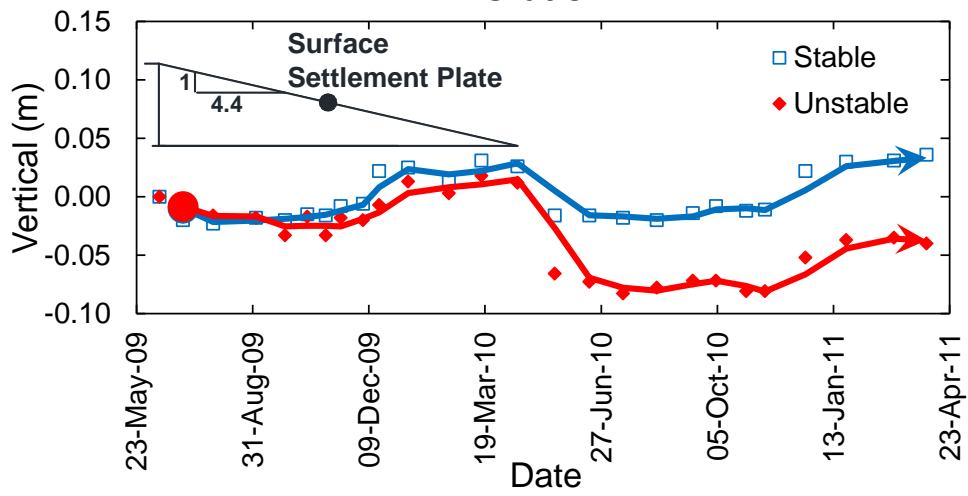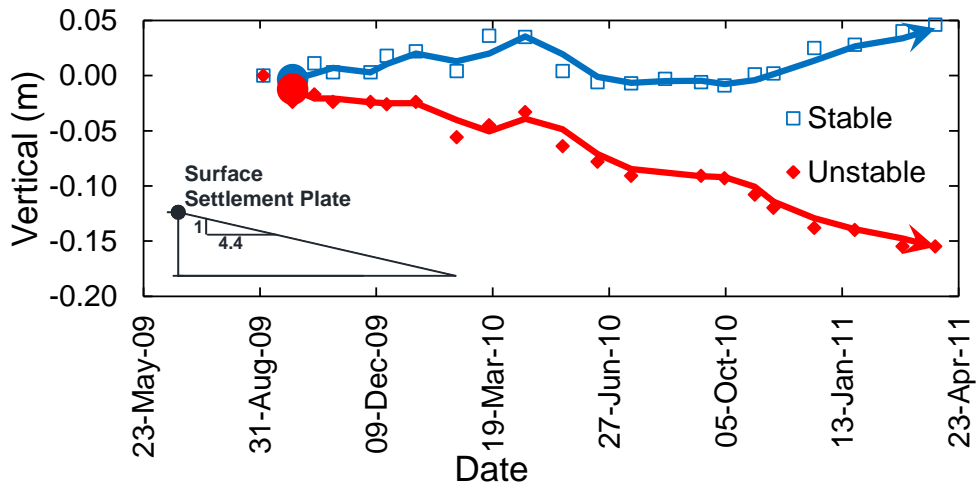
Figure 5.7: Vertical movements (settlements) at shoulder; mid-slope; and toe of the embankment.
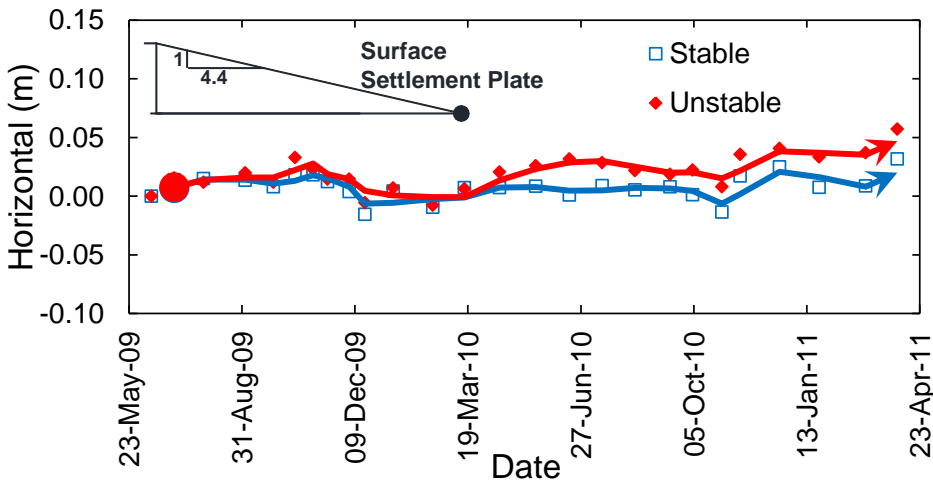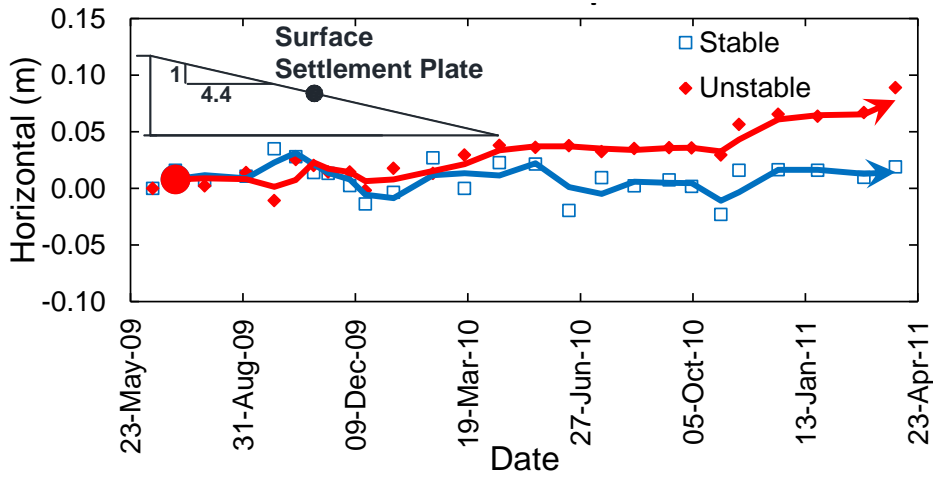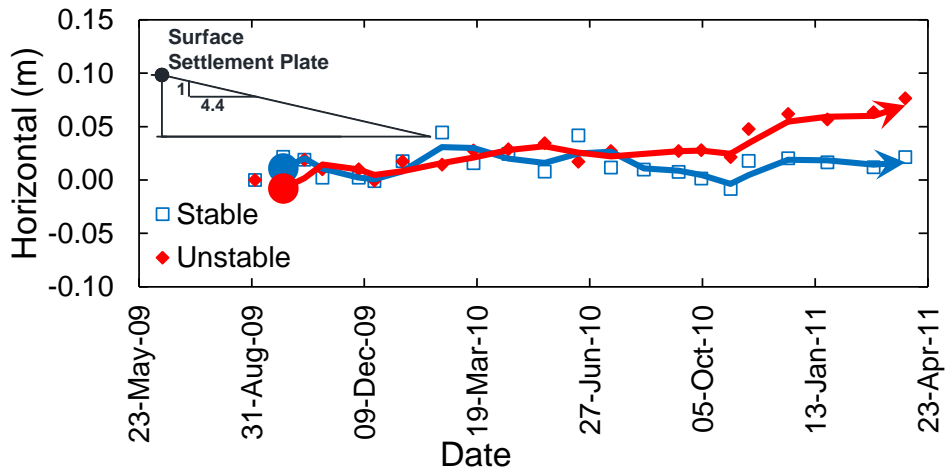
Figure 5.8: Horizontal movements in downslope direction at shoulder; mid-slope; and toe of the embankment.

148
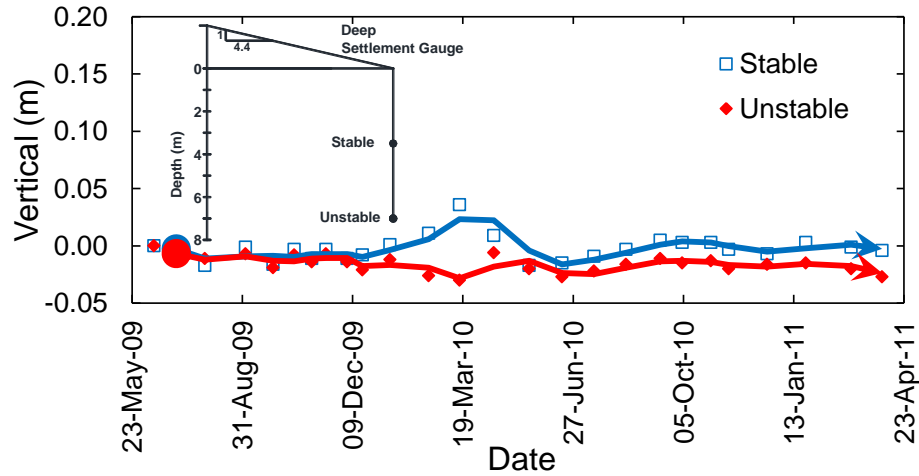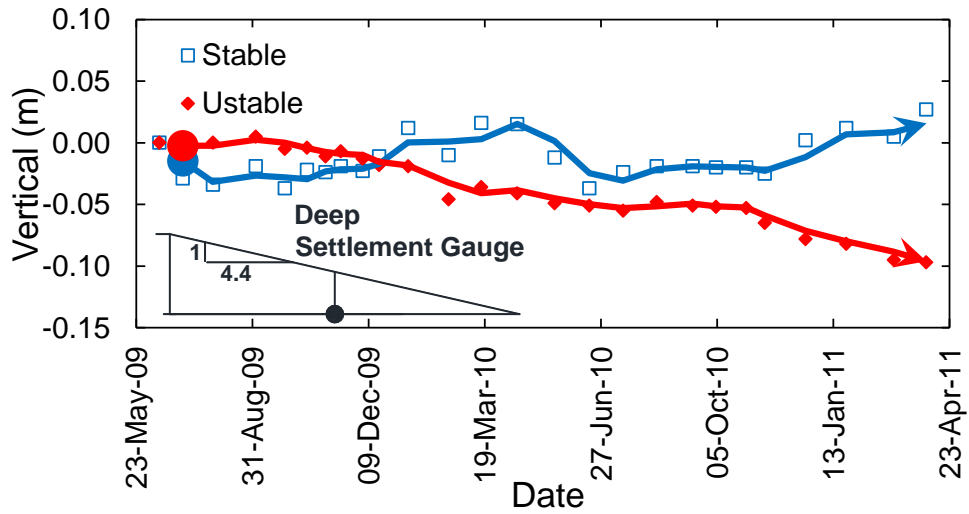
Figure 5.9: Vertical movements (settlements) at deeper locations at mid-slope; and toe of the embankment.
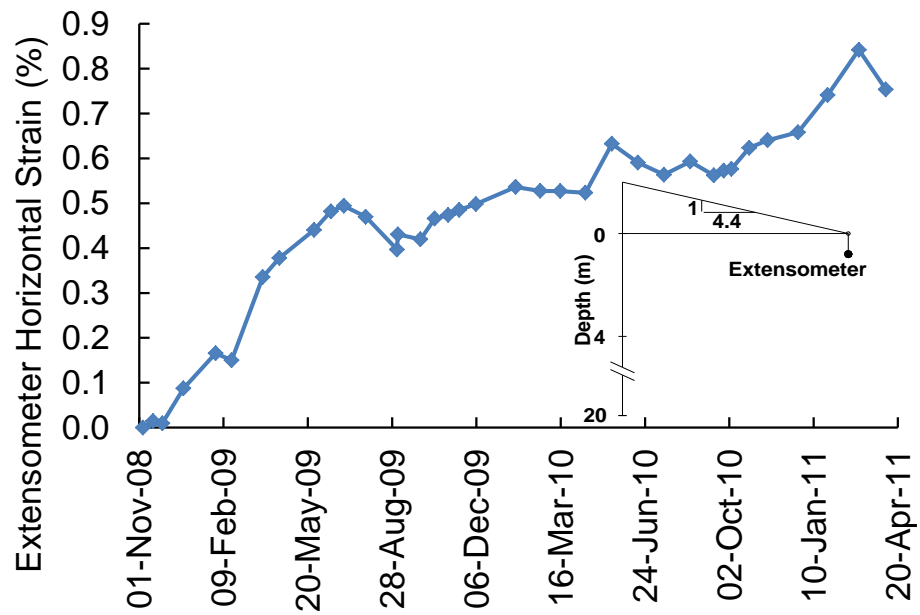
Figure 5.10: Extensometer horizontal strain vs. time at 0.8m depth at the toe of the unstable section.

a) stable section
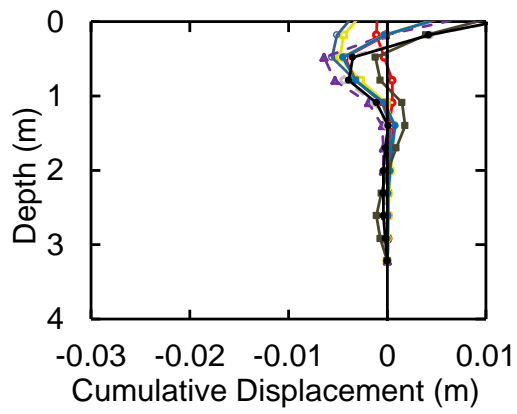
b) unstable section
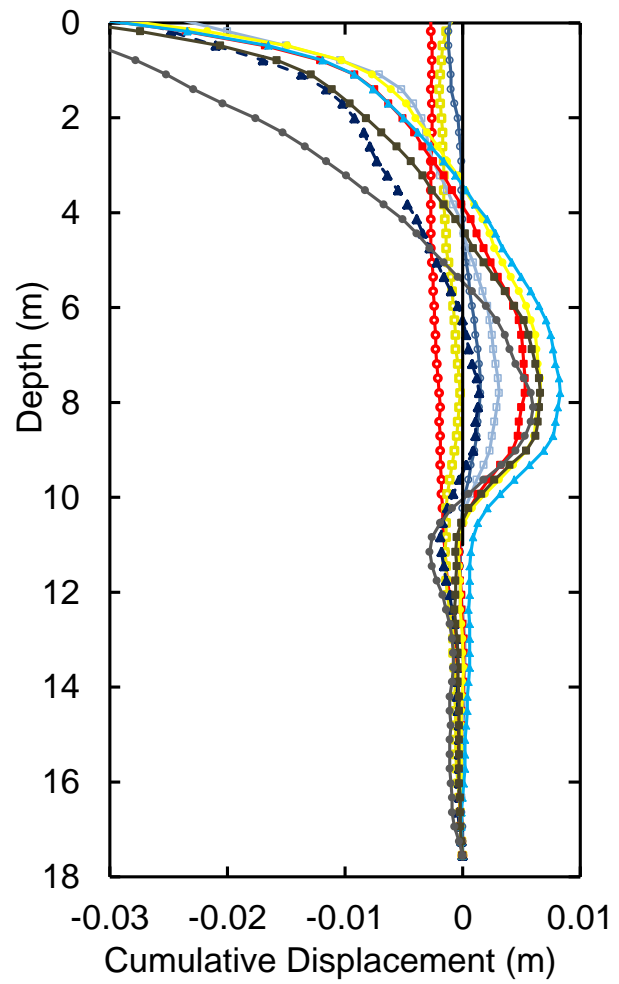
Legend:
- 19-Jun-09
- 27-Jul-09
- 30-Sep-09
- 21-Jan-10
- 15-Mar-10
- 15-Jun-10
- 16-Aug-10
- 04-Oct-10
- 16-Nov-10
- 26-Jan-11

Figure 5.11: Slope Inclinometer at the toe of the a) stable section; and b) unstable section.
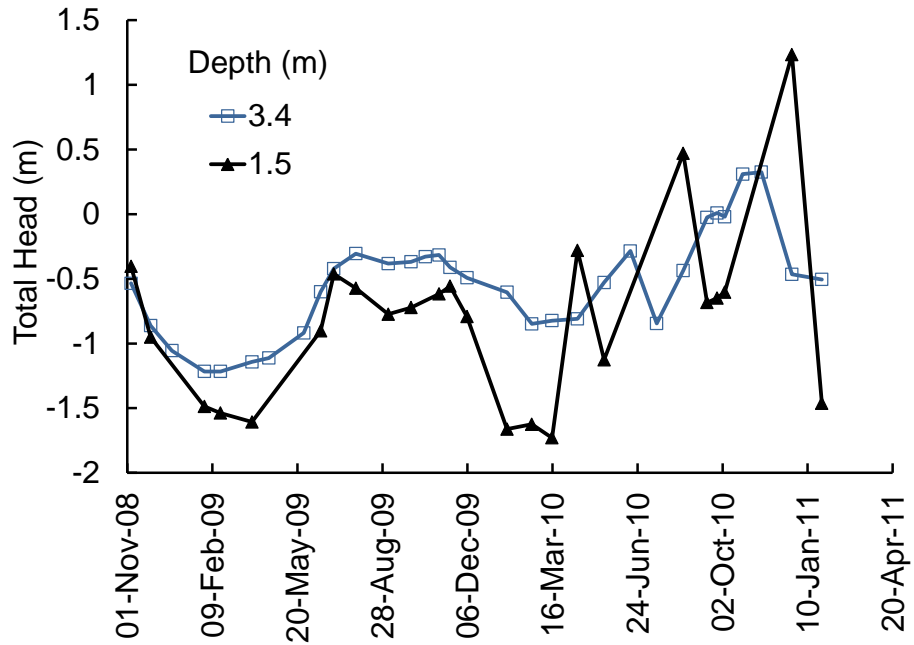
a) stable section
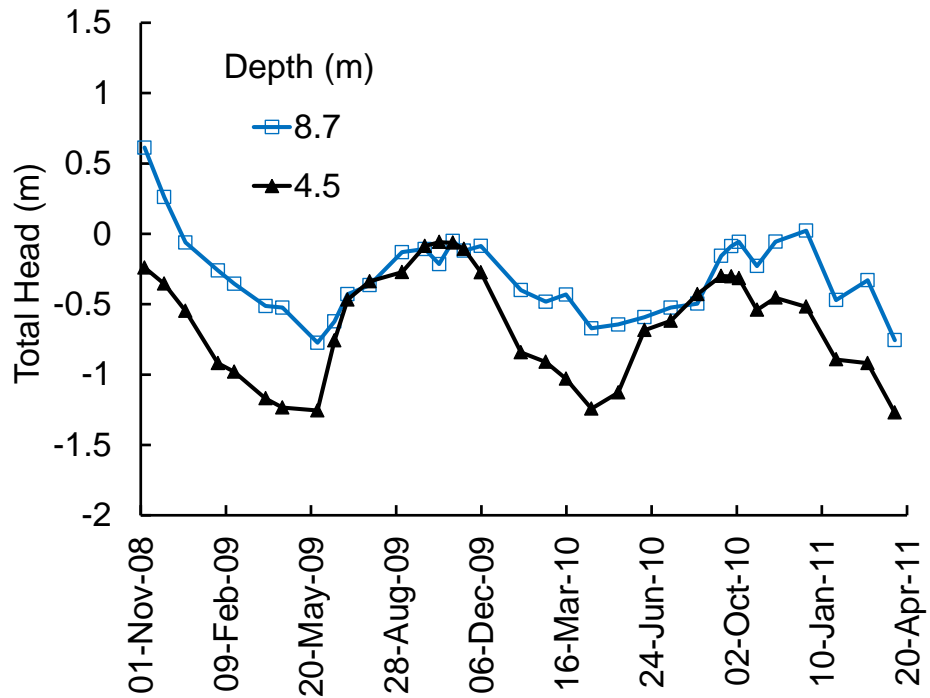
b) unstable section

Figure 5.12: Total head vs. time at different depths at the toe of the a) stable section; and b) unstable section.

CHAPTER 6:   Thermal Modelling and Frost Heave Prediction of PR391

Numerical modelling of the PR391 embankment has been developed to simulate the thermal changes and frost heave characteristics of the embankment. The approach used can also be used for other embankments. Thermal conductivity values of the soil from the PR391 test site embankment were measured in the laboratory and used as an input in the thermal modelling. Thermal conductivities of samples from PR391 were measured by the author's colleague and fellow Ph.D. student Mr. David Kurz and undergraduate summer student Mr. Graham Bartley, with some participation by the author. The results of these tests were then used by the author to analyse thermal conditions in the embankment as related to frost heaves, and specifically to develop a field value of segregation potential (SP).

The thermal modelling permitted simulation of temperature changes under the embankment. These simulated temperature changes provide an understanding of the behaviour of the foundation soil and allow calculation of frost heaves of the embankment. A second aspect of this modelling is the application of the frost heave approach known as the segregation potential (SP) method (Konrad & Morgenstern 1982) to field conditions. The goal of this portion of the work is to back-calculate

segregation potentials from the site observations and collected frost heave data by using the SP method, and to compare the results with other published results.

This chapter explains the thermal modelling, procedures for evaluating segregation potential, and analysis of the results. The interpretation of the results will be discussed in Chapter 7. All the modelling data, including the modelling files, calculations and spreadsheets, are included on the CD attached to this thesis (see Appendix A).

6.1 Thermal Modelling for PR391

Thermal modelling of the PR391 embankment used the commercially available software product TEMP/W (Geo-slope 2010). It is a finite element software code that can be used to model thermal changes in the ground due to environmental changes, or due to the construction of facilities, such as roads, buildings or pipelines. TEMP/W can simulate the real and physical process of heat flowing through a fully or partially saturated, frozen or thawed, particulate or solid medium.

6.1.1 Theory Used in Thermal Modelling

The principal mechanism for heat flow in soils is conduction (Andersland & Ladanyi 2004). This is the flow of heat by the passage of energy from one soil particle to another or through soil pore fluids. TEMP/W assumes that the heat flux (q) is

proportional to the thermal conductivity (k) and the temperature gradient ($\partial T/\partial x$), as in Fourier's law:

Equation 6.1 $\qquad q_i = -k_i \dfrac{\partial T}{\partial x}$

where T = temperature, and x = distance. The negative sign in Equation 6.1 indicates that the temperature decreases in the direction of increasing x; that is, the heat flows in the direction from high temperature to low temperature.

The symbol of thermal conductivity (k) was given as λ in Section 2.4.4.

The governing differential equation used in the formulation of TEMP/W is (Geo-slope 2010):

Equation 6.2 $\qquad \dfrac{\partial}{\partial x}\left(k_x \dfrac{\partial T}{\partial x}\right) + \dfrac{\partial}{\partial y}\left(k_y \dfrac{\partial T}{\partial y}\right) + Q = \lambda \dfrac{\partial T}{\partial t}$

where k_x = thermal conductivity in the x-direction, k_y = thermal conductivity in the y-direction, Q = applied boundary flux, λ = capacity for heat storage or heat capacity, and t = time.

This equation states that the difference between the heat flux entering and leaving an elemental volume of soil at a point in time is equal to the change in the stored

heat energy.   Under steady-state conditions, the flux entering and leaving an elemental volume balances the volumetric term. The right side of the Equation 6.2 is equal to zero:

Equation 6.3
$$\frac{\partial}{\partial x}\left(k_x \frac{\partial T}{\partial x}\right) + \frac{\partial}{\partial y}\left(k_y \frac{\partial T}{\partial y}\right) + Q = 0$$

In general, the heat capacity (λ) is composed of two parts. The first part is the volumetric heat capacity of the material (frozen or unfrozen) and the second part is the latent heat associated with heat being released or absorbed when there are phase changes between solids, liquids, and gases. In equation form:

Equation 6.4
$$\lambda = C + L\theta \frac{\partial \theta_u}{\partial T}$$

Where C = volumetric heat capacity of the material, θ = Volumetric water content at the initiation of freezing, L = Latent heat of freezing of water (334J/g), and $\partial\theta_u/\partial T$ = change in unfrozen water content of the soil with temperature.

Substituting λ in Equation 6.2 leads to the complete differential equation:

Equation 6.5
$$\frac{\partial}{\partial x}\left(k_x \frac{\partial T}{\partial x}\right) + \frac{\partial}{\partial y}\left(k_y \frac{\partial T}{\partial y}\right) + Q = \left(C + L\theta \frac{\partial \theta_u}{\partial T}\right)\frac{\partial T}{\partial t}$$

Equation 6.5 is applied to every node in a finite element domain to account for the change in temperature in a transient analysis.

6.1.2 Input Parameters and Boundary Conditions

Figure 6.1 shows the cross section, materials and finite element mesh at the stable and unstable sections. Symmetry was assumed at the centreline of the embankment to maximize computing efficiency. Since the model was set up to be symmetrical around the centreline, the influence of the north-facing or south-facing slopes has not been considered. The direction the slope is facing is important if the question of insolation, that is, the duration and direction of the sun's rays, is being studied.

The finite element meshes shown in Figure 6.1 are primarily made up of 4-node elements with some triangular elements in zones of transition between materials. They have the global element size of 0.25m. The mesh is more detailed in the upper part of the model domain to account for the greater variations of temperature near the surface.

The materials of the model were selected in a way to simulate the materials present at the stable and unstable sections of the PR391 embankment. The model has three materials: 1) coarse grained soil or gravel used as fill material, 2) clayey silt,

which is located at the upper layer of the ground, and 3) silty clay. The material properties required as input for the TEMP/W modelling are the values of unfrozen gravimetric water content (w_u), volumetric water content (θ), volumetric heat capacity (C), and thermal conductivity (k).

Unfrozen water content is a key factor in the thermal behaviour of frozen soils (Farouki 1985). For frozen fine-grained soils, some water remains unfrozen over a considerable range of negative temperatures. This water is adsorbed around the clay particles and can increase in amount with increasing specific surface area of the clay particles. It plays a very important role in the process of water migration to the freezing zone and in improving the thermal contact between the soil matrix and the ice. The unfrozen water content w_u, has been related to the specific surface area $S(m^2/g)$ and the temperature $T(°C)$ as follows (Anderson, Tice & McKim 1973) and (Farouki 2004):

Equation 6.6 $\qquad \log_e w_u = 0.2618 + 0.5519 \log_e S - 1.449 S^{-0.264} \log_e T$

In this study, the specific surface areas of the soil particles were not measured. Published graphs available in the literature (Farouki 1986) were used to determine the unfrozen water content function for the three materials in the model. Published graphs available in the literature were used to determine the unfrozen water content function and were entered in TEMP/W. Figure 6.2 show the graphs of unfrozen water content versus temperature for the materials used in the TEMP/W modelling.

The volumetric water content (θ) represents the fraction of the total volume of soil that is occupied by water. The volumetric water content can be expressed in terms of more common gravimetric water content and the degree of saturation according to the following equation:

Equation 6.7
$$\theta = \frac{w}{1+w}\left(\frac{\rho_b}{\rho_w}\right) = nS$$

where ρ_b = bulk density of the soil, ρ_w = water density, n = porosity, S = degree of saturation, and w = gravimetric water content. The values of volumetric water content were calculated from the results of laboratory testing (Chapter 4, Table 4.1) and used in the TEMP/W models. Table 6.1 shows values of volumetric water content for the materials used in the TEMP/W models.

Heat capacity (C) is the amount of heat required to raise the temperature of a unit mass of a substance by one degree. The volumetric heat capacity can be computed (Farouki 2004) by adding the heat capacities of the soil constituents in a unit mass soil as:

Equation 6.8
$$C(kJ/kg \; °C) = x_s C_s + x_w C_w + x_a C_a$$

where x_s = volume fraction of solids, C_s = heat capacity per unit volume of solids, x_w = volume fraction of water, C_w = heat capacity per unit volume of water, x_a = volume fraction of air, and C_a = heat capacity per unit volume of air.

For saturated soil, the volumetric heat capacities in the unfrozen and frozen conditions are respectively given by the following (empirical) equations (Farouki 1985):

Equation 6.9 $$C_u = \frac{\rho_d}{\rho_w}\left(0.18 + 1.0\frac{w}{100}\right)C_w$$

Equation 6.10 $$C_f = \frac{\rho_d}{\rho_w}\left(0.18 + 0.5\frac{w}{100}\right)C_w$$

The values of unfrozen and frozen volumetric heat capacities were calculated from the results of laboratory testing (Chapter 4) and the heat capacities per unit volume of the soil constituents available in the literature, and were used in the TEMP/W modelling. Table 6.1 shows values of volumetric heat capacity for the materials used in the TEMP/W modelling.

Thermal conductivity is a measure of the quantity of heat that will flow through a unit area of substance in unit time under a unit temperature gradient (Farouki 1985). For analysis of unfrozen soils, the thermal conductivity can be considered constant. However, for a frozen soil analysis, the thermal conductivity is function of the water

content, which at the same time is a function of the temperature. Since the thermal conductivity of ice can be four times the thermal conductivity of the water (Farouki, 1985), the thermal conductivity of the soil increases as the soil freezes. Thermal conductivity can also be expressed in terms of its variation with respect to the change in temperature.

Thermal conductivity was measured using a small non-steady-state thermal probe (TP08) manufactured by Hukseflux. The TP08 consists of a heating wire, representing a perfect line source, and a temperature sensor capable of measuring the temperature at this source (Hukseflux). The probe is inserted into the soil that is to be investigated. The probe principle relies on a unique property of a line source: after a short transient period the temperature rise ΔT, only depends on heater power Q, and the soil thermal conductivity k, which is given by the following equation:

Equation 6.11 $$\Delta T = \left(\frac{Q}{4\pi k} \right)(\ln t + B)$$

with ΔT = change of temperature (K), Q = heater power (W/m), k = thermal conductivity (W/mK), t = time (s), and B a constant. By measuring the heater power, and tracing the temperature in time, k can be calculated.

Thermal conductivities of the soil samples extracted from the mid-slope of the stable section were measured at the temperatures of -10°C (frozen), +3°C and +10°C

(unfrozen) following the (ASTM D5334-08). The percentage of clay and silt, natural gravimetric water contents and Atterberg limits (plastic and liquid limits) were also determined. The results are included in Table 6.2 and shown in Figure 6.3. As expected, the values of thermal conductivity increase as the soil freezes. The specimens with high percentage of clay (that is silty clay, such as HBP11) has a frozen thermal conductivity of 104kJ/day/m/°C and an unfrozen thermal conductivity of 78kJ/day/m/°C. The specimens with high percentage of silt (clayey silt, such as HBP10 and HBP14) have a frozen thermal conductivity of 209-200kJ/day/m/°C and an unfrozen thermal conductivity of 122-131kJ/day/m/°C. No gravel materials were available from the site for thermal conductivity testing.

There are also empirical methods to calculate the thermal conductivity of soils (Farouki 1986). The method developed by (Johansen 1975) is the most common and reliable approach to compute thermal conductivity. It is an interpolation technique between the dry and saturated thermal conductivity values and does not take into account possible moisture migration at intermediate degrees of saturation (Andersland & Ladanyi 2004). This method also requires knowing the amount of quartz fraction of the total solids content. Coarse grained soils are dominated by quartz, which have a relatively higher thermal conductivity compared with fine grained soils that are dominated by clayey minerals, which have lower thermal conductivities.

Values of thermal conductivities were calculated by the author using Johansen's empirical method. Since the mineral composition of the soils is not known, the calculations were based on graphs found in the literature that relate to the water content of the soil, its dry density and the percentage of saturation (Farouki 2004). Table 6.3 compares these calculated values with values measured using the thermal probe. The frozen and unfrozen values of thermal conductivity for the soils calculated by the Johansen's method are in the same range as the values measured in the laboratory, but do not appear to be correlated.

The author used both the measured and calibrated values of thermal conductivity in Table 6.3 for calibrating a new program of TEMP/W modelling. Preliminary work led by colleague Mr. Kurz used generic thermal conductivities taken from the literature, for example in (Farouki 1986). The results of calibration showed that measured thermal conductivity values in the TEMP/W produced a better simulation of the ground temperature at the PR391 embankment than the values calculated using Johansen's method. Results of calibration will be further discussed in the following section.

Boundary conditions for the new modelling include a zero flux boundary along the centreline of the embankment, constant temperatures at a depth of mean zero annual amplitude (DMZAA is approximately 9m underneath the unstable section, as indicated in Chapter 5), and a constant temperature and varying climate data at the

163

surface in steady state and transient models, respectively. No boundary condition was defined along the right side of the embankment. The TEMP/W software assumes a zero horizontal flux boundary along this line.

Historic climate data from Environment Canada's monitoring station at Thompson Airport were used in the modelling. The information from this station is available in the web page of the Environment Canada Weather Office at (http://www.climate.weatheroffice.ec.gc.ca). The selected set of data starts on October 1st, 2006 and ends on September 31st, 2011 (that is 5 years of climate data). The date of October 1st, 2006 was chosen to give the model two years of climate data before the field measurements began. This allowed potential effects of the initial steady state analysis to be dissipated within the model.

TEMP/W uses the selected climate data to calculate the ground surface boundary condition (Geo-slope 2010). The data include maximum and minimum temperatures for each day, relative humidity, wind speed, amount of precipitation, starting and ending period of the precipitation event, longitude and latitude. The ground surface boundary condition is the net heat flux arising from absorbed solar and long wave radiation and from sensible and latent heat transfer between the ground surface and the overlying air (Goodrich & Gold 1981). This net flux can be expressed by the energy balance equation as follows:

Equation 6.12 $$Q_G = -k\frac{\partial T}{\partial n} + Q_{SW} + Q_{LW} + Q_H + Q_E$$

where Q_G = ground surface heat flux, k = thermal conductivity at the ground surface, $\partial T/\partial n$ = heat gradient normal to and evaluated at the ground surface, Q_{SW} = net flux of solar radiation, Q_{LW} = net flux of long wave radiation, Q_H = net flux of sensible heat, and Q_E = net flux of latent heat associated with evaporation of moisture from the surface.

6.1.3 TEMP/W Modelling

The model was developed in two stages; a steady state condition to establish the initial isotherms in the model, and subsequent transient analysis using the climate data. Temperatures for the surface boundary in the steady state analyses were taken from the first day of the set of climate data. Calibration of the modelling compares the ground temperature values simulated by TEMP/W and the measured ground temperatures from thermistor strings at the PR391 embankment presented in Chapter 5.

Figure 6.4 to Figure 6.7 compare modelled (simulated) and measured temperature profiles with depth for the stable and unstable sections. The periods in winter (January and February), and summer (July and August) for 2010 and 2011 are shown for comparison of the modelled and measured values. These months are expected to correspond with the largest changes in ground temperature due to the

change in seasons. The figures show that the simulated and observed data follow the same general trends and that the ground temperatures underneath the embankment match the observed data with reasonable accuracy. The match between the model and measured values is significantly better at the unstable section than the stable section. This is perhaps because the value of the DMZAA was defined as a temperature point in boundary conditions at the unstable section. This boundary condition does not exist at the stable section. As mentioned previously in Chapter 5, the DMZAA could not be measured at the stable section because the bedrock was encountered at 4m depth and thermistor strings were not installed into the bedrock.

6.2 Frost Heave Measurements for PR391

The following section presents results of efforts to use the method of segregation potentials (SP) in reverse to back-calculate values of SP from the frost heave measurements presented in Chapter 5. The theory and concept of the SP method were explained and discussed in Chapter 2.

The SP method is normally used in design problems to calculate frost heaves from values of SP measured in laboratory freezing-thawing tests. The author has reversed this process. Here, measurements of settlement rates from the field instruments at PR391 are used to calculate the field value of SP, which is then compared with generic published values for similar clays.

The parameter SP is used to model frost heave by knowing or predicting the temperature gradient in the frozen fringe, and the water intake flux v_w (Konrad & Morgenstern 1980), (Konrad & Morgenstern 1981), and (Konrad & Morgenstern 1982). The rate of frost heave (dh/dt) can then be obtained using the relation:

Equation 6.13
$$\frac{dh}{dt} = 1.09v_w + 0.09\theta\frac{dX}{dt}$$

where dX/dt is the rate of frost penetration depth, θ is the volumetric water content (the porosity reduced to account for the percentage of in situ pore water that will not freeze), and 0.09 is the volumetric expansion that occurs when water is frozen. By obtaining the values of dh/dt from the surveyed vertical movements at PR391, the values of dX/dt from the ground temperature data of the PR391 embankment, and the values of θ from the laboratory testing results, the water intake flux v_w can then be calculated from Equation 6.13.

According to the SP method, the rate of water flow is directly proportional to the temperature gradient (grad T). The coefficient of proportionality is called the segregation potential and can be obtained from:

Equation 6.14
$$SP = \frac{v_w}{gradT}$$

In Equation 6.14, the rate of water flow can be estimated from measured settlements, and the temperature gradient from thermistor readings.

6.2.1 Segregation Potential (SP) Calculation of PR391

Measured vertical movements at PR391 were shown in Chapter 5 (see Figure 5.7). The results show that the toe of the PR391 embankment experiences the highest amount of frost-heave during the freezing season, while the mid-slope shows a lower amount, and the shoulder shows almost no frost heave. Values of SP were therefore calculated only at the toe of the stable and unstable section.

Figure 6.8 shows measured vertical movements and frost heave during two freezing seasons at the toes of the stable and unstable sections. The top two graphs show a large amount of frost heave at the toes of both sections at ground level. The bottom graph in Figure 6.8 shows a small amount of frost heave during the first winter underneath the toe of the stable section at a depth of about 4m. Linear trendlines were fitted to the frost heave data of each freezing season in order to measure the rate of frost heave (dh/dt). These values are shown in Table 6.4.

Temperature profiles were measured from thermistor strings at the toes of the stable and unstable sections. They were presented in Chapter 5 (the monthly temperature profiles in Figure 5.1a and Figure 5.2a). The frost penetration depth is the greatest

depth to which the ground freezes below 0°C in the active layer during a freezing season. The depth of 0°C, and therefore the depth of frost penetration, was obtained from the temperature results at the toes of the stable and unstable sections. Figure 6.9 shows the depths of frost penetration (depths of 0°C temperatures). Linear trendlines were fitted to the frost depth data for each freezing season in order to calculate the rate of the frost penetration depth (dX/dt). These values are included in Table 6.4.

Values of temperature gradients (grad T) in the active layer were obtained from the monthly temperature data at the toes of both sections. They are also included in Table 6.4. Values of volumetric water content (θ) were calculated from the laboratory testing results at the toes of both sections and these are also included in Table 6.4. Combining Equation 6.13 and Equation 6.14 allows field values of SP to be calculated using Equation 6.15:

Equation 6.15
$$SP = \frac{\frac{dh}{dt} - 0.09\theta\frac{dX}{dt}}{1.09 \text{gradT}}$$

Table 6.4 shows values of SP at the toes of both the stable and unstable sections. At the depth of 0m, the stable section has the SP values of 153mm^2/°C.day and 219mm^2/°C.day for the two freezing seasons that were examined. The unstable section at the same 0m depth has higher SP values of 476mm^2/°C.day and

244mm^2/°C.day respectively for the two seasons. These results show that the unstable section is more frost susceptible than the stable section.

At 4m depth below the toe of the stable section, the SP has the low value of 20mm^2/°C.day, that is about 10% of the SP value at the ground level (219mm^2/°C.day). This indicates the influence of applied surcharge and a lower tendency for frost heave at greater depth. The segregation potential of a given freezing soil decreases with increasing overburden pressure. This observation is consistent with the results reported by researchers in the literature review presented in Chapter 2. Further discussion of the SP results, comparison of the results with the published data, and the applicability of this method to field conditions will be provided in Chapter 7.

Material	Volumetric Water Content θ (m³/m³)	Volumetric Heat Capacity (kJ/m³/°C)	
		C_u	C_f
Gravel	0.40	2400	2300
Clayey Silt	0.45	3270	2510
Silty Clay	0.55	3220	2230

Table 6.1: Volumetric water content and volumetric heat capacity values

Test	Section	Depth (m)	w_P (%)	w (%)	w_L (%)	I_p (%)	I_L	Clay (%)	Silt (%)	Thermal conductivity (kJ/d/m/°C) at given temp. (°C)		
										10	3	-10
HBP10		1.3	18	25	32	13	0.5	38	62	122	124	209
HBP11		2.0	32	34	57	24	0.1	74	26	78	79	104
HBP12	Stable Mid-Slope	2.8	24	26	40	16	0.1	50	50	116	114	163
HBP13		3.5	24	28	38	14	0.3	43	57	122	114	178
HBP14		4.3	21	25	29	8	0.4	27	73	131	102	200

- w_P = plastic limit, w = gravimetric water content, w_L = liquid limit, I_P = plasticity index, I_L = liquidity index

Table 6.2: Results of thermal conductivity testing at the mid slope of the stable

section. (Results by David Kurz, Graham Bartley, and the author.)

Material	Thermal Conductivity (kJ/d/m/°C) measured in laboratory		Thermal Conductivity (kJ/d/m/°C) calculated by Johansen's method	
	k_u	k_f	k_u	k_f
Gravel	-	-	216	346
Clayey Silt	126	205	83	153
Silty Clay	78	104	108	209

Table 6.3: Comparison of thermal conductivity values measured in the laboratory

and calculated by Johansen's method

	dh/dt (mm/s)			dX/dt (mm/s)			Grad T (°C/m)			SP (mm²/°C.day)		
	Stable		Unstable	Stable		Unstable	Stable		Unstable	Stable		Unstable
	0m depth	4m depth	0m depth	0m depth	4m depth	0m depth	0m depth	4m depth	0m depth	0m depth	4m depth	0m depth
02-Nov-09 15-Nov-09 04-Dec-09 18-Dec-09 12-Jan-10 16-Feb-10 16-Mar-10	1.39E-05	4.63E-06	1.97E-05	1.63E-04	1.13E-04	1.47E-04	2.31	1.35	2.35	**219**	**20**	**476**
30-Oct-10 15-Nov-10 20-Dec-10 24-Jan-11 06-Mar-11 03-Apr-11	9.26E-06		1.16E-05	9.14E-05		9.03E-05	2.62		2.66	**153**		**244**
θ	0.51	0.42	0.42									

- θ = volumetric water content

Table 6.4: Results of SP calculations

173
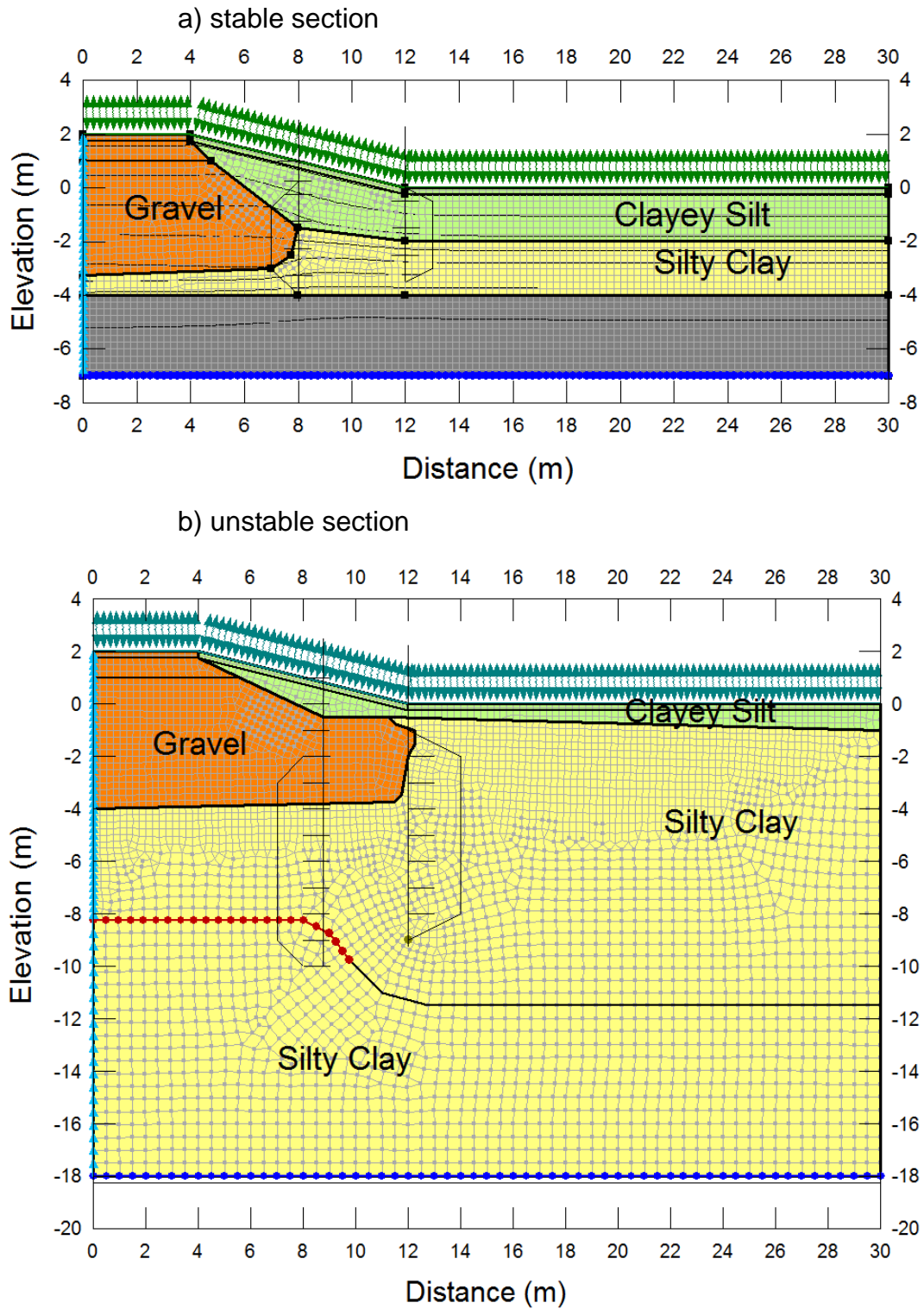
Figure 6.1: Cross sections, materials and finite element mesh at the a) stable section; b) unstable section

174
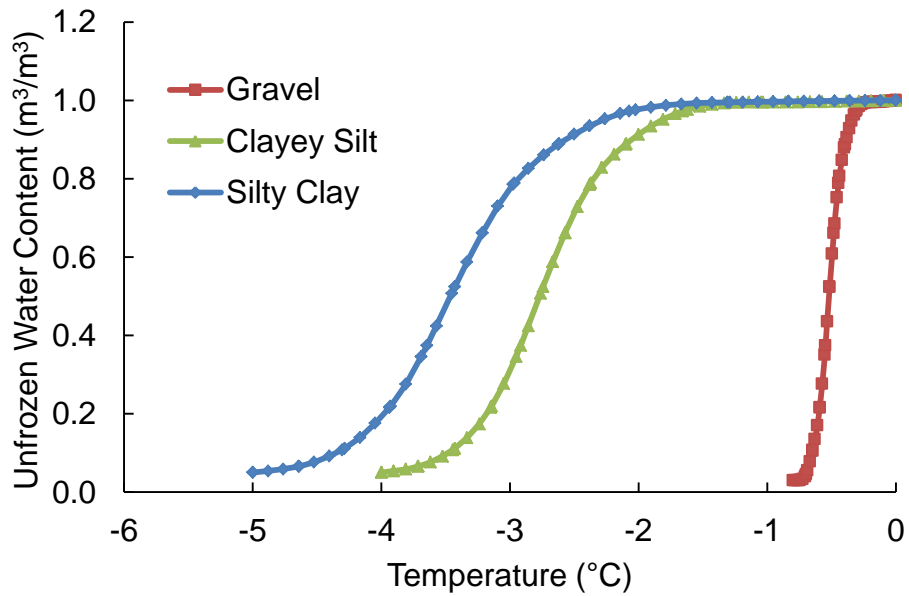
Figure 6.2: Unfrozen water content versus temperature
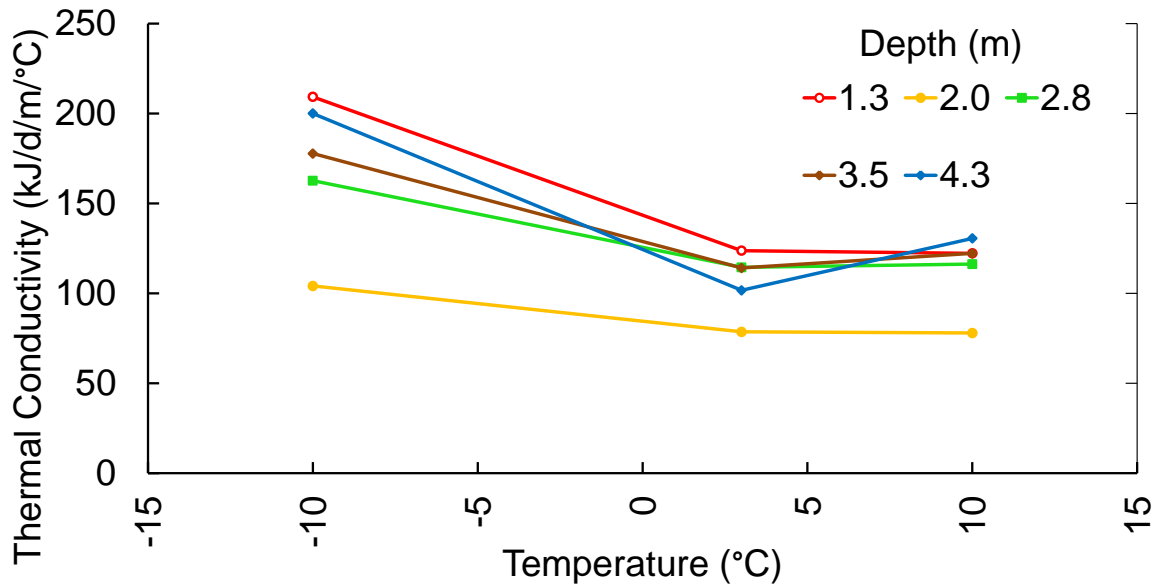
Figure 6.3: Thermal conductivity values versus temperature at the mid-slope of the stable section. (Results by David Kurz, Graham Bartley, and the author.)

175
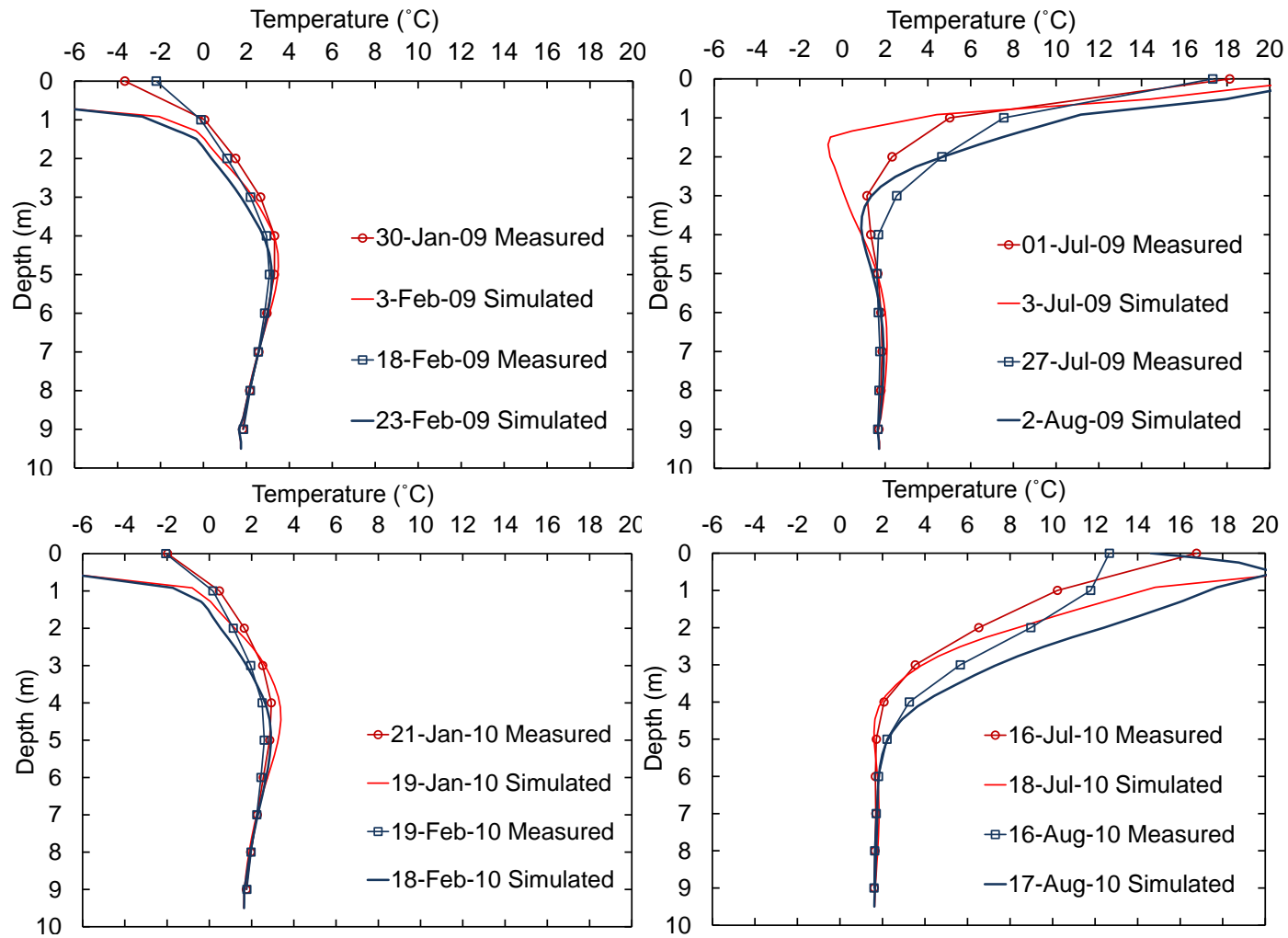
Figure 6.4: Modelling and measured results of temperature during winter and summer of 2009 and 2010 at the toe of the unstable section
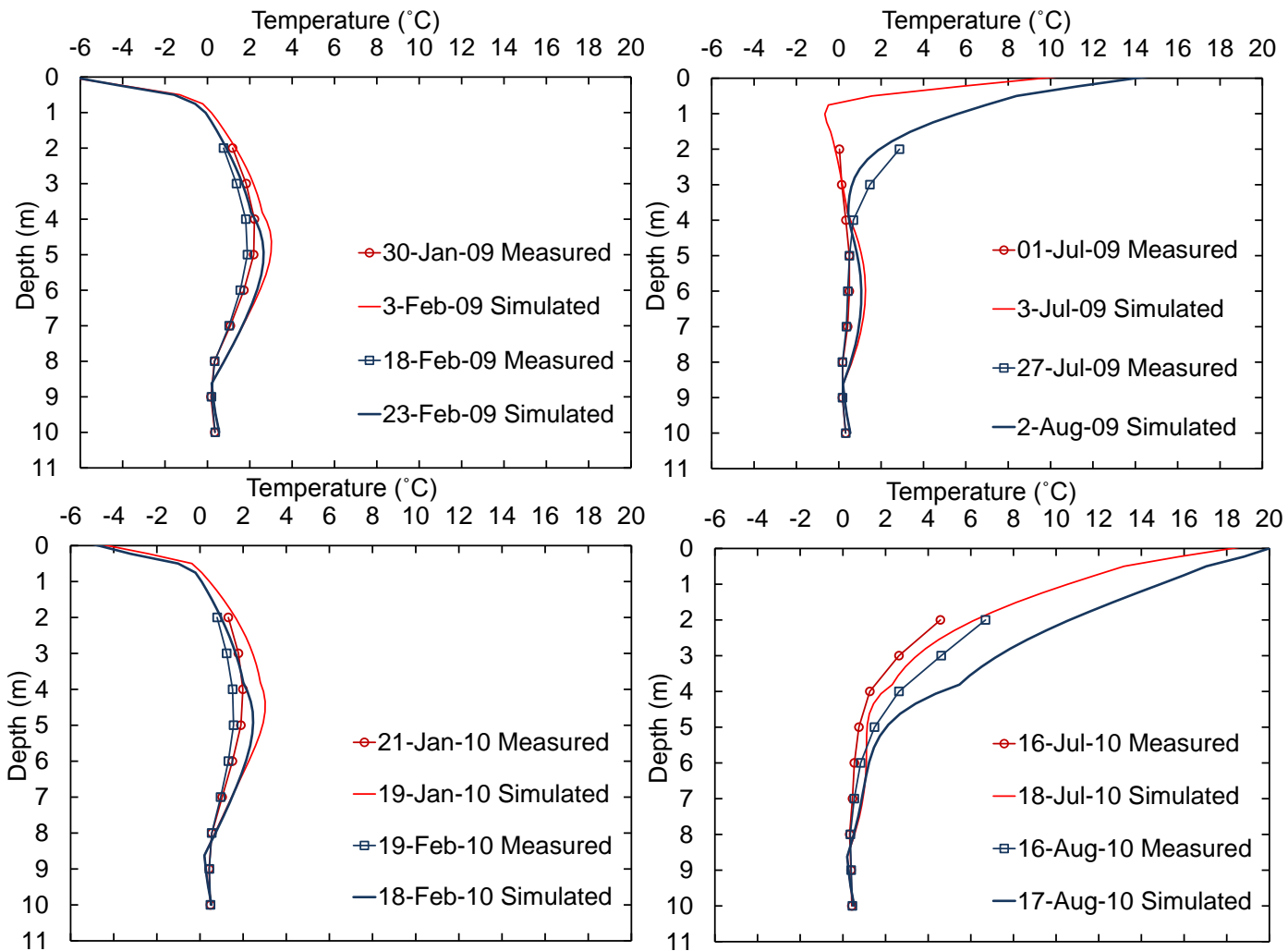
Figure 6.5: Modelling and measured results of temperature during winter and summer of 2009 and 2010 at the mid slope of the unstable section
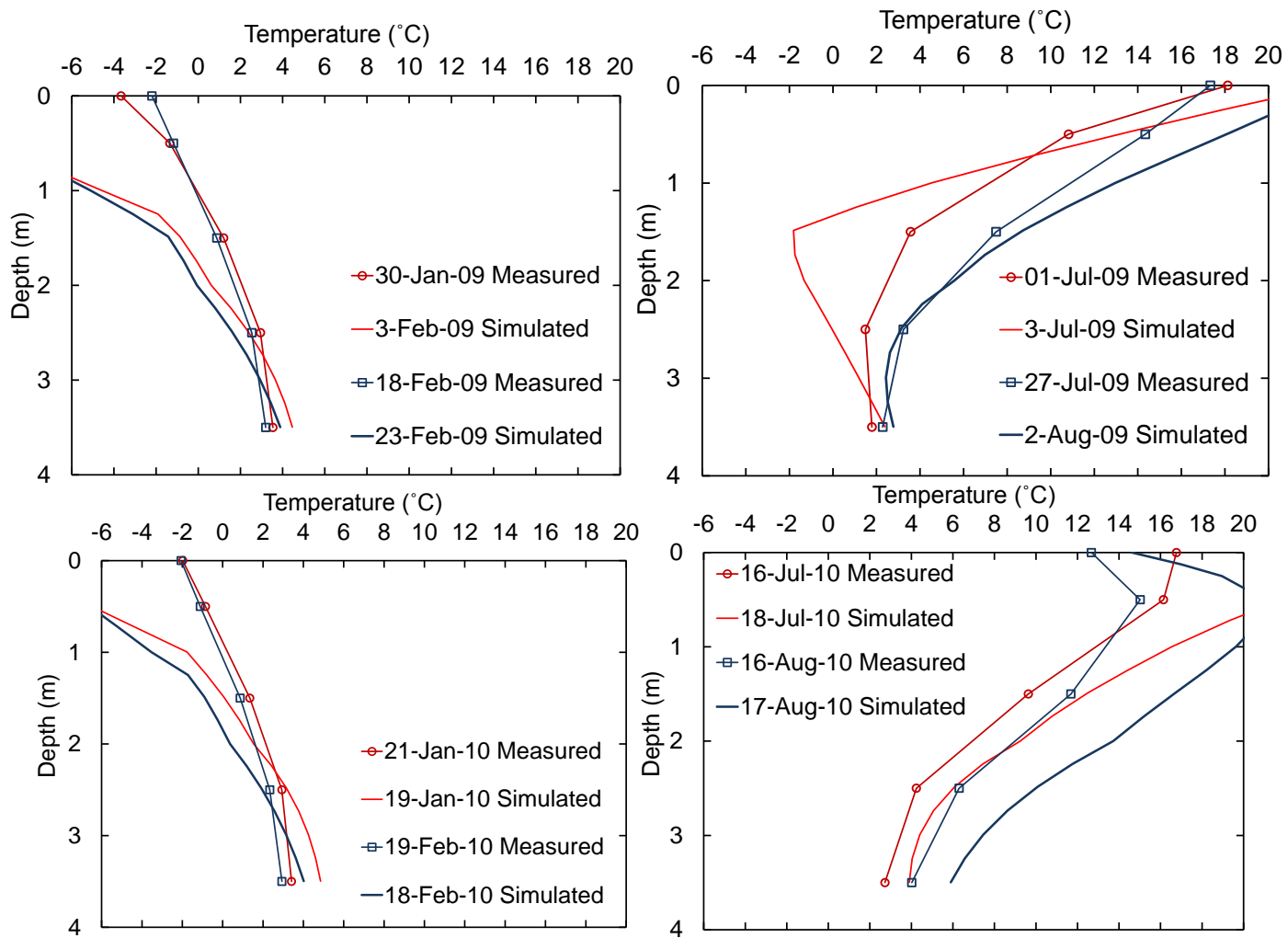
Figure 6.6: Modelling and measured results of temperature during winter and summer of 2009 and 2010 at the toe of the stable section
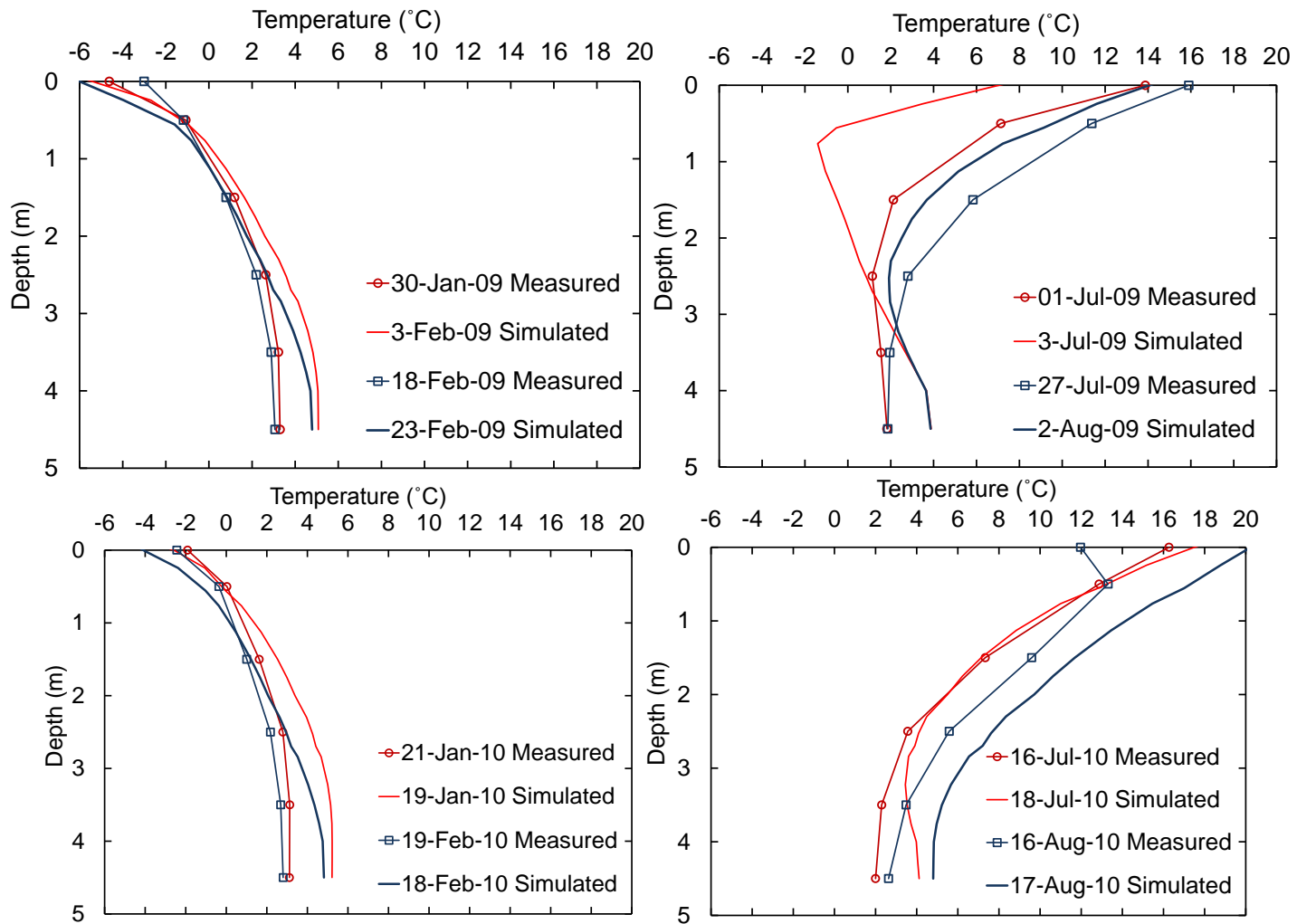
Figure 6.7: Modelling and measured results of temperature during winter and summer of 2009 and 2010 at the mid slope of the stable section
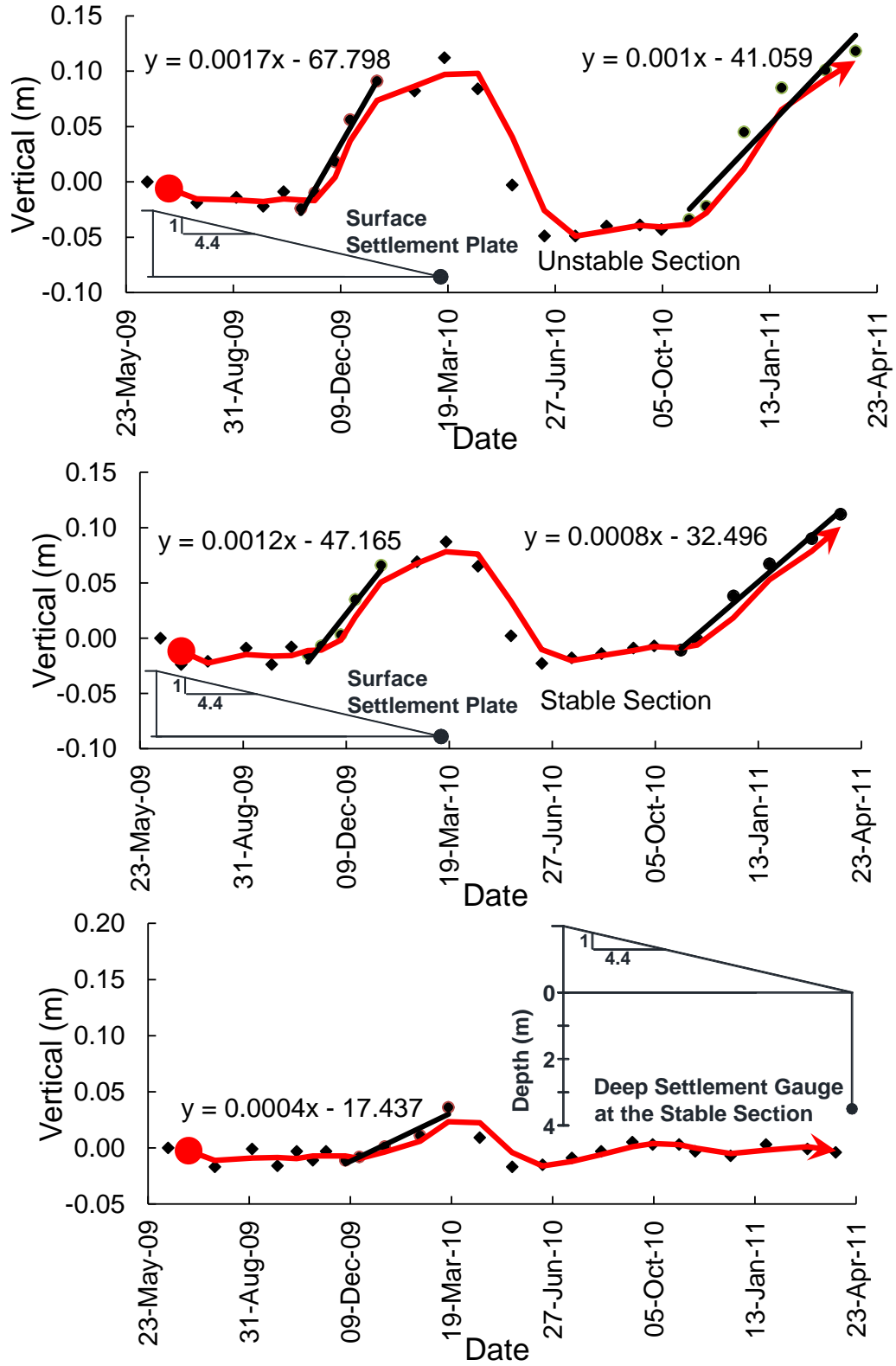
Figure 6.8: Frost heave data at the toes of the stable and unstable sections
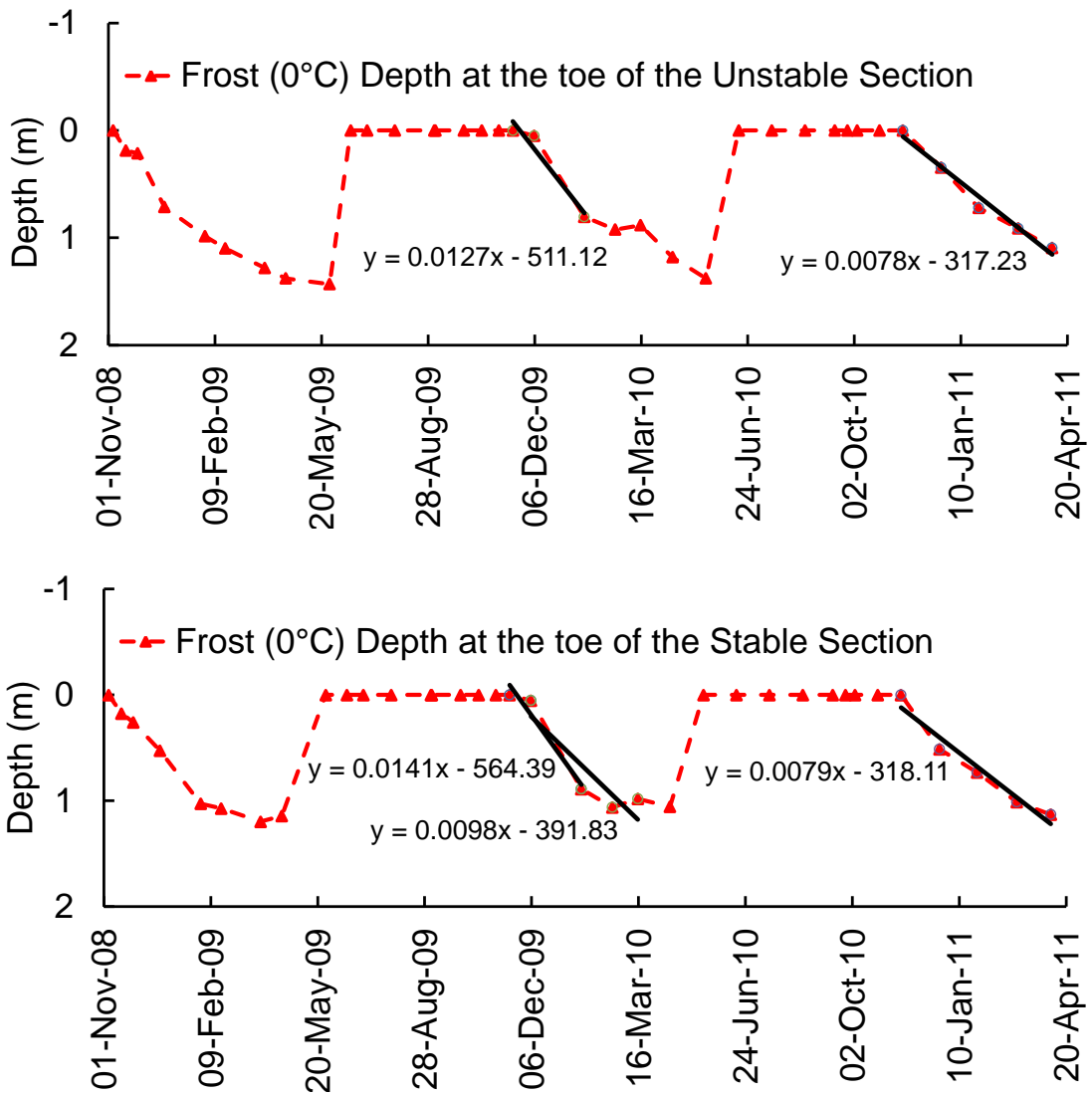
Figure 6.9: Frost penetration depth at the toes of the stable and unstable sections

CHAPTER 7:   Discussion and Synthesis

Earlier chapters presented the results and analyses of the laboratory testing, the data collected from the field instruments at the PR391 site, and thermal modelling and frost heave predictions. This chapter discusses, interprets, and synthesises the results of previous chapters into a single picture for the site. It also discusses the strengths and weaknesses of the overall research program. This leads in Chapter 8 to a number of design strategies and remedial measures.   Conclusions and recommendations for future work will be presented in Chapter 9.

7.1 Discussion of Laboratory Test Program

The hypothesis #1 proposed in Chapter 1 of this thesis was that soil properties measured at room temperatures may give faulty estimates of deformations at the lower temperatures in thawed permafrost. The laboratory testing program of this research provided results that included classification results (natural water content, Atterberg Limits and hydrometer analysis), and the mechanical properties, including the consolidation and shearing properties of the soils from the PR391 embankment, at two temperatures of 3°C and 21°C. The goal of the laboratory testing program was to study the effect of temperature on the mechanical behaviour of the soil extracted from the PR391 embankment. The results and analysis of laboratory

testing were provided in Chapter 4 and are discussed and synthesized in the following section.

Creep is an essential feature of the behaviour of clays. It arises from the viscoplastic rearrangement of interparticle contact forces over time. Viscoplastic behaviour is seated in the interaction of diffuse double layers (DDLs) of adsorbed water that surround the electrically charged surfaces of clay particles. Under constant effective stress, the separation of particles depends on potential distributions in the DDLs. It therefore depends on particle mineralogy, pore fluid chemistry and temperature, as expressed for example by Gouy-Chapman theory (Equation 2.1) (Mitchell & Soga 2005). The thickness of the DDL varies with temperature and with the dielectric constant, which itself varies with temperature. The results of the classification tests show that the foundation soil of the PR391 embankment has a large amount of silt content mixed with clay (On average, the ratio of clay/silt particles is around 50:50, in Figure 4.1 and Figure 4.2). The presence of silt as a granular soil with clay as a fine grained soil can alter the rearrangement of interparticle contacts in the diffuse double layer and reduce the proportion of soil that will exhibit viscous properties. This tends to lessen the effect of temperature on the measured mechanical behaviour of the PR391 soil, and specifically any differences associated with testing at room temperature while the in-situ material below the DMZAA is at much lower temperature.

In general, plastic clays, which have high surface activities, can be expected to exhibit high viscoplastic effects that depend on temperature. Evidence for the importance of viscoplasticity, which is important not only in compression but also in shear, has been recently identified by researchers (Kelln et al. 2008) (Kelln et al. 2009), who also commented that primary consolidation and creep must be considered concurrent mechanisms. Their work assumes that viscous behaviour is present through all stages of a soil's response to loading and that creep behaviour can be described by a single creep parameter $C_{\alpha e}$, which depends on plasticity index and temperature, but is otherwise constant in the same way that the compression index C_c and the unload-reload index C_r are constant.

The results provided in Chapter 4 (Table 4.1 and Table 4.2) showed that the values of $C_{\alpha e}$ / C_c for the Thompson clay are lower than one would expect for clay with moderate plasticity (I_P of 30 – 40%). Small and non-systematic variations of $C_{\alpha e}$, C_c, C_r, and friction angle with temperature are observed for the samples from PR391 at depths of less than 8m-9m (Table 4.2 and Table 4.3). These variations are somewhat more significant at greater depths where the clay content and plasticity indices are higher. They are still, however, somewhat smaller than were anticipated at the beginning of the project. That is, the mechanical and shearing properties of the soil collected from the PR391 embankment are not significantly affected by differences in temperature. Weathering processes in the foundation soil and active layer closer to the ground can cause destructuring of the soil material over time.

184

It is important to note the relationship between the plasticity characteristics and the mechanical behaviour of soil. The results of the 1-D consolidation and shearing properties of the samples from PR391 can be correlated with the results of the Atterberg limits (Table 4.1 to Table 4.3). In general, the characteristics of the primary and secondary compressions, and the shearing strengths correlate directly with the plasticity indices and clay fractions. That is, soils with higher plasticity characteristics and higher clay contents are more compressible (in both primary and secondary) and have lower angles of internal friction.

Most of the laboratory testing results reported by other researchers in the literature review (Chapter 2, Section 2.3) were performed on reconstituted samples prepared in the laboratory with known material properties. The results provided in this research program were obtained from tests performed on samples collected from the PR391 field site. One of the difficulties of the laboratory testing of this research program is that the examination of the changes of the material properties at different temperatures was made on vertically adjacent specimens from the same Shelby tube. That is, while the specimens came from the same sample tube they were from slightly different depths. Therefore the initial in-situ properties of the samples being tested were similar, but not necessarily identical. In geotechnical engineering, the material properties of soil in the ground can change drastically with small changes in depth. Good soil sampling, larger diameter Shelby tubes (100mm as opposed to the more common 50 mm or 76 mm), and having the least amount of disturbance during

both sampling and preparation of specimens are essential in obtaining high quality of the laboratory testing results. Another difficulty with the laboratory testing of PR391 samples is that specimens from the stable and unstable sections came from different depths and had therefore experienced different levels of weathering disturbance. Unfortunately, there was a considerable delay between sampling and testing. This may also have affected the quality of the results.

To sum up this section, the results of the laboratory testing program suggest strongly that the large differential settlements present at the unstable section of the PR391 are not caused by changes of temperature and related impacts on the hydro-mechanical behaviour of the foundation materials. On the basis of the literature review, the previous and current site investigations at PR391, and the extensive laboratory testing program, it is more likely that the thawing of discontinuous permafrost and change of phase in the foundation from solid to liquid has caused the destructuring of the foundation soil. After thawing and completion of phase change, the changes of temperature do not significantly affect the hydro-mechanical and shearing behaviour of the soil. From this, it can be noted that the results of laboratory testing at room temperature on the PR391 soil samples do not give faulty results compared to the laboratory testing completed in 3°C. The author believes that the following main factors must be taken into careful consideration in examining the foundation soil in permafrost areas:

1- Soil classification – the content of granular soil (silt or sand) present with clay

2- Plastic and liquid limits, and plasticity and liquidity indices of the material being investigated (for example in Table 4.1, Figure 4.1 and Figure 4.2)

3- Weathering processes such as freezing-thawing cycles and/or drying-wetting cycles that the soil is exposed to. These processes cause destructuring of the original soil fabric

7.2 Discussion of Data from Field Instrumentation

One of the primary contributions of this thesis to the literature has been the results of the field instrumentation data. Hypothesis #2 proposed in Chapter 1 was that deformations of highways and road embankments on thawed permafrost are associated with compression and shear strains, including creep strains in the foundation soils. To examine this hypothesis, instrument clusters were installed at the shoulder, mid-slope and toe of both the stable and unstable sections of the PR391 site embankment. (Details of instrumentation were discussed in Chapter 3).

Data have been collected from the instruments and analyzed during the first two years of operation, that is, over two freeze-thaw cycles. The data include monthly temperatures from the thermistor strings at 1m depth intervals, surveyed results from the surface settlement plates and deep settlement gauges, lateral displacements measured by slope inclinometers and horizontal VW extensometers, and pore water pressures measured by the VW piezometers. Only a few projects that are available from the literature have previously reported this type of work on this combination of

field instruments. Analyses of the data were provided in Chapter 5 and are discussed and synthesized in the following section.

The temperature results show the expected variations of temperature with seasonal changes (Figure 5.1 to Figure 5.4). Net heat flow into the ground was observed for both years of data collection (Figure 5.5 and Figure 5.6). This is possibly a confirmation of general warming in the area. Similar temperature data collection and observations were made by other researchers in northern cold region areas such as Canadian Arctic regions and reported in literature review (Chapter 2, Section 2.2.2). However, their conclusions were based on longer time periods of data collection (at least two decades of data collection). The author recommends similar duration of data collection from the instruments of this research site in order to further investigate the warming of ground in the long term.

The temperature data, (Figure 5.1), confirm field observations of the thawing of ice that was present in the previous drillings of the site in 1991 and 2005, but absent in recent drilling in 2008. The measured temperature at the DMZAA is above 0°C. The depth of DMZAA at the unstable section is about 8m-9m. This depth correlates with the depth at which the foundation soil was affected by weather processes and correlates well with results shown in the laboratory tests (Chapter 4, Section 4.2.2, see, for example, Table 4.2.)

The measured temperature at the DMZAA at the toe is higher than the measured temperature at the DMZAA at the mid slope (Figure 5.1). It is more likely that the thawing of permafrost begins at the toe of the embankment and then spreads towards the centre of the embankment. This is consistent with the findings of other researchers (Alfaro et al. 2009) and (Andersland & Ladanyi 2004). This observation could have been studied more if thermistor strings had been installed under the centre of the embankment. This was not possible due to concerns from the sponsor MIT about safety, snow clearing, and grading of the road. Considering the value of studying the temperature profile underneath the centre of the embankment, the author recommends the installation of thermistors in that location for future investigations. He understands that funding is currently being sought to make this possible.

The surface and deep measurements of deformation, (Figure 5.7 to Figure 5.11), indicate a combination of seasonal heaving, cumulative displacements, and lateral spreading. The cumulative displacements are larger at the shoulder, while the lateral displacements were larger at the toe of the embankment. As expected, the unstable section shows a significant amount of displacements while the stable section shows very little. The cumulative displacements collected by surface settlement and deep settlement gauges show downward vertical settlements, particularly at the shoulder and mid-slope, while the lateral deformations collected by the SI and VW extensometers show lateral movements away from the centre of the

embankment at greater depths. That is, shearing strains beneath the embankment push the lower levels of clay horizontally away from the centre of the embankment at greater depths. These combined measurements of deformations show that the displacements observed at the PR391 embankment are a combination of consolidation and shearing strain of the foundation material. The displacements are two dimensional (plane strain).

The pore water pressure results suggest the development of cyclic seasonal gradients of total head (Figure 5.12). These indicate hydrostatic water pressure conditions during summer months and upwards flow during the freezing season. These are believed to be caused by upward flow of water towards suction pressures (negative potentials) at the freezing front as it moves downwards during the winter. The effects of frost action involve a combination of frost heave during a downward advance of the freezing front, with the accompanying formation of ice lenses; and a subsequent reduction of shear strengths and higher compressibilities when the ice melts during the spring thaw.

Compiling the results of temperature, displacement, and pore water pressure data provides an improved understanding of the mechanisms and physics occurring at PR391. The PR391 embankment was constructed in a region of discontinuous permafrost. The unstable section was built on an 18 m thick layer of clay and silty clay, in the middle of which there was probably a layer of permanently frozen soil.

(Drilling reported frozen soil in the boreholes but there was no systematic investigation or instrumentation.) Because of the factors explained previously in Chapter 2, Sections 2.2.2 and 2.2.3 (including the human disturbances and climate warming), the mean ground temperature has increased, the frozen soil has thawed and changed into a thick layer of unfrozen soil and soft clay at deeper locations. Consolidation and shearing strain began in the foundation soils after the thawing. This was shown by the collected displacement data (Figure 5.7 to Figure 5.11). Because the thawed layer of soil is thick, the viscous consolidation and shear straining in the foundation will continue for a long period of time.

With the exception of one of the horizontal movement extensometers, the performance of the instruments was excellent. They were well-made, well-calibrated, well-installed and reliable. This was evidenced by the fact that all but one of them worked throughout the data collection period. The exception was one VW extensometer which is believed to have been damaged during the installation of the instrument. The accuracy of the measurements was considered to be of typical accuracy for this type of study. Additional instruments would have proved helpful in establishing more understanding of the processes underneath the PR391 embankment. Examples of additional instrumentation would include having a full set of instruments on both sides of the unstable embankment instead of only on one side. More useful would have been thermistors beneath the centre of the

embankment.   Neither of these improvements was possible with the funding

available.

7.3 Discussion of Thermal Modelling and Frost Heave Prediction of PR391

The numerical modelling of the PR391 embankment was developed to simulate the

thermal changes and frost heave characteristics of the embankment. The thermal

modelling shown in Figure 6.4 to Figure 6.7 provided simulation of temperature

changes under the embankment. The hypothesis #3 proposed in Chapter 1 of this

thesis was that frost heave prediction using segregation potential can be used in the

field to examine the frost susceptibility of the soil. To examine this hypothesis, a

second aspect of the modelling studied the application of the frost heave approach

known as the segregation potential (SP) method to field conditions. Segregation

potentials were back-calculated from the site observations and collected frost heave

data by using the SP method.   Chapter 6 outlined the thermal modelling,

procedures, evaluating segregation potentials and analysis of the results. These are

interpreted and discussed in the following section.

The TEMP/W thermal modelling of trends in ground temperature shown in Figure 6.4

to Figure 6.7 compare reasonably well with the data obtained from the thermistors

underneath the embankment.   Comparison of the thermal modelling results

explained in Chapter 6, Section 6.1.3, obtained from measured values of thermal

conductivity versus using calculated empirical values as input parameters shows that the precise estimate of thermal properties of soil (such as thermal conductivity) is a key factor in better simulating the thermal changes of ground. Another key factor is the definition of boundary conditions. Defining the boundary conditions in such a way that they include realistic temperature and depth of the DMZAA can significantly improve the results of thermal modelling (Figure 6.4 to Figure 6.7). As discussed in Chapter 6, Section 6.1.2, the thermal modelling was done using assumptions and values from published literature, because not all the required thermal properties of the PR391 soils were able to be measured. The author recommends that thermal characteristics of the foundation materials should be measured in laboratory testing in order to have better thermal modelling results.

The long term thermal modelling of a foundation can be developed by using the current thermal conditions of the foundation and the historic climate data of the site (Chapter 6, Section 6.1). This analysis is crucial for studying the thermal changes of the ground, potential thawing of frozen ground and the rate of thawing, sensitivity and thickness of the thawing layer, relative settlement, and eventually the extended performance of the embankment.

The primary contribution of the modelling section of this research has been the application of the SP method to field conditions (Chapter 6, Section 6.2). The author's use of the SP method to back-calculate values of SP from the frost heave

measurements of PR391 provided a useful full-scale comparison with values of SP which are usually measured in the laboratory on reconstituted or 'undisturbed' specimens. The SP modelling work in this research program explained the measured in-situ frost heave behaviour of freezing ground reasonably well. This indicates the validity of concept for field-scale projects. The soil properties used in this analysis were determined from data from the PR391 laboratory testing results (Table 6.1 to Table 6.3). To illustrate the accuracy of the model in a real situation, the calculated values from the site data should be compared with values of SP measured in the laboratory. Unfortunately, the author was not able to measure the values of segregation potentials in laboratory tests. Developing, manufacturing and commissioning equipment for measuring segregation potential was not possible in the time frame of this research. Therefore, the calculated values of SP were compared with available published data with similar material properties. The values of calculated SP values reported in Chapter 6 (Table 6.4) are generally of the same order of magnitude as laboratory values reported by researchers such as (Konrad 2005). He reported values of SP ranging 160 to 410 (mm^2/°C·day) for saturated sand–silt–clay mixtures, 52 to 325 (mm^2/°C·day) for till samples, and 84 to 329 (mm^2/°C·day) for quarry fines materials.

Research on the applicability of the SP method has been studied mostly under laboratory conditions. In laboratory frost heave tests, conditions often correspond only poorly to those in the field. The representativeness of the samples compared

194

with the soil profile is poor if the ground is anisotropic or heterogeneous. The author recommends that undisturbed samples drilled from the frozen ground should be used for frost heave testing in the laboratory. The natural structure of the soil will be damaged when a specimen from frozen ground is reconstituted in the lab. Irreversible deformations due to frost heave cycles can influence the values of SP for reconstituted samples.

In the segregation potential concept, segregation potential is a material property. It depends on environmental conditions such as in-situ stress, suction pressure, the rate of frost penetration, and climatic variations. If field measurements alone are applied in the way done in this project and the observation season is warm, the frost heave may differ significantly from the assumed design winter behaviour. The field observations should be carried out over several winters, and should be confirmed with representative laboratory tests.

In a cold region environment, there is often a need to limit the effect of frost action, such as heave in embankment soils, culverts and pipelines. Engineers must estimate the probable frost heave of a structure from the available soil data. They must take into account, the soil type and properties, the depth to the groundwater table, the dimensions and weight of the structure, thermal properties of the structure, and the weather conditions at the location during the period of analysis. At the preliminary stages, some level of relative frost heave or segregation potential should

195

be considered. Frost heave can be estimated by applying the SP frost heave method (Chapter 6, Section 6.2).

CHAPTER 8: Processes, Strategies and Remedial Measures to Improve Road Embankment Stability

The purpose of this chapter is to conduct a review of maintenance and engineering solutions to improve road embankment stability in areas of continuous and discontinuous permafrost, and to synthesize findings from the review into a summary of best practices. While this chapter does not deal directly with the author's research at the PR391 site, it builds on lessons learned from the research project at PR391, which formed the principal focus of this thesis document. It is presented here as an overview of highway embankment performance in cold regions and a presentation, with references, of techniques which the author hopes may be valuable to practitioners when designing and remediating highway embankments. The chapter discusses the need to understand the processes and physics of potential settlement problems, engineering design strategies and remedial measures, and selection of a proper design strategy for a road embankment.

8.1 Understanding the Processes and Physics of Potential Problems

Design, construction, and maintenance of infrastructure in cold regions require a full understanding of the framework of the project. Stability and settlement problems of embankments arise if the designs are not based on reliable knowledge about

properties of the foundation soil, the distribution of permafrost, frozen/unfrozen ground underneath the embankment, temperature distributions in the ground, freeze-thaw cycles, and the ice and water content of foundation soils.

Table 8.1 summarizes the physical processes that operate during the construction, operation, and maintenance phases of the life of an embankment. In sum, gradients of temperature, hydraulic potential, electrical potential, or chemical concentration produced by natural processes or during remediation can cause fluxes of heat, fluids, electrical current or ions.

In particular, if attempts are to be made to dry soils, and in this way to strengthen or stiffen them by decreasing their water content, then a number of physical processes are possible. Developing a flow of water (hydraulic flux) from a critical area can in principle be done by:

- Developing a temperature gradient – water flows away from hotter regions
- Changing the hydraulic gradient, often by improving drainage,
- Applying a potential difference between electrodes in the process known as electro-osmosis,
- Altering the chemistry of the pore water, perhaps by lowering cation concentrations in regions away from the site. This will have environmental challenges that must be examined carefully.

Geotechnical site investigation and characterization are essential for understanding the details of a project (Doré & Zubeck 2008). It helps engineers to identify the soil type and properties, location and characterization of thaw-sensitive areas, thickness of thaw-sensitive soils, potential settlements and lateral spreading. Information from the site investigation helps in the lifetime performance analysis of the project, in selecting proper construction techniques, and in designing the embankment. For existing embankments, site investigation provides understanding of processes and physics of the problems in thawing or thawed permafrost. This section discusses common practices and recommendations for site investigation prior to the construction of a new road embankment as well as investigation of an existing road embankment in cold regions.

(Doré & Zubeck 2008) reported a series of technical activities for geotechnical site investigation of road embankments in cold regions. The goals are to establish the nature, distribution, and properties of the soil along the embankment, provide information for embankment design, identify potential problems, and propose solutions to the problems. The following procedures discussed in this section are generally recommended when conducting a site investigation.

Topographical maps of the site include large quantities of information that can be compiled and used for site investigation. This information includes terrain

descriptions, site accessibility for investigation activities and potential technical problems associated with road construction at the suggested location.

Geomorphology and landform analysis are powerful and cost-effective techniques for preliminary study of road embankments (Doré & Zubeck 2008). They allow stereoscopic analysis of landforms and the possibility to observe the most significant features of the land surface. Information on landforms and land use, shape and characteristics of hydrographic networks, signs of soil and rock instability and erosion, presence and characteristics of exposed rock formations and boulders, presence and characteristics of soft and compressible soils can be gathered by examining the geomorphology of the site. Steep and irregular slopes can be identified by the topography of the surface and by the presence of irregular forested areas. These areas involve cut and fill construction and are likely to induce important differential settlement in road embankments. The presence of seepage faces and exposed rock and soil are indications of potential slope activity and special attention should be given to those features.

Information on flood zones, potential drainage problems, seepage problems, presence of swamps, and site access and restrictions can be identified by aerial photos and visual observations (Doré & Zubeck 2008). Low lands with flat surfaces can be potential problem areas. These areas are difficult to drain and can be subjected to flooding. Poor drainage conditions can be indicated by water ponding,

dark colored wet soils, and wetland vegetation. Soils are often fine grained and are likely to have low shear strengths and to be compressible and frost susceptible. When these fine grained soils are in direct contact with water-bearing coarser soils, severe consolidation and differential frost behaviour can occur. It is essential to identify these in the site investigation so that these features can be considered in the selection of the design strategy of the foundation, and the grading and drainage around the road embankment.

Drilling and soil sampling are primary techniques in understanding the soil properties. Obtaining undisturbed frozen samples is possible with various boring and coring techniques (Doré & Zubeck 2008). However, it is difficult to collect samples that remain frozen throughout the sampling process and transportation from the site to the laboratory facility. As previously discussed in Chapter 7, Section 7.1, collection of good quality samples of frozen soils is essential for the determination of frozen soil properties.

Analysis of relevant geological and technical reports is also an important step in site investigations. They can provide useful information such as the depth of bedrock, nature and characteristics of soils and rock units, depth to the groundwater level, bearing capacity and stiffness of soils, soil compressibility and shear strength, and presence of ice-rich soils in permafrost conditions.

The thermal stability and temperature profile of the ground should be examined in site investigations. This includes, but is not limited to, thermal modelling of the road embankment. As previously discussed in Chapter 7, Section 7.3, the long term thermal modelling of a foundation ground can be developed by using the current thermal conditions of the foundation and the historic climate data of the site. This analysis is crucial in studying the thermal changes of the ground, potential thawing of frozen ground, the rate of thawing, sensitivity and thickness of the thawing layer, relative settlement, and ultimately the extended performance of the embankment. The impact of long-term climate change (climate warming) should also be considered. It has an important bearing on the effectiveness of strategies to improve road embankment stability in areas of continuous and discontinuous permafrost.

8.2 Design Strategies

Several researchers have studied and recommended design strategies to improve road embankment stability in cold regions (Elias et al. 2001) (Andersland & Ladanyi 2004) (Esch & Stangl 2004) (Beaulac & Doré 2006) (Doré & Zubeck 2008) (Saboundjian 2008). This section presents findings from the literature review, including innovative and economically viable techniques and methods applicable to infrastructure built in continuous and discontinuous permafrost zones. Alternatives discussed in this section will help produce more high quality construction results with desirable performance in a cold region environment.

Replacing the soil with more competent soil:

Poor foundation soil conditions at construction sites in cold regions often contain ice-rich permafrost. Such foundation soils can be replaced by excavated more-competent soil materials that will provide subgrade-equivalent soils suitable for embankment construction (Saboundjian 2008). The replacement fill must have sufficient strength to support anticipated vehicle loadings or structures. Desirable soils must also possess good drainage capacity, as well as properties that support minimal compressibility, settlement, and long term creep. Categories of soils that generally fulfill the requirements of desirable subgrade soils for embankments include most soils with high gravel contents, low moisture contents, and only small quantities of silt, clay, or organic materials. Silty, clayey, or excessively organic soils tend to lack the required shear strength and resistance to consolidation or long term creep (Baxter & Veyera 2004). Such soils also have poor drainage properties, and tend to retain moisture. Soils with high moisture contents tend to initially consolidate (short term settlement) much more than comparable soils with lower moisture contents. Similarly, these fine grained soils and organic-rich soils have the possibility of creep (long term settlement), and may also be sensitive to freeze-thaw cycles, especially if there is an available supply of water from underlying coarser material. It is important to note that finding usable fill material can be difficult and expensive process in northern Canada.

Providing drainage for foundation soils and fill materials with high moisture content:

Fine grained soils exhibit high strength and low deformability (high stiffness) when compacted at moisture contents below optimum (Andersland & Ladanyi 2004). If the moisture content should increase after compaction, there is a significant loss of bearing strength, especially if freezing and thawing occur.

Proper design and installation of drainage in high moisture content foundations can accelerate foundation consolidation in order to minimize pre-construction and post-construction settlement (Esch & Stangl 2004). Use of Geodrains and Membrane Encapsulated Soil Layer (MESL) are common techniques for providing drainage in soils with high moisture content and low porosity.

Geodrains provide artificial drainage in soils with low hydraulic conductivity (Saboundjian 2008). They are a flattened tube drain formed of a nonwoven geotextile wrapped around a plastic core. Large geotextile tubes and bags may be used to contain and dewater fine-grained soils such as sands, silts, and sewage sludge. Large tubes are constructed of geotextiles appropriate in strength and filtration capabilities.

Electro-osmosis is a technique used for the consolidation and strengthening of soft, saturated clayey soils (Rittirong & Shang 2005). When a direct current voltage is applied to soil via electrode poles, the soil pore water will be attracted towards the direction of the negative terminal (cathode) due to the interaction of the electric field, the ions in the pore water and the soil particles (Shang 1998). The electrode poles consist of metallic rods or pipes installed vertically into the ground. Prefabricated vertical drains may sometimes be installed at the cathode as the drainage channel. If drainage is provided at the cathode and prohibited at the anode, consolidation will be induced by electro-osmosis, resulting in the lower soil water content, higher shear strength and lower compressibility. In addition, electrochemical reactions associated with an electro-osmotic process alter the physical and chemical properties of the soil and lead to a further increase in shear strength (Mitchell & Soga 2005). The effect of electro-osmosis technique on environment and electricity-related safety features must be studied before the construction.

Electrokinetic stabilization is a hybrid between electro-osmosis and chemical grouting (Rittirong & Shang 2005). The infusion of certain stabilization chemicals into silty and sandy soils is made more efficient by the application of an electrical potential difference to the soil mass. The procedure is more effective in silty soils that are otherwise difficult to grout ordinarily. More recently, the use of Electrokinetic Geosynthetics (EKG) to improve soft soils has been proposed and studied by

(Glendinning, Jones & Lamont-Black 2005). It is however important to note that this technique has not been studied in cold regions environments.

Membrane encapsulation serves to retain the desirable strength properties during freezing and thawing by preserving their moisture content at its initial low level of moisture content (Andersland & Ladanyi 2004). Soils must be placed and compacted at several percentage points below the optimum moisture content. The Membrane Encapsulated Soil Layer (MESL) technique begins with excavating the soil and spreading it out in the sun to dry (Saboundjian 2008). The dry soil is then transferred and encapsulated in impervious membranes to protect the soils from moisture acquisition. MESL construction involves much more excavation and materials handling than normal construction methods might require. Application of the MESL concept for construction purposes requires that suitable soil (low moisture content) be available within a reasonable haul distance or that the climate and rainfall be such that a reduction of soil moisture contents is economically feasible (Andersland & Ladanyi 2004). There will again be significant environmental issues to consider.

Various other methods can also be used to dry the soils (Saboundjian 2008). Chemicals can be used to accelerate the drying of the soil. Lime is the most common chemical used with clayey soils (Elias et al. 2001). Addition of lime at a

modification optimum percentage causes an instant reduction in plasticity and increased granulation of the soil (Townsend & Anderson 2004). This plasticity reduction is seen as an increase in plastic limit (I_P) and a slight decrease in liquid limit (I_L). The modification optimum percentage depends on the dry density of the soil. It is important to note that if the local clay is calcium-rich, the addition of lime may not produce useful increases in strength or compressibility.

Providing surface drainage:

Poor drainage and presence of surface water on site can have negative effects on the performance of an embankment. The presence and flow of surface water can influence the grading of drains and also impact ground temperatures (Holubec 2010). The presence of surface water often causes water to flow into the ground, which can lead to heat transmission, thawing of ice lenses, and thickening of the active layer over time (Table 8.1). The presence of excess water in the soil foundation causes lower effective stress, lower strength, and more settlements. It negatively affects stiff desiccated regions by elimination of suction (negative) pressures. It also causes the following difficulties during construction - erosion of final grading around the embankment, and initiation of ice lensing and frost heave during the freezing season. In swelling clays, the presence of surface water causes increased water contents, increased settlements, and decreased strengths and stability.

Surface drainage is the removal of excess water from the surface of the land. This can be accomplished by an open ditch parallel to the road embankment with culverts at regular intervals to disperse the run-off to local watercourses. Ongoing maintenance of all surface drainage is essential to good performance of highway embankments. Surface drainage is only present during the warm seasons of the year when snow thaws and rainfall is experienced.

Using Reinforcement to Improve Silts and Clay with Organics, High Water Content and/or Insufficient Strength:

When load is applied on the ground, deformation will occur. This is a result of soil movement to mobilize shear resistance to support the load applied (Yee 2005). Embankments constructed on soft soil foundations undergo large settlements and lateral deformations during and after construction. The loading from an embankment has vertical and horizontal components. The lateral earth pressure of the embankment fill applies an outward shear stress on the foundation, which will contribute to the lowering of the bearing capacity of the foundation (Jewell 1996). By placing a reinforcement layer spanning the differentially deforming foundation, the reinforcement will act as a tensioned membrane to support load (Yee 2005).

Geogrids are widely used for the reinforcement of soils in cold regions (Saboundjian 2008). The concept of geogrid reinforcement is to improve the performance of

subgrade by distributing traffic loads over a wider area. This reduces pumping and shear failure while maximizing the load bearing capacity of the subgrade. Geogrids are polyolefin products and so called "high modulus" geosynthetics (Townsend & Anderson 2004). That is, upon loading, geogrids do not require large strains (stretch) to develop maximum strength. These semi-rigid polymer-based grids are light and easy to transport and install.

Geosynthetics have been widely used to prevent collapse and control deformations of embankments on soft ground (Alfaro, Blatz & Graham 2006). They have also been used to reinforce embankments over discontinuous permafrost ground that includes voids (Kinney & Connor 1987) (Kinney & Connor 1990). The voids were assumed to represent weak zones in the ground caused by thawing of ice lenses/wedges. Kinney and Connor reported that properly selected geosynthetics could be used to span voids of up to 3m. This suggestion was based on measured surface displacements from test embankments. Geosynthetics can also be used in drainage structures to separate free-draining aggregate from lower-permeability surrounding materials to avoid contamination of the free-draining material (Kinney & Connor 1990).

Controlling thawing of embankment foundation:

Strategies to control thawing of embankment foundations can be implemented either prior to or after the construction of an embankment (Saboundjian 2008). In both cases, the strategies are implemented recognizing that it is not possible to ensure the long-term stability of the permafrost foundation.

Thawing of the foundation soil before construction (pre-thawing, Table 8.1) is applicable for areas of discontinuous permafrost or shallow ice-rich permafrost layers, but should be avoided when deeper ice is present (Saboundjian 2008). The pre-thaw process involves complete removal of the vegetation, providing proper drainage, scraping the local soil off the top of the permafrost and leaving the permafrost exposed (Esch & Stangl 2004). Pre-thawing involves time and flexibility, but does not require high costs (Beaulac & Doré 2006). The electro-osmosis technique as a form of heating the ground can be used for the pre-thawing of permafrost when deeper ice is present.

In continuous permafrost zones, keeping the permafrost stable can be achieved by applying methods and/or technologies which reduce the temperature of the road embankment (Saboundjian 2008). Insulation can also accomplish the same thing in cold regions. If permafrost remains frozen, it is effectively stable except for the possibility of long term creep. However, if climate conditions continue to exhibit

annual temperature increases, as has been the case over the last several decades (see Chapter 2, Section 2.2.2), the performance of the these methods can be estimated only if proper thermal modelling is completed.

Permafrost can be maintained at below freezing temperatures by several methods, including reducing solar radiation, inducing air convection, installing ventilation ducts, thermosyphons, or implementing a combination of these measures. The concept of thermosyphons was previously explained in Chapter 2, Section 2.2.5. The rest are discussed below.

Reduction of solar radiation can be achieved by using shading boards, or by applying a reflective surface to the aggregate or pavement (Saboundjian 2008). Snowsheds and sunsheds support cooling of embankments in winter by enabling cold air to circulate against the embankment and preventing insulation from snow. In summer, they reduce direct solar radiation on the embankment surface (Beaulac & Doré 2006). Installation of sheds requires a low cost deployable system compared to other methods, but involves a high-maintenance cost and does not have good durability.

Inducing air convection can be applied by using highly porous, poorly graded material (such as gravel or rock with a low fines content) to allow the passage of

cold air through voids in the rock fill of what are known as 'air convection embankments' (ACEs) (Saboundjian & Goering 2003). In winter, air temperatures and the upper portion of the embankment are colder than the underlying permafrost. As a result, an unstable air density gradient occurs within the embankment. This gradient induces air convection, if a porous material is used to construct the embankment. Thus, in winter, the ACE enables heat to be released from the embankment (Saboundjian 2008) (Beaulac & Doré 2006) (Wei, Guodong & Qingbai 2009) (Saboundjian & Goering 2003). In summer, the air density gradient within the embankment is stable, so cooler air remains at the bottom of the embankment and air convection is minimal. If the porous layer is sufficiently coarse, thermal conduction through the rock layer is also limited. Therefore heat absorption during summer is reduced. Construction of ACEs can be costly because of required sieving and crushing processes, and if competent coarse rocks are not available (Beaulac & Doré 2006).

Installing ventilation ducts is another method of cooling a road embankment (Saboundjian 2008). Ventilation ducts are hollow tubes (air culverts) placed horizontally in the road embankment (either longitudinally or transversely) which allow outside cool air to pass through and release heat from within the embankment to outside (Beaulac & Doré 2006). It is common to fit closing doors to each end of these ventilation ducts to minimize flow of warming air through the ducts during summer months.

Embankments can be insulated by embedding a layer of polystyrene or polyurethane insulation (Saboundjian 2008). The concept behind strategies to insulate an embankment is based on hindering the penetration of surface heat into the ground, thereby preventing degradation of the underlying permafrost (Cheng et al. 2004).

It is important to note that none of the cooling strategies establishes an ability to completely eliminate settlements. The cooling effect typically takes some time to occur and immediate thawing and settlement are induced by initial construction. These strategies are generally only effective at mitigating, not removing the negative impacts of permafrost degradation.

Reducing the applied load on embankment foundation:

A general strategy to improve the stability of road embankments involves the use of lightweight fill material (Saboundjian 2008). Lightweight fills have densities as low as 12kg/m^3 while compacted densities of conventional soils such as sands, silts, and clays range from approximately 1800kg/m^3 to 2200kg/m^3 (Stark & Arellano 2004). The reduction in applied load from the fill material improves the stability of the road embankment. In addition, certain types of lightweight fills may provide favourable performance in terms of improved insulative properties compared to conventional soils. Reduced embankment fill weight can be applied by using expanded

213

polystyrene geofoams (EPS), foamed concrete, rubber tire shreds or bales, or wood chips as fill material.

Perhaps the most promising approach for long-term stabilization of embankments is combining the specific strategies. Much of the most recent research focuses on the combinational effects of various strategies (Goering 2001) (Saboundjian 2008). More research is needed to further understand how to combine and optimize these design strategies.

8.3 Remediation of Embankments on Thawed Permafrost

The cooling and insulation methods to control thawing or to mitigate thawing and settlement are not capable of reversing the long-term thawing of foundations beneath embankments that were originally built on permafrost that has now thawed. These design strategies cannot ensure the long-term stability of embankments in areas with warm permafrost, particularly where the thawing of permafrost is advanced and/or a frozen foundation has already thawed.

In contrast, replacing the foundation soil with more competent soil, providing drainage for the foundation soils and fill materials with high water content, and reinforcing silts and clay with high water content and insufficient strength are the strategies which most likely promote long-term stability of embankments on thawed

permafrost. These specific strategies are effective in strengthening the soil structure and providing enough drainage to minimize post-construction settlements. However, applying these strategies to foundation soils of an existing embankment on thawed permafrost can be expensive. When feasible, relocation of the road embankment at an unstable section to an alternative route should also be considered.

8.4 Selection of a Design Strategy

Costs and benefits associated with different design strategies to improve embankment stability should be considered in the selection process of a proper strategy for the embankment being studied. The cost analysis involves addressing stability issues using standard maintenance practices. Better decisions are made by considering costs on a life-cycle basis which includes annualized capital and maintenance expenditures over the life period of a proposed strategy.

In order to select the proper design strategy, applicable methods and strategies must be analyzed. The following factors should be considered in an evaluation of a design strategy (Saboundjian 2008):

- Projected performance of the embankment
- The functional metrics of the embankment (including but not limited to stability requirements, allowable total and rate of settlement, level of maintenance) to establish required improvement
- Area, depth, weight, and total volume of soil to be treated

- Foundation soil type and properties

- Availability and mobilization of construction materials

- Availability and mobilization of equipment

- Local experience and preference

- Time available

- Costs and benefits

- Environmental factors such as erosion, waste disposal, water pollution and effects on adjacent facilities and structures, and fish habitat concerns

Flux	Potential Gradient			
	temperature	*hydraulic*	*electrical*	*chemical*
heat	thermal conduction	isothermal heat transfer	Peltier effect	Dufour effect
fluids	thermo-osmosis	hydraulic conduction (Darcy's Law)	electro-osmosis	normal osmosis
current	thermo-electricity	streaming current	electrical conduction (Ohm's Law)	Diffusion, membrane potentials
ions	Soret effect	streaming current	electrophoresis	diffusion (Fick's Law)

Table 8.1: Coupled processes in clay soils, from Table 9.6 in (Mitchell & Soga 2005)

CHAPTER 9:   Summary, Conclusions, and Recommendations for

Future Research

9.1 Summary

This research project investigated the understanding of the performance of a highway embankment on thawed permafrost. It was a project on Provincial Road PR391, about 18 km northwest of Thompson, Manitoba. The research on PR391 consisted of (1) a detailed geotechnical site investigation, (2) field instrumentation, (3) data collection, (4) laboratory testing, (5) constitutive analysis and (6) numerical simulations.

A comprehensive laboratory testing program was completed, focusing on the effects of low temperatures (near 0°C) on the consolidation and shearing properties of the soil at the PR391 test site. The one-dimensional consolidation (oedometer) tests and consolidated undrained triaxial tests with pore pressure measurement (CIŪ tests) were completed at temperatures of 3°C and 21°C. Soil characterization tests (such as Atterberg limits and grain size distribution) were undertaken to understand thoroughly the properties of the foundation material underneath the PR391 embankment and the effect of temperature change on the mechanical properties of soil.

Instrument clusters were installed at the PR391 site embankment, including thermistor strings at 1m depth intervals, vibrating wire piezometers and standpipes, surface settlement plates, slope inclinometers, and lateral displacement extensometers. The temperature, pore water pressure, and vertical and horizontal deformations of embankment were monitored. Data were collected from the instruments and analyzed during the first two years of operation, that is, over two freeze-thaw cycles.

Numerical modelling of the PR391 embankment was developed to simulate the thermal changes and frost heave characteristics of highway embankments. The modelling permitted simulation of temperature changes under the embankment. The second aspect of the modelling was to study the application of the frost heave approach known as the Segregation Potential (SP) method to field conditions. Segregation potentials were back-calculated from the site observations and collected frost heave data by using the SP method.

The author considers that the major contributions from this thesis project include:

1- Collection and interpretation of field data over 28 months from two well instrumented sections of a highway embankment at a site where previous permafrost has thawed.

2- At the test site, there is currently a net flow of heat into the ground from the surface.

3- A realization that embankment deformations are due not only to vertical settlements, but also to lateral movements under the toe of the side slopes.

4- The depth of measured DMZAA corresponds approximately to the depth above which temperature appeared to have little effect on material properties such as C_c and $C_{\alpha e}$, perhaps due to destructuring of the soil fabric.

5- The field data allow evaluation of segregation potentials that are broadly similar to those measured in laboratory testing.

6- It will be necessary to examine temperature distributions beneath the centre of the embankments.

7- Remote sensing of instruments is valuable and cost effective.

9.2 Conclusions

The following major conclusions can be drawn from this research.

1- Mechanical and shearing properties of the soil collected from the PR391 embankment are not significantly affected by differences in temperature.

2- Large differential settlements present at the unstable section of the PR391 are not caused simply by changes of temperature and their related impacts on the hydro-mechanical behaviour of the foundation materials.

3- The differential settlements were instead caused by thawing of discontinuous permafrost and change of phase in the foundation from solid to liquid, which in turn caused the destructuring of the foundation soil. After thawing and

completion of phase change, changes of temperature do not significantly affect the hydro-mechanical and shearing behaviour of the soil.

4- Displacements observed at the PR391 embankment are a combination of consolidation and shearing strain of the foundation material. The displacements are two dimensional (plane strain).

5- In situ frost heave characteristics can be estimated by applying the SP frost heave method in field conditions.

The following minor conclusions can also be drawn from this research.

1- Weathering processes in the foundation soil and active layer closer to the ground cause destructuring of the soil fabric over time.

2- Net heat flow into the ground observed for both years of data collection is possibly a confirmation of general warming in the area. Additional data over a longer time period would be helpful.

3- The temperature data show that measured temperature at the DMZAA is above 0°C. This confirms field observations of the thawing of ice that was present when the embankment was initially constructed.

4- Thawing of permafrost begins at the toe of the embankment and then spreads towards the centre of the embankment.

5- Development of cyclic seasonal gradients of total head indicated hydrostatic water pressure conditions during summer months and upwards flow during the freezing season. These are believed to be caused by upward flow of water

towards suction pressures (negative potentials) at the freezing front as it moves downwards during the winter. This causes reduction of shear strengths and higher compressibilities when the ice melts during the spring thaw.

6- Long term thermal modelling of the foundation for an embankment can be developed by using the current thermal conditions of the foundation and the historic climate data of the site

9.3 Recommendations for Future Research

The following is a list of suggestions recommended for future research:

1- Long term monitoring and data collection from the instruments at the PR391 site in order to investigate the performance of embankment and warming of ground in the long term

2- Installation of additional instruments at the site including having a full set of instruments on both sides of the embankment, and thermistors beneath the centre of the embankment.

3- Conduct frost heave tests in laboratory in order to compare the values of SP measured in the laboratory with the calculated values from the site data.

Bibliography

Alfaro, MC, Batenipour, H, Graham, J, Kurz, DR & Ng, TNS 2009, 'Highway embankments on degrading and degraded permafrost', *17th International Conference on Soil Mechanics & Geotechnical Engineering - The Academia & Practice of Geotechnical Engineering*, Alexandria, Egypt.

Alfaro, MC, Blatz, JA & Graham, J 2006, 'Geosynthetic Reinforcement for Embankments Over Degrading Discontinuous Permafrost Subjected to Pressressing', *Lowland Technology International*, vol 8, no. 1, pp. 47-54.

Alfaro, MC, Ciro, GA, Thiessen, KJ & Ng, TNS 2009, 'Case Study of Degrading Permafrost beneath a Road Embankment', *Journal of Cold Regions Engineering*, vol 23, no. 3, pp. 93-112.

Allard, M, Wang, B & Pilon, JA 1995, 'Recent cooling along the southern shore of Hudson Strait, Quebec, Canada, documented from permafrost temperature measurements', *Arctic and Alpine Research*, vol 27, no. 2, p. 157–166.

Andersland, OB & Ladanyi, B 2004, *Frozen Ground Engineering*, 2nd edn, John Wiley & Sons, Inc.

Anderson, D, Tice, A & McKim, H 1973, 'The Unfrozen Water and the Apparent Specific Heat Capacity of Frozen Soils', *Proceedings of the 2nd International Conference on Permafrost*, Yakutsk, U.S.S.R.

ASTM D2216-10, 'Standard Test Methods for Laboratory Determination of Water (Moisture) Content of Soil and Rock by Mass', *Annual Book of ASTM Standards. American Society for Testing and Materials*.

ASTM D2435-96, 'Standard Test Method for One-Dimensional Consolidation Properties of Soils', *Annual Book of ASTM Standards. American Society for Testing and Materials*.

ASTM D422-63, 'Standard test method for particle-size analysis', *Annual Book of ASTM Standards. American Society for Testing and Materials*.

ASTM D4318-05, 'Test Method for Liquid Limit, Plastic Limit, and Plasticity Index of Soils', *Annual Book of ASTM Standards. American Society for Testing and Materials.*

ASTM D4767, 'Standard test method for consolidated undrained', *Annual Book of ASTM Standards. American Society for Testing and Materials.*

ASTM D5334-08, 'Standard Test Method for Determination of Thermal Conductivity of Soil and Soft Rock by Thermal Needle Probe Procedure', *Annual Book of ASTM Standards. American Society for Testing and Materials.*

Batenipour, H, Alfaro, MC, Graham, J & Kalynuk, K 2011, 'Deformations of a highway embankment on degraded permafrost', *14th Pan-American Conference on Soil Mechanics and Geotechnical Engineering & 64th Canadian Geotechnical Conference*, Toronto, Ontario.

Batenipour, H, Kurz, DR, Alfaro, MC & Graham, J 2009a, 'Effect of Temperature on the 1-D Behaviour of Plastic Clay', *62nd Canadian Geotechnical Conference & 10th Joint CGS/IAH-CNC Groundwater Conference*, Halifax NS.

Batenipour, H, Kurz, DR, Alfaro, MC, Graham, J & Kalynuk, K 2010, 'Results from an Instrumented Highway Embankment on Degraded Permafrost', *63rd Canadian Geotechnical Conference & 6th Canadian Permafrost Conference*, Calgary, Alberta.

Batenipour, H, Kurz, DR, Alfaro, MC, Graham, J & Ng, TNS 2009b, 'Highway Embankment on Degrading Permafrost', *14th Conference on Cold Regions Engineering*, Duluth, Minnesota, USA.

Baxter, C & Veyera, G 2004, 'Liquefaction Potential of Inorganic and Organic Silts', RIDOT, Providence, RI, Research in Progress, Transportation Research Board, National Research Council, Washington, DC.

Beaulac, I & Doré, G 2006, 'Permafrost degradation and adaptations of airfields and access roads, Nunavik, Quebec, Canada', *Proceedings of the Annual Conference of the Transportation Association of Canada*, Charlottetown, Prince Edward Island.

Black, PB 1995, *RIGIDICE Model of Secondary Frost Heave.*

Boudali, M 1995, 'Comportement tridimensionnel et visqueux des argiles naturelles', PhD Thesis, Université Laval, Sainte-Foy, Quebec.

Brown, RJE 1960, 'The distribution of permafrost and its relation to air temperature in Canada and the USSR', *Arctic*, vol 13, pp. 163-177.

Brown, RJE 1965, 'Distribution of permafrost in the discontinuous zone of western Canada', *Canadian regional permafrost conference*, National Research Council of Canada, Ottawa, Ontario.

Brown, RJE 1967, 'Permafrost in Canada', Geological Survey Map 124A, first edition, Canada.

Brown, RJE 1969, 'Distribution of Permafrost in Canada', *Third Canadian Conference on Permafrost*, Division of Building Research, National Research Council, Ottawa.

Brown, RJE 1997, 'Disturbance and recovery of permafrost terrain', in *Disturbance and Recovery in Arctic Lands: An Ecological Perspective*, Kluwer Academic Publishers, Dordrecht, The Netherlands.

Brown, RJE, Hinkel, KM & Nelson, FE 2000, 'The Circumpolar Active Layer Monitoring (CALM) program: Research designs and initial results', *Polar Geography*, vol 24, no. 3, p. 165–258, (file code: ECV-T7-permafrost-ref-01(CALM) program - GCOS-Imp).

Budhu, M 2007, *Soil Mechanics and Foundations*, 2nd edn, Wiley, Hoboken, NJ.

Burghignoli, A, Desideri, A & Miliziano, S 1992, 'Deformability of clays under non isothermal conditions', *Rivista Italiana Di Geotecnica*, vol 26, no. 4, pp. 227-236.

Campanella, RG & Mitchell, JK 1968, 'Influence of temperature variations on soil behavior', *Journal of the Soil Mechanics and Foundations Division*, vol 94, pp. 709-734.

CCCSN 2009, 'Canadian Climate Change Scenarios Network, Arctic Ensemble Scenarios'.

Cheng, G, Zhang, J, Sheng, Y & Chen, J 2004, 'Principle of thermal insulation for permafrost protection', *Cold Regions Science and Technology*, vol 40, pp. 71-79.

Chiu, SL 1996, 'Behaviour of normally consolidated clay at elevated temperature', Ph.D. Thesis, The University of Sydney, Sydney, Australia.

Claridge, FB & Mirza, AM 1981, 'Erosion control along transportation routes in northern climates', *Arctic*, vol 34, no. 2, p. 147–157.

Ctori, P 1989, 'The Effects of Temperature on the Physical Properties of Cohesive Soil', *Ground Engineering*, vol 22, no. 5, pp. 26-27.

DGE Slope Indicator 2004a, 'Multi-Level Vibrating Wire Piezometer manual'.

DGE Slope Indicator 2004b, 'Water Level Indicator manual'.

DGE Slope Indicator 2006, 'Digi-Pro for Windows Systems (Version 1.34.1)'.

Doré, G & Zubeck, H 2008, *Cold Regions Pavement Engineering*, McGraw-Hill.

Elias, V, Welsh, J, Warren, J & Lukas, R 2001, 'Ground Modification Technical Summaries Volumes I and II', Federal Highway Administration, Publication No. FHWA-SA-98-086R.

Eriksson, LG 1989, 'Temperature effects on consolidation properties of sulphide clays', *12th International Conference on Soil Mechanics and Foundation Engineering*, Rio de Janeiro.

Esch, DC & Stangl, KO 2004, 'Performance of Yukon-Kuskokwim Delta Airport Embankments'.

Farouki, O 1985, 'Ground Thermal Properties', in *Thermal Design Considerations in Frozen Ground Engineering*, American Society of Civil Engineers, ASCE., New York.

Farouki, O 1986, *Thermal properties of soils*, Trans Tech Publications.

Farouki, O 2004, 'Ground Thermal Properties', in *Thermal Analysis, Construction, and Monitoring Methods for Frozen Ground*, American Society of Civil Engineers, ASCE.

Freden, S 1965, 'Some aspects on the physics of frost heave in mineral soils', *Surface chemistry*, pp. 79-90.

Geo-slope 2010, *Thermal Modeling with TEMP/W 2007*, Geo-slope International Ltd., Calgary, Alberta, Canada.

Ghahremannejad, B 2003, 'Thermo-Mechanical Behaviour of Two Reconstituted Clays', PhD Thesis, The University of Sydney, Sydney, Australia.

Glendinning, S, Jones, C & Lamont-Black, J 2005, 'The Use of Electrokinetic Geosynthetics (EKG) to Improve Soft Soils', in *Ground improvement: case histories*.

Goering, DJ 2001, 'ACE and Thermosyphon Design Features – Loftus Road Extension Project', Alaska Department of Transportation & Public Facilities Report No. FHWA-AKRD-RD-02-01.

Goodrich, LE & Gold, LW 1981, 'Ground Thermal Analysis: Permafrost Engineering Design and Construction', John Wiley & Sons.

Graham, J, Tanaka, N, Crilly, T & Alfaro, MC 2001, 'Modified Cam Clay Modeling of Temperature Effects in Clays', *Canadian Geotechnical Journal*, vol 38, no. 3, pp. 608-621.

Habibagahi, K 1977, 'Temperature effect and the concept of effective void ratio', *Indian Geotechnical Journal*, vol 7, no. 1, pp. 14-34.

Halsey, LA, Vitt, DH & Zoltai, SC 1995, 'Disequilibrium response of permafrost in boreal continental western Canada to climate change', *Climate Change*, vol 30, p. 57–73.

Heginbottom, JA 2000, 'Permafrost distribution and ground ice in surficial materials', in *The physical environment of the Mackenzie Valley, Northwest*.

Henry, KS 1998, 'The use of geosynthetics to mitigate frost heave in soils', PhD Thesis, Civil Engineering Department, University of Washington, Seattle.

Hinkel, KM, Nelson, FE, Park, W, Romanovsky, V, Smith, O, Tucker, W, Vinson, T & Brigham, LW 2003, 'Climate Change, Permafrost, and Impacts on Civil Infrastructure', United States Arctic Research Commission: Permafrost Task Force Report, Special Report 01-03.

Hoekstra, P 1969, 'Water movement and freezing pressures', *Soil Science Society of America Proceedings*.

Holubec, I 2008, 'Flat Loop Thermosyphon Foundations in Warm Permafrost', Prepared for the Government of the Northwest Territories Asset Management Division of Public Works and Services and the Climate Change Vulnerability Assessment of the Canadian Council of Professional Engineers.

Holubec, I 2010, 'Geotechnical Site Ivestigation Guidlines for Building Foundations in Permafrost', Department of Public Works and Services, Government of the Northwest Territories.

Houston, SL, Houston, WN & Williams, ND 1985, 'Thermomechanical behavior of seafloor sediments', *Journal of Geotechnical Engineering*, vol 111, no. 11, pp. 1249-1263.

'http://gsc.nrcan.gc.ca/permafrost/images/wheredoes1.jpg' August 2011, Geological Survey of Canada, Natural Resources Canada.

Hueckel, T & Baldi, G 1990, 'Thermoplasticity of saturated clays: experimental constitutive study', *Journal of Geotechnical Engineering*, vol 116, no. 12, p. 1778–1796.

Hueckel, T & Pellegrini, R 1989, 'Modelling of thermal failure of saturated clays', *NUMOG3, 3rd International Symposium on Numerical Models in Geomechanics*, Elsevier, Niagara Falls, Ontario.

Hukseflux, 'TP08 Small Size Non-Steady-State Probe for Thermal Conductivity Measurement manual'.

IPCC 2007, 'Summary for policymakers', in *Climate change 2007: The physical science basis. Contribution of Working Group I to the Fourth Assessment Report of the Intergovernmental Panel on Climate Change*, Cambridge University Press, Cambridge, UK, and New York, NY.

Jewell, RA 1996, 'Soil Reinforcement with Geotextiles', *Construction Industry Information Association, Thomas Telford, London*, 1996, p. 237–273.

Johansen, O 1975, 'Thermal Conductivity of Soils', PhD Thesis, CRREL draft translation 637, Trondheim, Norway.

Kelln, C, Sharma, J, Hughes, D & Graham, J 2008, 'An Improved Framework For An Elastic-Viscoplastic Soil Model', *Canadian Geotechnical Journal*, vol 45, pp. 1356-1376.

Kelln, C, Sharma, J, Hughes, D & Graham, J 2009, 'Finite element analysis of an embankment on soft estuarine deposit using an elastic-viscoplastic soil model', *Canadian Geotechnical Journal*, vol 46, pp. 357-368.

Kinney, TC & Connor, B 1987, 'Geosynthetics supporting embankments over voids', *ASCE Journal of Cold Regions Engineering*, vol 1, no. 2, pp. 102-112.

Kinney, TC & Connor, B 1990, 'Geosynthetic reinforcement of paved road embankment on polygonal ground', *ASCE Journal of Cold Regions Engineering*, vol 4, no. 4, pp. 158-170.

Konrad, J-M 1984, 'Soil freezing characteristics versus heat extraction rate', *National Research Council of Canada, DBR Paper No 1257*, p. 7.

Konrad, J-M 1989a, 'Influence of cooling rate on the temperature of ice lens formation in clayey silts', *Cold Regions Science and Technology*, vol 16, pp. 25-36.

Konrad, J-M 1989, 'Physical processes during freeze-thaw cycles in clayey silts', *Cold Regions Science and Technology*, vol 16, no. 3, pp. 291-303.

Konrad, J-M 1994, 'Sixteenth Canadian Geotechnical Colloquium: Frost heave in soils: concepts and engineering', *Canadian Geotechnical Journal*, vol 31, pp. 223-245.

Konrad, J-M 2005, 'Estimation of the segregation potential of fine-grained soils using the frost heave response of two reference soils', *Canadian Geotechnical Journal* , vol 42, no. 1, pp. 38-50.

Konrad, J-M 2008, 'Freezing-induced water migration in compacted base-course materials', *Canadian Geotechnical Journal*, vol 45, pp. 895-909.

Konrad, J-M & Morgenstern, NR 1980, 'A mechanistic theory of ice lens formation in fine-grained soils', *Canadian Geotechnical Journal*, vol 17, no. 4, pp. 473-86.

Konrad, J-M & Morgenstern, NR 1981, 'The segregation potential of a freezing soil', *Canadian Geotechnical Journal*, vol 18, no. 4, pp. 482-91.

Konrad, J-M & Morgenstern, NR 1982, 'Prediction of frost heave in the laboratory during transient freezing', *Canadian Geotechnical Journal*, vol 19, no. 3, pp. 250-59.

Konrad, J-M & Morgenstern, NR 1983, 'Frost susceptibility of soils in terms of their segregation potential', *4th International Conference on Permafrost*, National Academy Press, Fairbanks, Alaska.

Koyama, M & Sasaki, H 1967, 'Frost Heave of Roads in Hokkaido and Its Countermeasures', *Physics of Snow and Ice : proceedings*, vol 1, no. 2, pp. 1323-1331.

Kuntiwattanakul, P, Towhata, I, Ohishi, K & Seko, I 1995, 'Temperature effects on undrained shear characteristics of clay', *Soil and Foundations*, vol 35, no. 1, pp. 147-162.

Laguros, JG 1969, 'Effect of Temperature on Some Engineering Properties of Clay Soils', Highway Research Board, Special Report 103, Washington D.C.

Leroueil, S & Marques, MES 1996, 'Importance of strain rate and temperature effects in geotechnical engineering', in TC Sheahan, VN Kaliakin (eds.), *Measurement and modeling time dependent soil behabiour, Geotechnical Special Publication*, ASCE, Reston, Va.

Linell, KA 1973, 'Long-term effects of vegetative cover on permafrost stability in an area of discontinuous permafrost', *Permafrost, Second International Conference Proceedings, North American Contribution.*, National Academy Press, Washington, D.C.

Lingnau, BE, Graham, J & Tanaka, N 1995, 'Isothermal modelling of Sand-Bentonite mixtures at elevated temperatures', *Canadian Geotechnical Journal*, vol 32, pp. 78-88.

Lingnau, BE, Graham, J, Yarechewski, D, Tanaka, N & Gray, MN 1996, 'Effects of temperature on strength and compressibility of sand-bentonite buffer. 41 1, 1, 3, 4, pp.', *Engineering Geology*, vol 41, no. 1-4, pp. 103-115.

Marques, MES, Leroueil, S & Almeida, MDS 2004, 'Viscous behaviour of the St-Roch-de-l'Achigan clay, Quebec', *Canadian Geotechnical Journal*, vol 41, no. 1, pp. 25-38.

McBean, GA, Alekseev, G, Chen, D, Forland, E, Fyfe, JC, Groisman, PY, King, R, Melling, H, Vose, R & Whitfield, PH 2005, 'Arctic Climate: Past and Present', in *Arctic Climate Impact Assessment*, Cambridge University Press.

Mesri, G 1973, 'Coefficient of secondary compression', *Journal of the soil mechanics and foundations division*, vol 99, no. SM1, pp. 123-137.

Mesri, G, Feng, TW & Shahien, M 1995, 'Compressibility Parameters During Primary Consolidation', *Invited Special Lecture. International Symposium on Compression and Consolidation of Clayey Soils, Hiroshima, Japan, Lectures and Reports Volume*, May 1995, pp. 201-217.

Mesri, G & Godlewski, PM 1997, 'Time and Stress Compressibility Inter relationship', *Journal of the Geotechnical Engineering Division*, vol 103, no. GT5, pp. 417-430.

Mikkelsen, PE 2002, 'Cement-bentonite grout backfill for borehole instruments', *Geotechnical News*, 2002, pp. 38-42.

Mitchell, JK 1964, 'Shearing resistance of soils as a rate process', *Journal of the Soil Mechanics and Foundations Division*, vol 90, pp. 29-61.

Mitchell, JK & Soga, K 2005, *Fundamentals of Soil Behavior*, 3rd edn, John Wiley & Sons.

Moritz, L 1995, 'Geotechnical properties of clay at elevated temperatures', Report: 47, Swedish Geotechnical Institute.

Murayama, S 1969, 'Effect of Temperature on the Elasticity of clays', Highway Research Board, Special Report 103, Washington D.C.

Nelson, FE & Outcalt, SI 1982, 'Anthropogenic geomorphology in northern Alaska', *Physical Geography*, vol 3, pp. 17-48.

Nixon, JF 1991, 'Discrete ice lens theory for frost heave in soils', *Canadian Geotechnical Journal*, vol 28, no. 6, pp. 843-59.

Nixon, JF 1992, 'Discrete ice lens theory for frost heave beneath pipelines', *Canadian Geotechnical Journal*, vol 29, no. 3, pp. 487-97.

Nixon, JF, Ellwood, JR & Slusarchuk, WA 1981, 'In-situ frost heave testing using cold plated', *4th Canadian Permafrost Conference*, NRCC, No. 20124, Calgary, Alberta.

Noble, CA & Demirel, T 1969, 'Effect of Temperature on Strength behaviour of Cohesive Soil', Highway Research Board, Special Report 103, Washington D.C.

O'Neill, K & Miller, RD 1982, 'Numerical solutions for a rigid ice model of secondary frost heave', Technical report, CRREL Rep 82-13.

O'Neill, K & Miller, RD 1985, 'Exploration of a rigid ice model of frost heave', *Water Resources Research*, vol 21, no. 3, pp. 281-296.

Osterkamp, TE & Lachenbruch, AH 1990, 'Thermal regime of permafrost in Alaska and predicted global warming', *Journal of Cold Regions Engineering*, vol 4, pp. 38-42.

Penner, E 1972, 'Influence of freezing rate on frost heaving', *Highway Research Record 393*, 1972, pp. 56-64.

Penner, E & Goodrich, LE 1980, 'Location of segregated ice in frost susceptible soil', *The 2nd International Symposium on Ground Freezing*, Trondheim, Norway.

Perkins, S & Sjursen, M 2009, 'Effect of cold temperatures on properties of unfrozen Troll Clay', *Canadian Geotechnical Journal*, vol 46, no. 12, pp. 1473-1481.

Péwé, TL 1954, 'Effect of permafrost upon cultivated fields', *U.S. Geological Survey Bulletin*, vol 989F, p. 315–351.

Plum, RL & Esrig, MI 1969, 'Some temperature effects on soil compressibility and pore water pressure', *Effects of temperature and heat on engineering behaviour of soils. Highway Research Board, Special Report 103*, 1969, p. 231–242.

Rittirong, A & Shang, JQ 2005, 'Electro-Osmotic Stabilization', in *Ground improvement: case histories*.

RST 2008a, 'Casagrande Standpipe Piezometer manual', RST.

RST 2008b, 'Thermistor Strings manual'.

RST 2008c, 'Vibrating Wire Extensometer manual'.

Saboundjian, S 2008, 'Evaluation of Alternative Embankment Construction Methods', Alaska Department of Transportation, Juneau.

Saboundjian, S & Goering, DJ 2003, 'Air Convective Embankment For Roadways: Field experimental study in Alaska', *Transportation Research Record: Journal of the Transportation Research Board*, vol 1821, pp. 20-28.

Shang, JQ 1998, 'Electroosmosis-enhanced preloading consolidation via vertical drains', *Canadian Geotechnical Journal*, vol 35, pp. 491-499.

Sheng, D 1994, 'Thermodynamics of freezing soils, theory and application', PhD Thesis: 141D, Lulel University of Technology.

Sherif, MA & Burrous, CM 1969, 'Temperature effect on unconfined shear strength of saturated cohesive soils', *an international conference on Effects of Temperature and Heat on Engineering Properties of Soils*, Special Report 103, Highway Research Board, Washington, D.C.

Skempton, AW 1954, 'The pore pressure coefficients A and B', *Geotechnique*, vol 4, no. 4, pp. 143-147.

Slaughter, CW, Racine, CH, Walker, DA, Johnson, LA & Abele, G 1990, 'Use of off-road vehicles and mitigation of effects in Alaska permafrost environments: A review', *Environmental Management*, vol 14, no. 1, pp. 63-72.

Smith, SL, Burgess, MM, Riseborough, D & Nixon, FM 2005, 'Recent trends from Canadian permafrost thermal monitoring network sites', *Permafrost and Periglacial Processes*, vol 16, pp. 19-30.

Stark, TD & Arellano, D 2004, 'Guideline and Recommended Standard for Geofoam Applications in Highway Embankments', NCHRP Report 529, Transportation Research Board, National Research Council, Washington, DC.

Tanaka, N 1995, 'Thermal elastic plastic behaviour and modelling of saturated clays', PhD Thesis, University of Manitoba, Winnipeg, Manitoba.

Tanaka, N, Graham, J & Crilly, T 1997, 'Stress-Strain Behaviour of Reconstituted Illitic Clay at Different Temperature', *Engineering Geology*, vol 47, pp. 339-350.

Tang, AM, Cui, YJ & Barnel, N 2008, 'Thermo-mechanical behaviour of a compacted swelling clay', *Géotechnique*, vol 58, no. 1, pp. 45-54.

Tidfors, M & Sällfors, G 1989, 'Temperature effect on preconsolidation pressure', *Geotechnical Testing Journal*, vol 12, no. 1, pp. 93-97.

Towhata, I, Kuntiwattanaku, P & Seko, I 1993, 'Volume change of Clays induced by heating as observed in consolidation tests', *Soils and Foundations*, vol 33, no. 4, pp. 170-183.

Townsend, FC & Anderson, JB 2004, 'A Compendium of Ground Modification Techniques', University of Florida.

Wei, M, Guodong, C & Qingbai, W 2009, 'Construction on permafrost foundations: Lessons learned from the Qinghai-Tibet railroad', *Cold Regions Science and Technology*, vol 59, pp. 3-11.

Williams, PJ 1986, *Pipelines & Permafrost: Science in a Cold Climate*, Carleton University Press, Don Mills, Ontario.

Yee, TW 2005, 'Ground Improvement with Geotextile Reinforcements', in *Ground improvement: case histories*.

Yin, J-H, Zhu, J-G & Graham, J 2002, 'A new elastic viscoplastic model for time-dependent behaviour of normally and overconsolidated clays: theory and verification', *Canadian Geotechnical Journal*, vol 39, pp. 157-173.

Appendix A

Original data from the field, laboratory, and computing parts of this project have been compiled into a single CD. Following paragraphs list the contents of the CD and how they can be accessed. The data are contained in four folders with, respectively, the following contents:

- *Folder 1:* Information about the wiring and program required to run the software for the Campbell Scientific data acquisition system. The program (file name: Q012225_UofM_CR3000_1MIN_rev_Hamid.CR3, required software: LoggerNet by Campbell Scientific (Canada) Corp.) and wiring diagram (file name: ELE0415A_WOQ012225.pdf, required software: Adobe Reader) of the DA system explained in Chapter 3.

- *Folder 2:* The results and calculations of the geotechnical testing program outlined in Chapter 4. Single folders for each test of Chapter 4 contain Excel files with raw data, spreadsheet calculations and plots. The summary of the results are also included (file name: 111028 Lab testing Restuls.xlsx, required software: Microsoft Excel).

- *Folder 3:* The results and calculations of the field instruments data collected from the PR391 embankment presented in Chapter 5. The Chapter 5 folder contains an Excel file of raw data, spreadsheet calculations and plots of the field data, including the data collected by the DA system and the surveyed

settlement data (file name: 111107 DA +Surverying.xlsx, required software: Microsoft Excel).

- *Folder 4:* The results and calculations of thermal modelling and frost heave predictions of PR391 presented in Chapter 6. The Chapter 6 folder contains the TEMP/W thermal modelling files (file names: 111028 - SS_Model-Hamid.gsz and 111102 - US_Model-Hamid.gsz, required software: GeoStudio by GEO-SLOPE International Ltd.), and the Excel file of spreadsheet calculations and plots of the SP frost heave prediction of PR391 (file name: 111107 DA +Surverying.xlsx, required software: Microsoft Excel).

The CD containing the data that form the basis of this thesis can be obtained from the author, from Dr. Marolo Alfaro at the Department of Civil Engineering, University of Manitoba; or from Manitoba Infrastructure and Transportation.